Master Thesis

Detection of forest parameters
using
imaging spectroscopy

submitted by Anne Reichmuth
seminar group 10/063/71
matriculation number 30795
study course Geoinformation und Management
handed in 2nd April 2013

Hochschule für Technik und Wirtschaft (HTW) Dresden
University of Applied Sciences Dresden
Faculty of Spatial Information

Deutsches Zentrum für Luft- und Raumfahrt e.V. (DLR)
German Aerospace Center
German Remote Sensing Data Center
Department Land Surface

Supervisors:

Prof. Dr. Martin Oczipka (HTW Dresden)
Dr. Nicole Pinnel (DLR Oberpfaffenhofen)

Contents

List of Figures

List of Tables

Abbreviation

ALS	Airborne Laser Scanning
BRDF	Bidirectional Reflectance Distribution Function
CAO	Carnegie Airborne Observatory
CASI	Compact Airborne Spectrographic Imager
CIR	Colour Infrared
DEM	Digital Elevation Model
DFD	German Remote Sensing Data Center
DGPS	Differential Global Positioning System
DLR	German Aerospace Centre
DN	Digital Number
DSM	Digital Surface Model
EnMAP	Environmental Mapping and Analysis Program
FDI	Forest Discrimination Index
FOV	Field of View
FWHM	Full Width of Half Maximum
GA	Genetic Algorithm
GPS	Global Positioning System
HYDICE	Hyperspectral Digital Imagery Collection Experiment
HyMap	Hyperspectral Mapper
HyspIRI	Hyperspectral Infrared Imager
Hz	Hertz
IAS	Iterative Adaptive Smoothing Filter
IMF	Remote Sensing Technology Institute
INS	Internal Navigation System
IR	Infrared
LDA	Linear Discriminant Analysis
LiDAR	Light Detection And Ranging
LWF	Landesanstalt für Wald und Forstwirtschaft
ML	Maximum likelihood
NDBRI	Normalised Difference Brick Roof Index
nDSM	Normalised Digital Surface Model
NDVI	Normalised Difference Vegetation Index
Radar	Radio Detection and Ranging
PC	Principal Component
PCA	Principal Component Analysis

RGB	Red Green Blue
RMS	Root Mean Square
SA	Spectral Angle
SAM	Spectral Angle Mapper
SPOT	Satellite Pour l'Observation de la Terre
SRTM	Shuttle Radar Topography Mission
SWIR	Short Wave Infrared
TM	Thematic Mapper
VNIR	Visible Near Infrared
WV2	Worldview-2

Abstract

The main tree species in Bavaria is spruce, which is being strongly affected by the climate change, because of its anthropogenic influenced distribution in non-typical site ranges. Through climate change, biotic and abiotic factors, such as bark beetles, fungi, storm, snow and water stress are occurring more often and are stressing spruce in these unsuitable sites. Due to these changing conditions it is getting more important to detect forest types as a feature of its own, but also other tree species and spruce in particular.

This thesis presents a spectral analysis of detecting deciduous and coniferous forest as forest type and independently European beech, European fir and Norway spruce as tree species. The analysis was carried out using hyperspectral HySpex VNIR and multispectral Worldview-2 images, each with 2 m ground resolution from a heterogeneous and stratified temperate forest in southern Germany. This type of forest exhibits characteristics of sustainable prospective temperate forests. A total of 2008 and 2009 reference spectra from HySpex VNIR and Worldview-2 were extracted and analysed with Principal Component Analysis for possible discrimination. A combination of eight uncorrelated bands, that were optimised for forest type discrimination and another eight bands, also optimised for tree species discrimination were extracted from HySpex VNIR imagery, using a Genetic Algorithm. The extracted eight bands from HySpex VNIR and the eight bands from Worldview-2 served as input for Linear Discriminant Analysis. The overall accuracies achieved from HySpex VNIR are 94.4 % for forest type and 88.3 % for tree species discrimination. Worldview-2 achieved an overall accuracy of 87.8 % for forest type and 86.7 % for tree species discrimination. The successful spectral based classification for forest type and tree species were transferred onto the corresponding images for spatial description of their occurrence.

The promising results of this thesis confirms the advantage of airborne hyperspectral images for forest type and species detection. The transferability of this approach to spaceborne multispectral images with spectral information, relevant for vegetation purposes seems feasible.

1 Introduction and Objective

1.1 Introduction

Forest cover in Germany amounts to approximately 11.1 million hectares which is 31 % of the area of Germany (BMELV, 2002). Bavaria has 2.5 million hectares of forest, which covers approximately 36.3 % of the federal state. Spruce (*Picea abies*) is the main tree species in Germany with 28.2 % and also the main species in Bavaria accounting for 43.8 % of forest cover (BMELV, 2002). As a result of historical development in forest management and the first and second world wars, reparation payment changed forest tree species composition to fast growing species with clear felling system. This resulted in single aged and homogenous forest stands comprising dominantly European spruce. Consequently, spruce occurs predominantly on unsuited sites outside of the natural habitat.

Forest, and associated resources are highly affected by biotic and abiotic influences. Climate change and its consequences impact forest and tree species composition. The climate change trend is towards higher annual temperatures and constant amount of annual precipitation (LfU, 2012, P. 12). Winter hydrology shows a significant increase of up to 15 % in precipitation and summer hydrology in the opposite decrease of 10 % in total (LfU, 2012, P. 13). Through temperature increase it is predicted that the amount of snowfall will decrease and days of rainfall will increase. Also summer temperatures will rise and increase the possibility of extreme temperatures (LfU, 2012, P. 9). This development can change the seasonal conditions for native flora and fauna and increase the threat of longer dry periods.

Climate change has also a potential impact on natural and cultivated spruce forests. The natural spruce forest might decline by 90 % with high fragmentation of occurrence (Müller-Kroehling et al., 2009, P.). There is also evidence that spruce stands will be affected significantly beyond natural growing areas by climate change (Kölling and Ammer, 2006) and will further increase the vulnerability of spruce in these areas.

For example, warm and dry summers might benefit insect outbreaks in natural and managed tree compositions (Schelhaas et al., 2003, P. 1630). Insect outbreaks and other biotic calamities are mostly resulting from foregoing abiotic damages such as storms (Schelhaas et al., 2003, P. 1625). Increasing amount of growing stock, especially of trees on unsuited sites, might increase the problem of abiotic damage and subsequently biotic infests. Spruce is naturally vegetated in higher elevations on northern slopes with sufficient water supply and may be highly sensitive to an increasingly warm and dry climate.

In the last century forests had more of an economic focus, whereas nowadays ecologic and socioeconomic value have great importance. Thus there is a need for forest modification and sustainable forest management practices with close regard to natural forestry. This

is realised through a mixture of site adapted tree species with respect to multi-storey and multi-age forest structure.

1.2 Objective

Remote sensing has more become an important tool for forest applications, such as forest monitoring. With support of diverse remote sensing data several researchers have already detected different forest parameters, such as forest types, tree species and age classes (Clark et al., 2005; Clark and Roberts, 2012; Elatawneh et al., 2012; Reuter, 2010; Schlerf et al., 2003).
Hyperspectral remote sensing is becoming widely available and offers many advantages contrary to multispectral remote sensing. Specifically, the high number of contiguous spectral bands provide opportunities of delimiting forest parameters by their spectral features.
The mapping of tree species is crucial for scientific research and for management of forest resources. The knowledge about tree species distribution and their occurrence is essential for observing the impacts of climate change, which affects tree species differently. The impacts are biotic and abiotic damages of single trees and forest in general. Beside observation of impacts it is important to monitor forest modification towards sustainable close to natural forests.

The aim of this study is to:

1. Analyse whether optical remote sensing is suitable for tree species discrimination using airborne hyperspectral data from HySpex Visible Near Infrared (VNIR) and multispectral satellite data from Worldview-2
    - Use ground truth data to collect image based spectral libraries of different forest type and tree species and assessing the ability to discriminate between them
    - Transfer the spectral tree species classification to HySpex VNIR and Worldview-2 imagery
2. Develop an approach of tree species discrimination that is based on existing statistical analysis tools and test whether this approach is repeatable and objective, enabling it to be implemented as an operational processing chain
3. Conclude about the qualification of HySpex VNIR and Worldview-2 data for forest tree species discrimination. Subsequently the applicability of large-scale analysis can be stated

1.3 Hypothesis

The hypothesis of this thesis is that

1. the spectral discrimination of different tree species based on their spectral features is possible
2. hyperspectral remote sensing is appropriate for the species discrimination
3. the hyperspectral approach can be transferred to multispectral data for large-scale application

This study is intended to show that inter-specific variability of tree species exceeds the intra-specific variability that enables tree species separation.

2 Study Area

This chapter describes the forest and area of Traunstein. Section 2.1 describes the geography of the area, section 2.2 the climate and landscape formation and section 2.3 and 2.4 describe the history and characteristic of the forest of Traunstein.

2.1 Geographical area

Traunstein (47 ° 52'10.00" N and 12 ° 38'50.60" E) is the capital of the rural district of the same name in south eastern Bavaria, see figure 2.1.

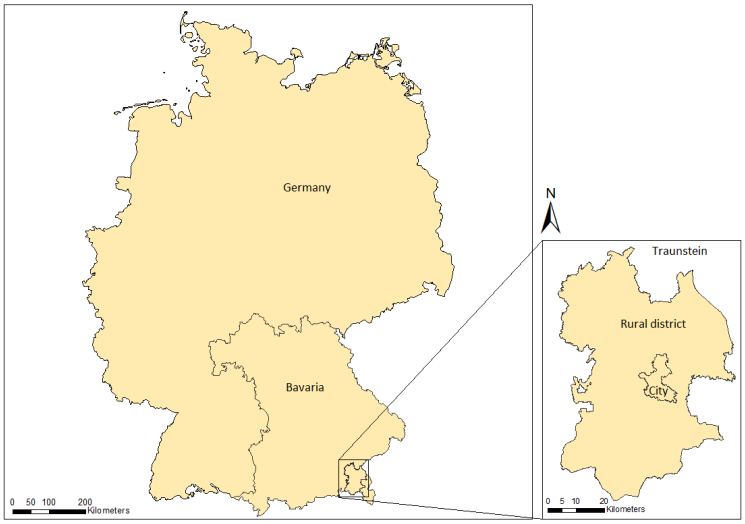

Figure 2.1: Location of rural district and city of Traunstein within Germany

At 1,533.95 km^2 it is the second biggest rural district in Bavaria. The city Traunstein is inhabited by 20,316 residents and is located 10 km east of the Chiemsee and 15 km north of the Chiemgau alps. The establishment reaches back to the late medieval time. Seven city forest areas belong to the city, with two studied in this project. All areas of the city forest are with a distance of 15 km around Traunstein, see figure 2.2. Their total size amounts to 600 ha with elevation ranging from 590 m to 675 m above sealevel. In 1949 forest management was assigned to the forestry faculty of the Technische Universität (TU) of Munich (Stadtverwaltung Traunstein *a*). The two main study areas are Heiligengeistwald and Bürgerwald and lie east of the city. Inventory plots and the hyperspectral and multispectral images used in this analysis cover these areas.

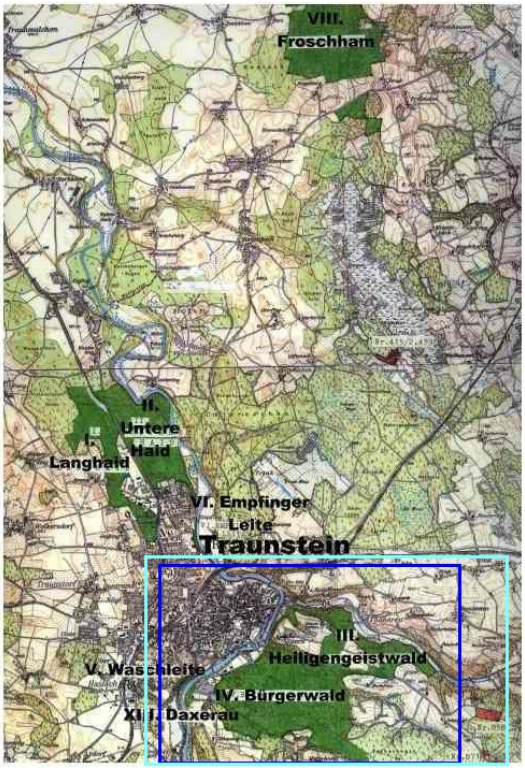

Figure 2.2: City forest areas of Traunstein with highlighted area of sensor acquisition, HySpex VNIR (light blue) and Worldview-2 (dark blue)
Stadtverwaltung Traunstein *a*, adapted

2.2 Climate and landscape

The climate of Traunstein is warm-temperate and characterised by the change of maritime west to continental east european climate. The mean annual precipitation of the study area amounts to 1,500 mm (Stadtverwaltung Traunstein *a*). The precipitation results from the closeness of the alps, which serve as water parting when warm moist air rises and cools down for passing the alps (Stadtverwaltung Traunstein *a*). Also the mean annual temperature of 7.5 ° C results from much variation during the year with summer temperatures above 20 ° C and winter temperatures below 0 ° C. The vegetation period in Traunstein ranges from April to October.

The existing landscape of the city and the study area was formed by several glacial periods of the alps during the Pleistocene. The last glacial period was Würm. At its maximum, the alps were covered with glaciers up to the elevation of 3000 m and the ice shield covered the area of Traunstein. The Chiemsee glacier and Salzach glacier formed the area around Traunstein. Their origin was the Central Alps between the Engadin and the Brenner Pass. During this period the glacier deposited fragments of granite, gneiss, mica schist and ser-

pentine to the Alpine foreland (Darga, 2009, P.9). Ablating of these glaciers happened in various stages which left behind the transported material and formed the present subsoil. The ablating also formed drainage channels, such as the Traun river running through Traunstein. The forest area of the study site is located on a moraine that formed a hilly surface with ridges and drumlins (LfU, 2010).

2.3 Forest history of Traunstein

Birch and pine were the first tree species that established after the last glacial period. Through succession more diversity of tree species families afforested Bavaria with the area almost completely covered with forest. Through anthropogenic influence during the neolithic, some forest was converted to agricultural land. During the medieval times the forest was intensively cleared for agricultural purposes and the remaining parts were used as pasture for livestock, charcoal burning, litter and fuel wood collection. By 1350 approximately one third of the original forest cover was left (StMELF, 2009). Due to this depletion of forest goods and permanent extraction of soil nutrition, the forest was damaged and scarcely stocked. After 1568 many sovereigns started to enforce forest laws to counter the shortage of forest products. As a result of many wars such as the Thrity Year's War and epidemics it took another 200 years before a careful forestry could be established (StMELF, 2009).
During the industrial revolution timber was needed for construction and as fuel, as such fast growing coniferous tree species, in particular spruce and pine, were planted in pure stands. With this development there occurred more often calamities of biotic (insects, funghi) and abiotic (windfall, snowbreak) origin on the depleted sites, which caused economic damage. After the First and Second World Wars timber was needed for reparations and rehabilitation of the countries economy.
With the economic expansion changed the forest management from completely wood production to a many purpose objective where economical, ecological and social aspects were also considered. Forest die-back also enforced the concept of forest modification towards sustainable mixed stands. New concepts within forestry departments scheduled forest modification for serving these different aspects and for improving the resistance of forest stands regarding biotic and abiotic impacts. The modification of the Stadtwald in Traunstein started around 60 years ago, which was 20 years before it has been constituted in Bavarian forest law.

2.4 Forest distribution and tree species composition

Bavaria is one of the most densely wooded federal states in Germany. The forest area conducts 36.3 % of the federal state area of 70,551 km^2. Main and mostly stand-forming tree species in Bavaria is Norway spruce (*Picea abies* [L.] Karst) with 43.8 % (Average of Germany is 28.2 %) (BMELV, 2002). Apart from this development, Traunstein city forest is

a stratified heterogeneous forest based on the species, age and height composition. Each age class shows a significant high amount of spruce, but with the trend of decline. This is an effect of close-to-nature forestry with site adapted tree species, which has been enforced by the forestry faculty of the Technische Universität Munich (see section 2.1). Since the forest management has been assigned to the faculty, new silvicultural research findings were applied.
Remote sensing of forest is highly influenced by the tree components and their physical state. The typical tree characteristics vary by season and affect the spectral information. The knowledge about these characteristics enhances the analysis of spectral tree features.

2.4.1 Important tree species for analysis

European beech (*Fagus silvatica* [L.])
The distribution of that tree species spans over the moderate and warm moderate climate in Europe. Due to its lack of drought-tolerance, areas with special drought periods are not vegetated by European beech. Its growing area is bordered in the south by northern Greece, Sicily, Corsica and northern Spain in the west by the Atlantic ocean. In the north it also vegetates southern England and southern Scandinavia and in the east the border reaches from the Baltic sea, Warsaw to the Black sea. These climatic borders exist because of the lack of tolerance to frost and spring frost as well as already mentioned missing drought resistance. (Felbermeier and Mosandl, 2006, P. 242)
Morphological characteristics of beech is the smooth bark even in older age. A short stem and sweeping crown in free standing and long almost branchless stem in established forest, where it can reach a maximum height of 45 meters.
The appearance of the leafs are different and vary by season and leave surface. In spring time the leafs are light green and silky fuzz. Later in the year around summer time the upper surface turns darker green and glossy and the lower surface is lighter in colour. Likewise, the aspect of leafs at the tree differ, depending on the preceding year solar irradiation on the tree. It develops two diverse types, the sun-leaf and shade-leaf. Sun-leafs develop a thicker cuticle and have a higher number of stomata, which helps them to regulate the heat and solar radiation. Shadow influenced leafs are usually larger and thinner than sun-leafs. They occur more often in the crown and the sum of shadow-leafs carry out approximately the same amount of photosynthesis as the total of sun-leafs. (Felbermeier and Mosandl, 2006, P. 245-246)
European beech starts propagating with age of 60 to 80 years in closed stands and are monoecious with unisexual flowers, which bloom in May (Stiftung Unternehmen Wald *a*). After germination the seeds start to develop to brown beech-nuts, which achieve maturity in october of the same year.
European beech establishes primarily a taproot and secondarily a heart root system through

branching of the primary root. This gives a strong halt to the tree. *Fagus silvatica* shows a low sensitivity to biotic infests compared to the following tree species. Though it is sensitive towards chemical pollution of air and soil. This results mostly increasing short shoots, which lead to a progressing crown transparency.

European silver fir (*Abies alba* [M.])

The natural aerial distribution of *Abies alba* is constrained in moist collinear to subalpine regions of central and southern Europe. The actual propagation in the west is bordered by the western Black Forest. In the north the region around Warsaw limits its area and in the east the European silver fir reaches over the whole Carpathians. The mountain ranges of the Balkans and the Apennines border it in the south. Throughout that whole region, it is delimited by lowlands or arid regions as stated above. It demands a vegetation period without frost of 3 months and wintertime of the same duration, but extreme temperatures, spring frost, frost drought and low precipitation limit the distribution of *Abies alba*. At least 800 mm of precipitation are needed but with sufficient soil water content this fir is able to compensate lower rates. (Bucher, 2004, P. 9)

In several areas of Bavaria this specimen has once covered 24 to 80 % of forest area, which has declined to 6 to 33 % (secondary literture by (Bucher, 2004, P. 3)) This change is due to the clear felling system, biotic infests, overexploitation and other anthropogenic influences.

The appearance of European silver fir is monopodia with main branches grouped by false whorls (several whorls that just appear as one), as well as convoluted smaller branches (Bucher, 2004, P. 4). Needles are oriented convoluted but vary from shadow needles with horizontal parted to light influenced needles with radial arrangement. They all remain at the tree for several years, but their size and shape vary dependent of the tree age and position in the trees crown. Shadow influenced needles have a dark green upper and light green lower surface with two white bands of stomata. Light influenced needles are shorter than shaded needles, as well as more stiff and slim and have stomata all over . (Bucher, 2004, P.5)

This specimen starts with propagation in age of 30 to 40 years in free stands and 60 to 70 years in closed stands (Stiftung Unternehmen Wald *b*). They are monoecious and flower in May to June. Male yellow flowers are located in the upper crown. Female staminate cones stand up on the upper side of strong one year old sprouts and after germination and maturity their size can reach up to 16 cm and turn to a green brown colour. At seed maturation they loose their seeds and the remaining parts can last for several years at the tree. (Bucher, 2004, P.5)

Abies alba develops a taproot system in younger age which turns into a heart root later. This species root grows deeper than many other species even in unsuited stands. This helps it to overcome drought periods. Other characteristics of it is the sensibility towards immissions, specially regarding SO_2.

Norway spruce (*Picea abies* [L.] Karst)

Distribution of Norway spruce has increased strongly in Europe through cultivation on unsuitable sites. The natural propagation is mainly in boreal forest in Scandinavia and baltic countries with an elevation boundary of 100-400 m. In central Europe the distribution is mainly in low mountain ranges, e.g. Carpathians, Tatra, Bavarian Forest and Harz. The elevation boundary is in Harz below 1000 m, in Bavarian Forest below 1450 m and in the Carpathians below 1770 m (Stiftung Unternehmen Wald *c*). In southern Europe spruce is represented in alpine regions and the natural cultivation boundary is below 2100 m. Occurrence of spruce is also naturally in lowlands with special site characteristics.

This specimen demands a cool-continental climate with sufficient precipitation. Sites with high amount of chalk, compressed soil and/or water accumulation can interfere the growth of it. Due to the reason stated in section 2.3, spruce has been planted frequently on unsuited sites, due to its fast growth characteristic. Also inappropriate forestry practices foster the incidence of calamities, such as storm breaks, snow breaks, insects or fungi.

The growth of spruce is monopodia where main branches are grouped as false whorls same as *Abies alba*. Also the branches are monopodia and have different variations of growth habit, depending on the origin. The needles of *Picea abies* are oriented convoluted and vary in colour, depending on the position in the crown, usually they last for 6 years on the tree. Sun influenced needles show a lighter grey green dull colour, which results from the high amount of wax on the needle surface. Shadow and sun influenced needles have both stomata lines all-around. (Schmidt, 2004, P. 271)

Norway spruce is monoecious with flowers in the light influenced crown and are April to May in blossom. Male flowers are red-yellow in colour and approximately 2,5 cm long. Female flowers are 2 to 4 cm long cones and magenta in colour before germination. After germination they grow up to 16 cm long and turn brown when maturity is reached in October. Spruce cones differ from fir cones by hanging down from branches. In the following late winter to spring they release their seeds and fall off. *Picea abies* starts with propagation in age of 10 to 40 years which can vary in closed stands. (Stiftung Unternehmen Wald *c*)

On suited sites with adequate aerated soil Norway spruce can establish a root system of up to 2 m depth. On unsuitable sites with e.g. water accumulation, spruce develops a shallow root, which gives few halt and results windthrow during storm. Other damage caused mainly by anthropogenic influence (see above) fosters the conversion of pure to mixed stands.

3 Basic Principle of Remote Sensing

The following sections describe the basic principles of remote sensing including the background of the physics in section 3.1. Section 3.2 describes the application of remote sensing through sensor systems.

3.1 Background of the physics

Remote sensing is the science of obtaining information from an object, through analysing data acquired by a sensor without having direct contact to the object. The basic principle of remote sensing is, that electromagnetic radiation is reflected by all objects except of the perfect black body. Electromagnetic radiation is theoretical an energy spreading in harmonic, sinusoidal fashion with light velocity c (Lillesand and Kiefer, 1994, P. 4). The wave period is referred as wavelength λ with a frequency ν measured in Hertz (Hz), see equation 3.1 (Albertz, 2009, P. 10).

$$\lambda = \frac{c}{\nu} \tag{3.1}$$

The electromagnetic radiation has various wavelengths with different characteristics, see figure 3.1. These wavelengths are separated into several groups by manner of emergence and their effect. The visible range is located between 400 and 700 nm and is the lowest relevant radiation for remote sensing. Shorter wavelengths are highly influenced by the atmosphere, see subsection 3.1.1. Wavelengths between 700 nm and 1,000,000 nm are referred as infrared with different divisions. Near infrared is located from 700 to 1,300 nm, the middle infrared has a range of 1,300 to 3,000 nm and subsequently the far infrared, also known as thermal infrared. Following wavelengths are microwaves and radio waves from 1 mm up to 1 m Hz. For remote sensing, important wavelengths vary from visible to middle infrared.

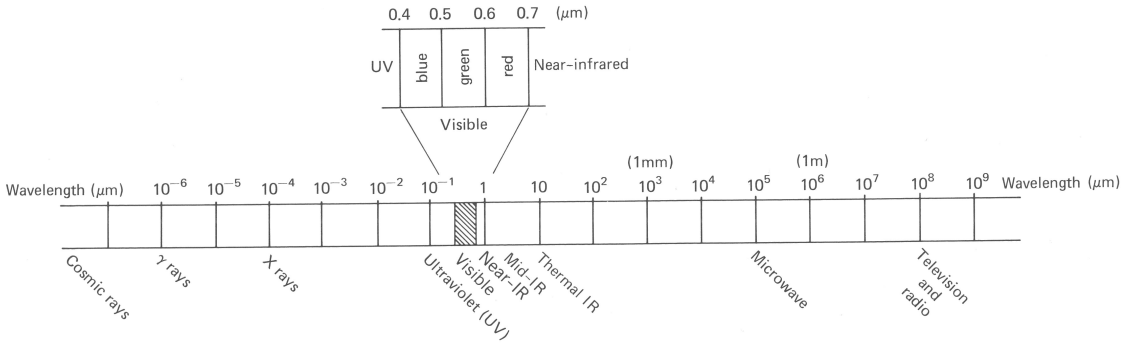

Figure 3.1: Wavelength ranges of electromagnetic radiation of light
(Lillesand and Kiefer, 1994, P. 5)

3.1.1 Atmospheric influences

The solar radiation has to pass through the atmosphere where some wavelengths are absorbed and others pass through. Only wavelengths with the ability to pass are considered for remote sensing. For optical remote sensing the atmosphere needs to be cloudless. The solar radiation is influenced by two main atmospheric impacts, absorption and scattering:
Absorption is the conversion of electromagnetic radiation into several forms of energy, such as warmth. Many constituents of the atmosphere absorb radiation and commonly are water vapour, carbon dioxide and ozone (Lillesand and Kiefer, 1994, P. 10). Water vapour absorbs most of the light compared to the other two components. It affects mainly mid and thermal infrared, see figure 3.2, in the lower atmosphere below 100 km and varies by time and place on earth (Campbell, 2006, P. 41). Ozone absorbs ultraviolet radiation and carbon dioxide absorbs mid and thermal infrared radiation, see figure 3.2 of atmospheric transmittance. Carbon dioxide occurs almost evenly spread in the atmosphere, whereas ozone varies by place on earth.

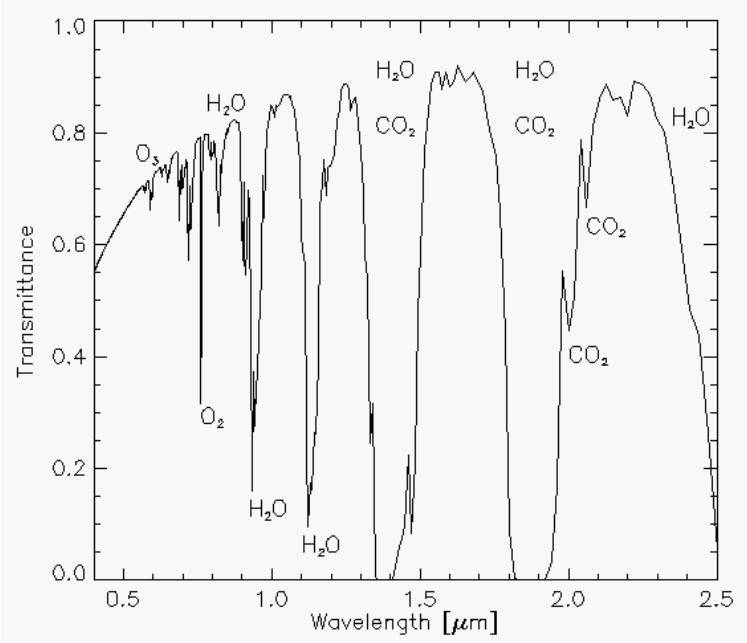

Figure 3.2: Atmospheric transmittance of electromagnetic radiation
(Richter and Schläpfer, 2012a, P. 14)

Scattering also plays an important role in atmospheric influences. It redirects the electromagnetic radiation through particles, called aerosol or molecules in the atmosphere. The scattering depends on the atmosphere depth, such as aerosol size, shape, material and density, and is wavelength dependent. The amount of aerosol is strongly dependent on location and time (Richter and Schläpfer, 2012a, P. 15). When aerosols are smaller than the wavelength of light Raleigh scattering occurs, even in an atmosphere with low aerosol content. Short wavelengths such as ultraviolet and blue are scattered more intense than longer wavelengths and cause a blue sky.
Two important parameters for describing the scattering of atmosphere are visibility and optical thickness. Visibility is described as maximum horizontal distance where a human eye can distinguish a dark body against light sky (Richter and Schläpfer, 2012a, P. 14).
Optical thickness is the equivalent for vertical space and considers the amount of contributors such as aerosol, water vapour, ozone, carbon dioxide and other molecules. The maximum visibility and minimum optical thickness is reached when the air does not contain any aerosol or molecules in lower and higher atmospheric layers. These atmospheric impacts are considered as noise and need to be corrected.
Two different types of radiation reach the ground surface, namely indirect and direct radiation. Indirect radiation is the sky radiation, the atmospheric scattered radiation. Whereas the residual radiation reaches direct the ground surface. Both are combined as global flux

(Albertz, 2009, P. 15). Global flux is highly variant and dependent on sun elevation and haze content of the atmosphere.

3.1.2 Surface reflectance

Different materials show characteristic reflectance, absorption and transmittance, which enables them to be distinguished from one another in remotely sensed data. Equation 3.2 explains the proportion of radiant power (ϕ) with the reflectance (ϕ_r), absorption (ϕ_a) and transmittance (ϕ_t), which percentage adds up to (ϕ = 1).

$$\begin{aligned} reflection\ degree\ \varrho &= \frac{\phi_r}{\phi} \\ absorption\ degree\ \alpha &= \frac{\phi_a}{\phi} \\ transmission\ degree\ \tau &= \frac{\phi_t}{\phi} \\ \varrho + \alpha + \tau &= 1 \end{aligned} \tag{3.2}$$

Also the physical state, coarseness, illumination and the geometry of object and sensor influence the appearance of objects (Albertz, 2009, P. 17).
Reflectance is the redirection of incident light and depends on the roughness of surfaces, see figure 3.3. Smooth objects redirect all or almost all of the radiation into one direction which is called specular reflectance. Objects of that type are e.g. mirrors, windows or calm water bodies. Rough surfaces reflect diffuse or isotropically which means that the radiation is scattered in all directions almost equally. Lambertain surfaces are considered ideal objects that reflect diffusely in every direction equally and the object appears homogenous bright (Albertz, 2009, P. 18).

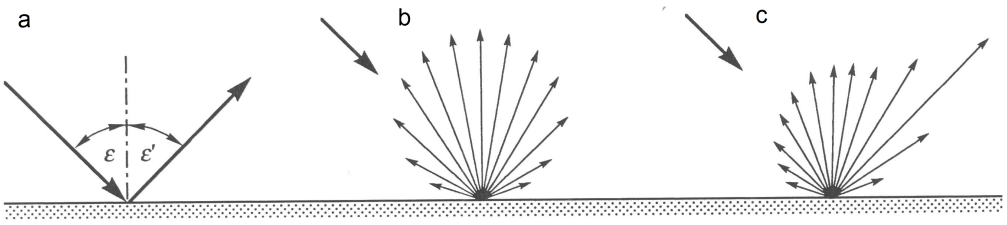

Figure 3.3: Reflectance depending on object surface; specular reflectance (a), Lambertain reflectance (b), diffuse reflectance (c)
(Albertz, 2009, P. 18)

For analysis of objects in optical remotely sensed data ϱ is plotted per wavelength. Usually the reflectance curve is influenced by several effects as mentioned above, but the shape is typical for each object component. The curves in figure 3.4 show reflectance of three specific objects in the range from visible to short wave infrared. Due to analysing the shape of a reflectance curve, it is possible to distinguish between different objects.

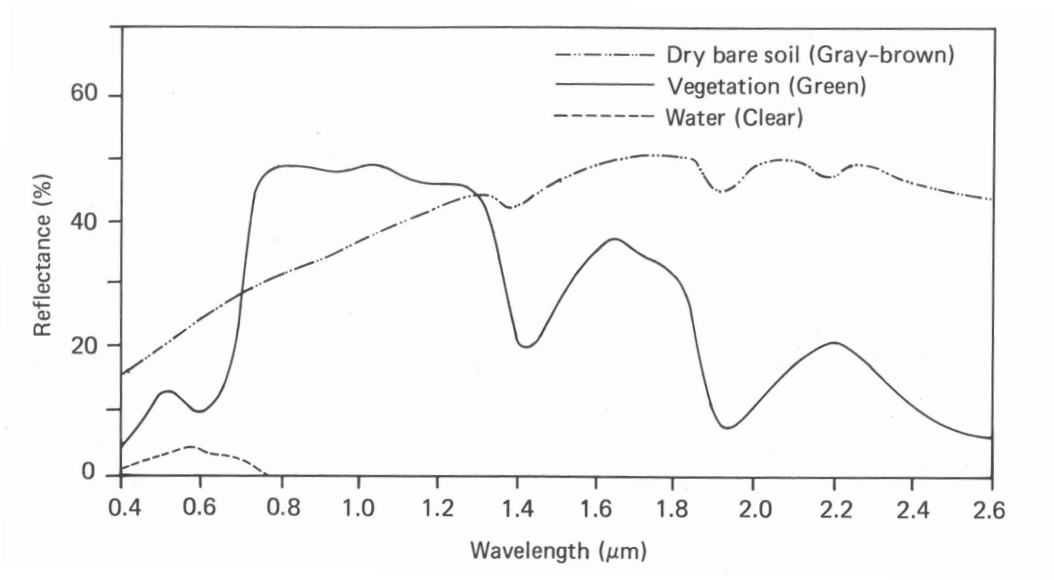

Figure 3.4: Reflectance curves of different objects with spectral characteristic of theses objects due to pigment content (vegetation), dryness (soil) and clearness and depth (water)

(Lillesand and Kiefer, 1994, P. 18)

3.2 Sensor systems

Sensors collect the radiation that is reflected by objects. Thereby it needs to be differentiated in two sensor types.

3.2.1 Passive sensors

Passive sensor types receive object reflectance that is illuminated from an additional light source, such as the sun. Optical sensors are usually passive sensors. These sensors collect different spectral ranges, that are called bands and can vary in their number and width per sensor.

Multispectral sensors

Multispectral sensors receive data in several spectral ranges simultaneously. Each band carries the spectral information of an object and all bands plotted, creates the reflectance

curve, which is called a spectrum. The spectrum is typical for that object and spectral range. The more bands a sensor is able to collect, the more spectral information of that object can be extracted. Last decades have improved the development of spatial and spectral resolution of sensors.
The first civilian satellite program was Landsat for gathering information about the earths natural resources. Landsat 1 collected spectra in 4 multispectral bands with spatial resolution of 56 x 79 m and was launched in 1972 (Baumann, 2009). Several more Landsat satellites and other satellite systems from other countries such as Satellite Pour l'Observation de la Terre (SPOT) from France were developed.
The new generation of satellite systems with high spatial resolution are e.g. RapidEye (6.5 m spatial and 5 band spectral resolution), Quickbird-2 (2.62 m spatial and 4 band spectral resolution) and Worldview-2 (1.86 m spatial and 8 band spectral resolution).

Hyperspectral sensors

Hyperspectral remote sensing, also referred as imaging spectroscopy, became more relevant for earth remote sensing in 1985 (Goetz and Gregg, 1985, P. 1147).
The advantage of imaging spectroscopy is the acquisition of object reflectance simultaneously in many narrow bands, that creates a continuous spectral curve. Hyperspectral data are usually depicted in a spectral cube with three dimensions of x and y as $pixel_i j$ and z as λ, see figure 3.5.

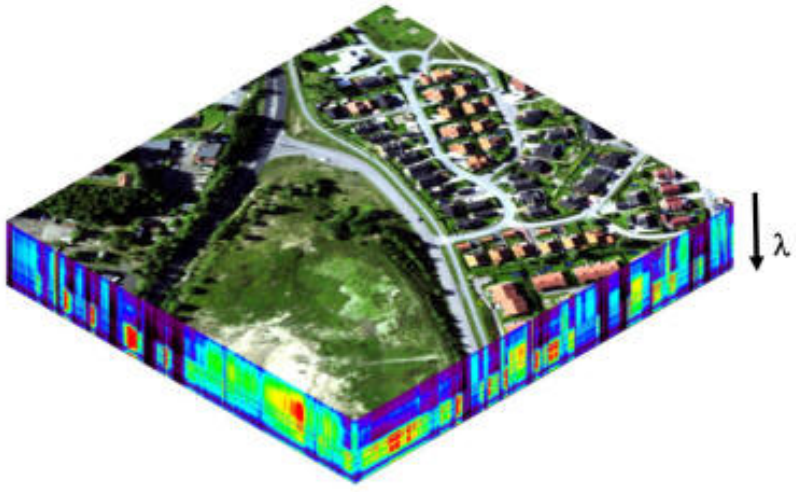

Figure 3.5: Data cube of hyperspectral imagery with x,y pixel location and z as wavelength in λ

(Norsk Electro Optikk AS, 2012, P. 1)

Hyperspectral sensors collect large amount of data in a short time, which leads to issues regarding data storage volume and data storage rate (Thenkabail et al., 2011, P. 11). Before the launch of Hyperion Earth Observing-1 (30 m spatial and 220 bands spectral resolution) as first spaceborne imaging spectrometer in 2000, imaging spectrometers were only airborne sensors. The spatial resolution vary by their flight height between 0.5 and 10 m. The spectral resolution are e.g. Hyperspectral Mapper (HyMap) (128 spectral bands), Airborne Visible/Infrared Imaging Spectrometer(AVIRIS) (224 spectral bands), HySpex (406 spectral bands). Prospective satellite sensors will follow, e.g. Environmental Mapping and Analysis Program (EnMAP) and Hyperspectral Infrared Imager (HyspIRI).

3.2.2 Active sensors

In contrary to passive sensors send active sensors radiation to the object and receive the scattered reflectance. Radio detection and ranging (Radar) remote sensing is active and uses microwave spectral range. Another active system is Light Detection And Ranging (LiDAR).

4 Literature Review

The following sections provide a review of scientific literature about forest appearance in remote sensing data and forest tree species classification methods in multispectral and hyperspectral data, respectively. Additionally several approaches of combining hyperspectral and LiDAR data is reviewed. Also the method of delineating forest from non-forest is an important issue towards tree species classification and is discussed in this chapter. Cho et al. (2012); Clark et al. (2005) and Clark and Roberts (2012) provide broad reviews about tree species classification using remote sensing data. Additionally Buddenbaum et al. (2005); Heinzel and Koch (2012) and Schlerf et al. (2003) have analysed the forest tree species classification in a temperate mixed forest similar to Traunstein forest.

4.1 Forest appearance in remotely sensed data

The appearance of vegetation in remote sensing data is indicated by low reflectance and high absorption in the visible wavelength with exception of the green range near 500 nm (Jones and Vaughan, 2010, P. 37). Between red and near infrared, also referred to as red edge, increases the reflectance. In near infrared between 700 and 1,000 nm the reflectance reaches the climax. Spectra between 1,000 nm and 2,500 nm are mainly characterised by water absorption features (Jones and Vaughan, 2010, P. 37).

The surface appearance of vegetation, as well as their leave structure influences the reflectance significantly. Variations in reflectance is indicated in de Boer (1993) and Jones and Vaughan (2010) by the position and distribution of leaves in the crown. This variation within a specimen is caused by different reflectance, transmission and absorption characteristics of several crown parts, such as leaves and woody branches. Whereas, Howard (1991) states that young leaves possess high amount of waxes, older ones may lose it during the vegetation period, which also changes the reflectance and causes intra-specific variability.

The inter-specific variability is caused by different leave structure and surface texture based on specific genetics (Jones and Vaughan, 2010, P. 37). This variability is the spectral difference among tree species. Many tree species show high amount of hair on the leaves or also different amount of waxes, as well as different thickness of cuticle, that prevents the leaves from water loss during high sun altitude.

However, the reflectance of vegetation in remotely sensed data is highly influenced by the phenology state and the senescence of the leaves. Senescence can occur uncorrelated to the phenological state and might be an indication for vitality.

The chemical composition of leaves indicate these stages by the pigment content. Two main pigment groups occur in leaves in different amount depending on the condition of leaves.

Chlorophyll a and b are essential pigments for photosynthesis (e.g. Blackburn (1998, P. 273), Blackburn (2007, P. 255), Curran et al. (1990, P. 33) and Gitelson et al. (2003, P. 272)). The absorption peaks are at chlorophyll a 430 nm and 660 nm and chlorophyll b at 450 nm and 660 nm (Howard, 1991, P. 32).
Further main pigments are the carotenoids, which also contribute to photosynthesis and cause yellow, orange and red colour of the vegetation. This group consists of carotine and xanthophyll (Jäger et al., 2003, P. 371). Howard (1991) explains that during senescence the chlorophyll content decreases and carotenoids increases, which causes the blue shift, as shown in figure 4.1.

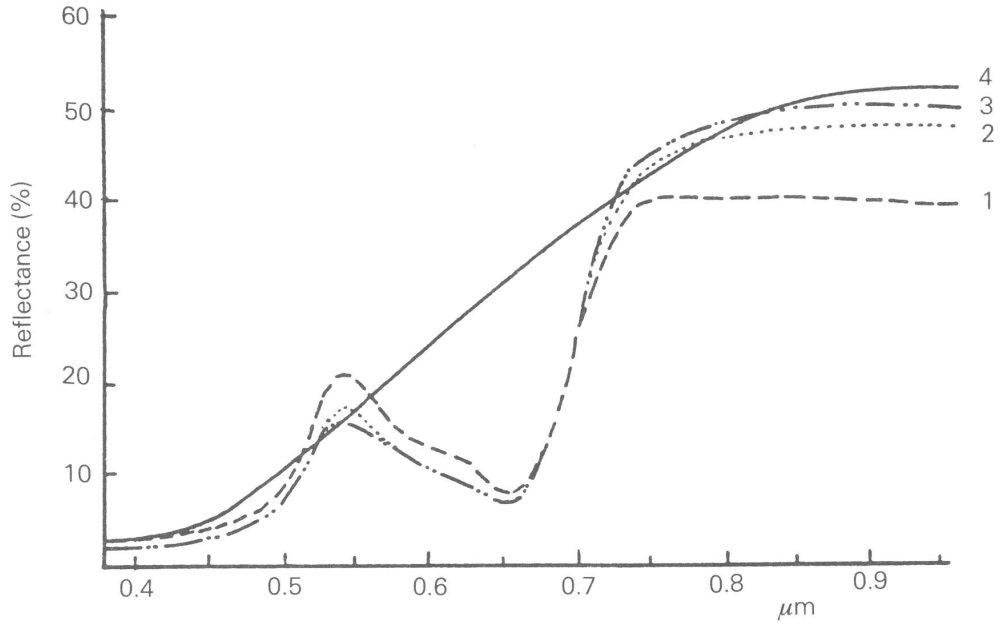

Figure 4.1: Spectral characteristics of deciduous leaves in different phenological stages; 1 shows spectral curve of young yellow green leave in spring time, 2 shows in comparison expanded green leave, 3 mature green leave, 4 dead leave with brown colour

(Howard, 1991, P.46)

The blue shift can be caused by natural senescence, but also biotic or abiotic impacts cause the leaves die back. The near infrared region is not affected by pigment changes but is highly influenced by changing water content (Howard, 1991, P. 32). The more water the leaves contain, the lower appears the reflectance in near infrared, see figure 4.2.

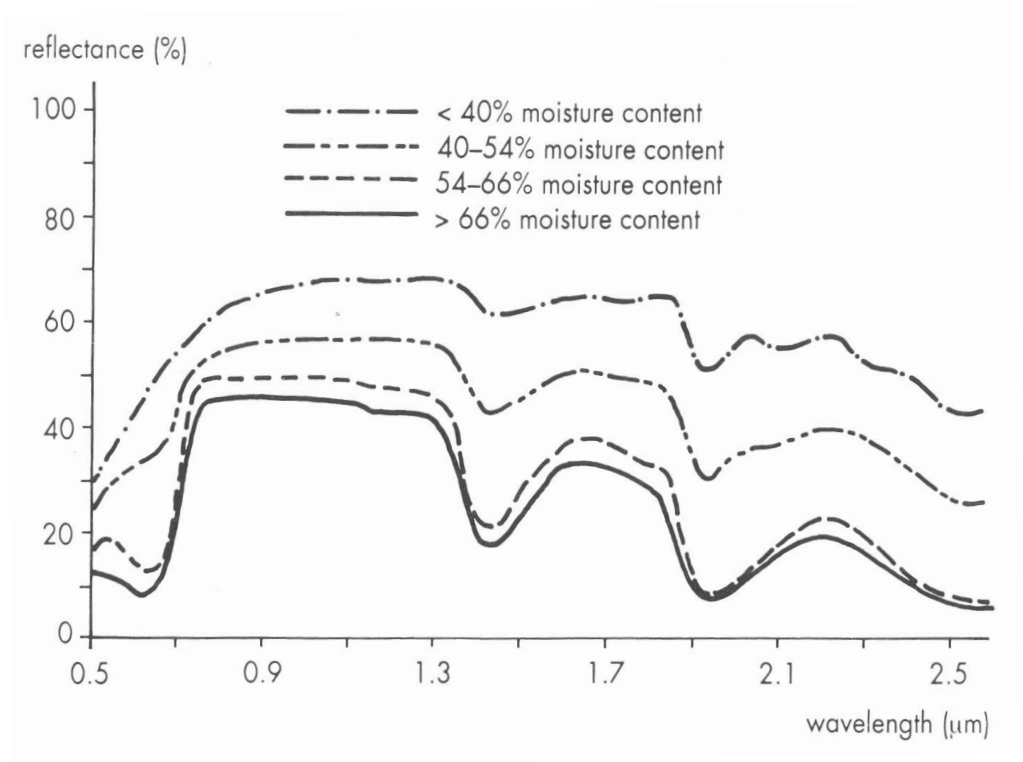

Figure 4.2: Spectral characteristics of vegetation with different moisture content (de Boer, 1993, P.46)

Forest canopy consists of many different object types such as leaves, branches, bark, buds, flowers, fruits and influence the relative amount of shading (Clark et al., 2005, P. 393). The anisotropic multiple scattering of light radiation is determined through the geometry of sun, object and sensor, as well as illumination differences of similar objects and cause the Bidirectional Reflectance Distribution Function effects (BRDF) (among others Clark et al. (2005, P. 393) and Schaepman-Strub et al. (2006, P. 30)). These objects receive direct solar radiation and radiation scattered or transmitted through other objects (Goel, 1988, P. 16). Also the scattered radiation can be scattered once, several times by different canopy components or additionally by soil. This reflectance is highly influenced by the leaves physical and chemical characteristics (Jacquemoud and Baret, 1990, P. 75). They are affected by the different pigments, water and nutrient content (Jacquemoud and Baret, 1990, P. 75). According to Blackburn (1998) and Carter and Knapp (2001) spectral characteristics of reflectance can help to derive the plants physiology, phenology and stress of a plant. Clark et al. (2005) also hypothesises that there exist differences in crown structure at species level, that affect the volume scattering of different tree species.

4.2 Current research approach in forest classification

The following subsections address the research approach in forest and tree species classification using passive, e.g. multispectral and hyperspectral sensors and active, e.g. LiDAR, remote sensing systems.
Different studies analysed if and how forest stands and tree species can be detected through remote sensing (e.g. Bunting and Lucas (2006); Cho et al. (2012); Clark and Roberts (2012); Elatawneh et al. (2012) and Heinzel and Koch (2012)).
The difficulty is not to investigate this on forests with low vertical and horizontal stand diversity, but on a temperate forest with stand diversity affected by sustainable close to nature forestry, as stated by Heinzel and Koch (2012, P. 102).
Regardless of the forest composition the successful discrimination of tree species depends strongly of the relation between intra- and inter-specific variation. It demands a significantly smaller spectral variation within and among crowns of one specimen than the variation among different species (Zhang et al., 2006, P. 130).

4.2.1 Generating a forest mask and crown delineation using remotely sensed data

Remote sensing of forest tree species becomes important for supporting forest management and forest research. In general the first step of forest analysis is the derivation of a forest mask, delineating forest from non-forest and thus improving the classification results. Several different approaches are known from literature.
Heinzel and Koch (2012) calculated a mask derived by the height metrics of LiDAR data. They used a threshold of 2 m for extracting vegetation from non-vegetation where no urban areas occurred, otherwise this approach would not be sufficient. They also delineated single tree crowns. The tree delineation was derived from a normalised Digital Surface Model (nDSM) calculated on basis of LiDAR data. However, inadequate smoothing of the nDSM can result in inaccurate segmentation.
Also Wang et al. (2008) used the approach of deriving a forest mask through LiDAR data using a *K x K* Kernel. This approach defines only pixel with height greater than 3 m as forest. It also tests, if within the kernel the forest cover amounts to a minimum of 20 %, as it is defined in the Swiss National Forest Inventory. This can improve the forest masking through elimination of urban areas. Depending on the resolution of LiDAR data and their height accuracies, they deliver adequate results. Although the high costs for height data acquisition need also to be considered.
In contrary to segmentation or height delineation Buddenbaum et al. (2005) and Schlerf et al. (2003) used a spectral approach with unsupervised classification technique using isodata algorithm on hyperspectral data. This was useful in spectral separation of coniferous from deciduous forest. Since the spectral delineation was successful it might also be feasible

to separate at least different forest types by spectral characteristics.
Whereas Bunting and Lucas (2006) derived a forest mask by applying a Forest Discrimination Index (FDI) using three bands in blue, red and near infrared region of hyperspectral Compact Airborne Spectrographic Imager (CASI). This approach was surprisingly successful as remote sensing data were acquired during dryer vegetation time in Australia when the contrast between vegetation and non-vegetation was highest.
A combination of spectral features with height metrics might also be a successful approach for forest classification. Using spectral indices could split height metrics, which lead to the separation of urban areas from trees. Many studies use methods to delineate tree crowns successfully, such as object oriented methods or texture analysis. However most of their data have a pixel resolution less than 1m (Bunting and Lucas (2006); Chubey et al. (2006); Heinzel and Koch (2012) and Leckie et al. (2003)). Additionally, in study areas with high tree densities in a heterogeneous forest, crown and single tree delineation can become difficult (Bunting and Lucas, 2006, P. 246). This approach was not followed in this study as spatial resolution of 2 m and below tends to be insufficient.

4.2.2 Application of multispectral sensors for forest classification

Multispectral sensors and their data are mostly applied for environmental studies.
Different research was done on the usability of multispectral sensors for forest structure and forest species detection, respectively. Chubey et al. (2006) analysed Ikonos-2 data for forest structural classification with spatial resolution of 1 m panchromatic and 4 m multispectral, with 4 multispectral bands ranging from 445 - 853 nm. The study site was mature forest in Alberta, Canada with coniferous and deciduous forest, both occurring in mixed and pure stands with pine, spruce and aspen. Before classification the image was segmented. Also texture analysis using the panchromatic band was conducted. Two different decision tree classification approaches were applied on 87 image object metrics derived from the input data. This yielded a tree species and a land-cover classification. The land-cover classification accomplished an overall accuracy of 93 %. Pine, spruce and aspen dominated forest was delineated with 81 % to 93 % producers and 83 % to 100 % users accuracy. Chubey et al. (2006) suggested to undertake further research in forest classification using object segmentation for reducing cost and enhancing operational forest inventory. The classification accuracies are not surprising, however since pure stands were observed beside mixed stands.
Also Ozdemir and Karnieli (2011) investigated the possibility of multispectral imagery, namely Worldview-2 data, for classification of forest structure. Study area was an almost pure Aleppo pine stand low in age and height variability. Different structure indices were calculated and correlated to image derived texture features such as contrast, orderliness and descriptive statistics (Ozdemir and Karnieli, 2011). Results of this analysis was the correla-

tion of structural to textural features with a range of 0.23 to 0.67 R^2 whereas three of eight correlations are above 0.50. The conclusion was that the additional bands of Worldview-2 sensor compared to the before mentioned Ikonos-2, namely the yellow, red-edge and additional near infrared range, are appropriate for forest structure prediction and should be taken into consideration for further research.
Cho et al. (2012) also concluded the usefulness of additional Worldview-2 bands in pigment absorption regions and other chemical parameters for species mapping. Even if the spectral range only covers the visible near infrared region is it still appropriate. Additionally they stated the possibility of using Worldview-3 for further studies with integrated short wave infrared red spectral region which will be launched in 2014.
Beside Worldview-2 also RapidEye offers a red-edge channel, that is appropriate for vegetation analyses. Concluding both Worldview-2 and RapidEye are the most appropriate satellite systems with regard to band number and the spectral range they cover. With consideration of the additional near infrared band and the higher spatial resolution Worldview-2 is considered as most appropriate multispectral sensor for forest application.

4.2.3 Hyperspectral approach of forest classification

Hyperspectral remote sensing data are often used for differentiating between land cover types or vegetation parameter estimation and show higher accuracies than multispectral images (Lee et al. (2004, P. 508) and Ustin and Xiao (2001, P. 1794)).
Reuter (2010) analysed the possibility of tree species classification in a temperate mixed forest stand. The sensor was AISA HAWK hyperspectral airborne sensor with a spatial resolution of 1.5 m and 235 spectral bands in the short wave infrared spectral region. The overall accuracy of the analysis was 78 %. Additional to the hyperspectral data also colour infrared (CIR), red-green-blue (RGB) images and bands of SPOT were used. All spectral data were applied for calculating band ratios. Significant band ratios for tree species differentiation were used together with a digital canopy model to classify crowns. The overall goal of this study was to evaluate different spectral information and to delimit spectral bands that are appropriate for tree species classification. One of the main issues in this study was the lack of red edge spectral information, but also the varying spatial resolution of the different datasets, which could not lead to reliable results.
Another approach of tree species classification in a temperate mixed forest stand using imaging spectroscopy was analysed by Schlerf et al. (2003). The hyperspectral HyMap data with 128 contiguous spectral bands covering the spectral range of 400 to 2,500 nm and 5 m spatial resolution. The spatial resolution was resampled to 30 m additionally to 5 m resolution. The original and resampled datasets were compared to synthetic Landsat Thematic Mapper (TM) data also with 5 and 30 m spatial resolution derived of the HyMap data. The overall accuracy showed that both datasets had lower rates for 5 m than for 30 m resolution

data. Furthermore it results that the hyperspectral data had higher accuracies ranging from 81.4 to 95 % than Landsat TM data with 55.9 to 69.5 %. Schlerf et al. (2003) concluded that a high spectral resolution is of great importance, but spatial resolution does not yield better classification results.

Similar study by Buddenbaum et al. (2005) used the same data set. The classification input parameters were the data set itself, co-occurrence matrix based texture measures and geostatistical methods such as pseudo-cross madograms. Every parameter separately and all combined were classified. The individual parameters obtained overall accuracies between 58.6 % and 64.8 %, whereas the combined classification achieved 71.1 %. Buddenbaum et al. (2005) pointed out the high influence of geostatistical channels to classification results and recommended an object based approach for further research.

Apart from temperate forst the analysis of Clark and Roberts (2012) focused on tropical rain forests using Hyperspectral Digital Imagery Collection Experiment (HYDICE) data with a spatial resolution of 1.6 m and spectral range of 400 to 2,500 nm. Laboratory spectra of different tissue material, such as leaves and bark were collected for comparison. Different metrics were derived from these data and separated with random forest classifier. This classifier has the ability to sort all features, in this case the metrics by their importance for classification. The analysis showed that metrics in near infrared and short wave infrared have most importance for classification accuracy, which was 86.8 % for leaves and individual tree crowns 71.5 %. Also pixel spectra with an overall accuracy of 70.6 % and 87.4 % was observed.

Similar results are achieved in a former approach with same hyperspectral sensor. Prior classification a band selection technique was used to reduce the data dimensionality. Subsequent classification methods were applied, Spectral Angle Mapper (SAM), Linear Discriminant Analysis (LDA) and Maximum Likelihood (ML). LDA achieved highest classification rates with 86 % overall accuracy (Clark et al., 2005, P. 389) with 1.6 m spatial resolution of hyperspectral sensor compared to considerably less accuracy of simulated Ikonos and Landsat TM.

Clark et al. (2005) and Clark and Roberts (2012) emphasis the usage of hyperspectral imagery for tropical tree species classification with significance of the spectral range in near infrared and short wave infrared region.

Taking the adequate accuracy of tropical tree species classification into account, which is not of less difficulty as temperate mixed forest, the LDA classification is best qualified as method combined with data reduction methods.

4.2.4 Combined systems for forest and tree species classification

Since tree species discrimination, using individual multispectral and hyperspectral data is possible, combined methods might lead to higher accuracies and more precise statements. Heinzel and Koch (2012) investigated different data sources to classify four tree species in a temperate, heterogeneous mixed forest stand. Five feature groups were used for this analysis, namely texture, full-waveform LiDAR data with hight metrics, CIR and hyperspectral images. Texture was first derived by LiDAR data and secondly by CIR image data. The five features were used individually, as well as all together for final classification. Best results were achieved with all features combined with an overall accuracy of 88.03 %. Hyperspectral HyMap images of 4 m ground resolution had better overall accuracy of 64.67 % than CIR images (overall accuracy of 50.71 %) even if the CIR had a spatial resolution of 0.25 m. This proves the importance of spectral over spatial resolution according to Schlerf et al. (2003). Heinzel and Koch (2012) recommended to test tree species discrimination using higher spatial resoluted hyperspectral data.
Also Cho et al. (2012) investigated the results of combining LiDAR data for tree height together with optical data in african savannah. The optical data were acquired from Carnegie Airborne Observatory (CAO) hyperspectral, as well as simulated multispectral Worldview-2 and Quickbird data. Spatial resolution of CAO data was 1.12 m and the spectral region spans from 385 nm to 1054 nm with 72 bands. Simulated Worldview-2 image alone and combined with LiDAR data resulted the best overall accuracies with 76.8 % and 79.3 %, respectively. Even simulated Quickbird data, without important spectral ranges in the red edge, showed with 65.1 % similar accuracy as CAO data with 65 %. Band selection of hyperspectral data might improve the classification accuracy due to elimination of redundant band information (Cho et al., 2012, P. 222). Also parametric classification methods that are appropriate for multispectral and hyperspectral selected bands can be used e.g. ML or LDA (Cho et al., 2012, P. 222). Another classification approach of high dimensional data is the non-parametric random forest. This method reaches robust accuracies, comparable to parametric classifiers (Breiman (2001, P. 29) and Cutler et al. (2007, P. 2789)), which is applied in many different studies (e.g. Hapfelmeier and Ulm (2013), Latifi et al. (2012) and Rodriguez-Galiano et al. (2011)).
Elatawneh et al. (2012) investigated the detection of different forest stand types using hyperspectral HyMap as well as multispectral and multi-temporal RapidEye data, both with 5 m spatial resolution. This investigation concentrated on three problems. First deriving the forest structure on basis of the image and second classifying stand types with comparison of hyperspectral to multispectral imagery. The third question was whether object heights derived from DSM can enhance the classification accuracy. The conclusion of this study was, using the hyperspectral data set had no benefit compared to the RapidEye data. But com-

bined with height information it is possible to enhance the classification of forest stand types. Also Dalponte et al. (2008); Feret and Asner (2012) and Jones et al. (2010) achieved higher accuracies for tree species classification combining hyperspectral and LiDAR data.
In the end multispectral images combined with additional features such as LiDAR data or derived texture tend to be efficient enough for tree species detection at least in african savannah. Although in temperate forest stands hyperspectral data combined with additional height metrics showed the best classification results.

5 Data Set and Preprocessing

Data sets from different sensors were selected for the analysis of forest tree species classification.Technical details of these sensors are explained in section 5.1. Section 5.2 characterises the remote sensing data. Forest inventory data that were used as in-situ reference are described in section 5.3. The last section illustrates the preprocessing steps that were necessary for preparing the remote sensing data prior analysis.

5.1 Technical description

Different sensor types, multispectral, hyperspectral and lidar data, were used in this study and are described in more detail in the following subsections.

5.1.1 Multispectral data

Multispectral sensor systems were first developed as opto-mechanical scanners that used discrete detectors. They segment the acquired radiation in singular spectral ranges. The newer generation use line arrays that acquire spectral data simultaneously (Albertz, 2009, P. 47). Since multispectral sensors obtain spectral data over a few broad wavelength ranges, the spectrum of vegetation will differ from hyperspectral continuous spectra, see figure 5.1.

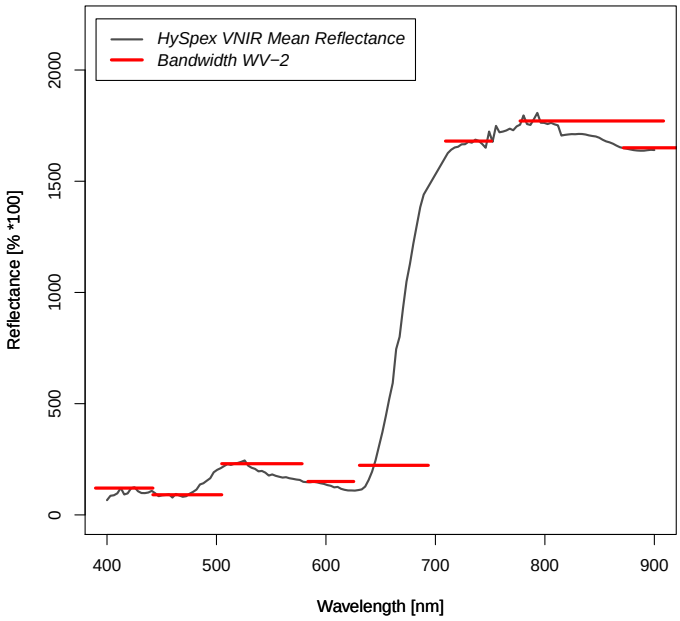

Figure 5.1: Mean spectra of coniferous forest species obtained by hyperspectral Hyspex VNIR sensor; the bandwidths of Worldview-2 are plotted in red

5.1.2 Hyperspectral data

Imaging spectrometers show two types of imaging spectrometer detector systems, that are commonly used. Line arrays that acquire spectral data simultaneously in one line, where each wavelength is obtained separately by a detector. This system is referred as push-broom sensor. Whereas scanline imaging spectrometers with high spatial resolution have additional area arrays. They provide a detector for each cross-track pixel, additional to a detector obtaining each wavelength separately of that pixel (Goetz, 1992, P. 21). The advantage of push-broom sensors are the similar geometry within a line but scanline sensors show a possible higher spatial resolution. However this higher spatial resolution shows several trade-offs, such as Field Of View (FOV), calibration and signal-to-noise-ratio (Goetz, 1992, P. 21). Characteristic for imaging spectrometers is the acquisition of a continuous spectrum across a specific wavelength range (see figure 5.1).

5.1.3 Airborne active data

LiDAR is an active systems and is usually operated as airborne laser scanning (ALS). Each compressed light beam is a coherent laser pulse for ensuring the collimation, providing spatial filtering and preventing the transmission of other radiation such as broadband signals (Measures, 1992, P. 213). The outcome is not an image but height measurements as a point

cloud from several pulses. Time travel measurement enables the calculation of object or ground height on condition, that the flight height above sea level is known, with speed of light (c), time of travel (t) and the resulting distance (s).

$$s = \frac{c * t}{2} \tag{5.1}$$

Usually LiDAR data are obtained for deriving a Digital Surface Model (DSM) and Digital Elevation Model (DEM), since stereoscopic image analysis is not useful in dense vegetated areas. A DEM is a 3 dimensional representation of the terrain surface. Furthermore LiDAR is often used as additional input data set for research, such as forest canopy delineation or forest biomass estimation.

5.2 Data description

The hyperspectral airborne data and multispectral satellite data were both acquired on cloudfree days, see table 5.1. Their acquisition date varies only by one week in June 2012. Spatial resolution of both sensors is 2 m.

Table 5.1: HySpex VNIR and Worldview-2 sensor specifications of acquired data

specifications	HySpex VNIR-1600 sensor	Worldview-2 sensor
Acquisition date	18th June 2012	12th June 2012
Spectral range	0.4 - 1.0 µm	0.4 - 1.04 µm
Spectral resolution	160 bands	1 panchromatic and 8 multispectral bands
Spatial resolution	2 m	2 m
Swath width	3.2 km	17.7 km

5.2.1 Hyperspectral airborne data

Since the beginning of 2012 the DLR holds its own hyperspectral sensor the HySpex VNIR-1600 and also HySpex SWIR-320 developed by *Norsk Electro Optikk*. Table 5.1 shows the main specifications of the data set used for this analysis. Only HySpex VNIR with 160 contiguous bands was applied due to comparable spectral range of the Worldview-2 sensor, see table 5.2.
The HySpex VNIR data were acquired with a spatial resolution at ground scale of 2 m. This sensor was equipped with a FOV expander of 34 $^\circ$, which is the opening angle of the lens that determines the swath width and the ground coverage consequently. Through this FOV expander the opening angle is widened but decreases the spatial resolution.

Table 5.2: HySpex VNIR band numbers and Wavelengths [nm] with Full Width of Half Maximum (FWHM) of 3.5 nm for each band

Band	Wavelength	Band	Wavelength	Band	Wavelength	Band	Wavelength	Band	Wavelength	Band	Wavelength
1	415.65	28	513.48	55	611.31	82	709.14	109	806.97	136	904.80
2	419.27	29	517.10	56	614.93	83	712.76	110	810.59	137	908.42
3	422.90	30	520.73	57	618.56	84	716.39	111	814.21	138	912.04
4	426.52	31	524.35	58	622.18	85	720.01	112	817.84	139	915.67
5	430.14	32	527.97	59	625.80	86	723.63	113	821.46	140	919.29
6	433.77	33	531.60	60	629.43	87	727.26	114	825.08	141	922.91
7	437.39	34	535.22	61	633.05	88	730.88	115	828.71	142	926.54
8	441.01	35	538.84	62	636.67	89	734.5	116	832.33	143	930.16
9	444.64	36	542.47	63	640.30	90	738.13	117	835.96	144	933.79
10	448.26	37	546.09	64	643.92	91	741.75	118	839.58	145	937.41
11	451.88	38	549.71	65	647.54	92	745.37	119	843.20	146	941.03
12	455.51	39	553.34	66	651.17	93	749.00	120	846.82	147	944.65
13	459.13	40	556.96	67	654.79	94	752.62	121	850.45	148	948.28
14	462.75	41	560.58	68	658.41	95	756.24	122	854.07	149	951.90
15	466.38	42	564.21	69	662.04	96	759.87	123	857.69	150	955.52
16	470.00	43	567.83	70	665.66	97	763.49	124	861.32	151	959.15
17	473.62	44	571.45	71	669.28	98	767.11	125	864.94	152	962.77
18	477.25	45	575.08	72	672.91	99	770.74	126	868.57	153	966.40
19	480.87	46	578.70	73	676.53	100	774.36	127	872.19	154	970.02
20	484.49	47	582.32	74	680.15	101	777.98	128	875.81	155	973.64
21	488.12	48	585.95	75	683.78	102	781.61	129	879.43	156	977.26
22	491.74	49	589.57	76	687.40	103	785.23	130	883.06	157	980.89
23	495.36	50	593.19	77	691.02	104	788.85	131	886.68	158	984.51
24	498.99	51	596.82	78	694.65	105	792.47	132	890.30	159	988.13
25	502.61	52	600.44	79	698.27	106	796.10	133	893.93	160	991.76
26	506.23	53	604.06	80	701.89	107	799.72	134	897.55		
27	509.86	54	607.69	81	705.52	108	803.35	135	901.18		

5.2.2 Multispectral satellite data

Since the importance of spectral information in red-edge range for vegetation purposes, a satellite with red-edge information and high spatial resolution was necessary. Worldview-2 is a satellite of the newer generation and provides these features. This satellite was launched in October 2009 and is planned to operate for 10 to 12 years (Digital Globe). Table 5.3 states the satellite specifications.

Table 5.3: Worldview-2 sensor specifications (Digital Globe)

specifications	Worldview-2
Orbit	Sun-synchronous, altitude 770 km
Sensor bands	1 Panchromatic
	8 multispectral
Spatial resolution	Panchromatic: 0.46 m GSD at nadir
	0.52 m GSD at 20° off-nadir
	Multispectral: 1.85 m GSD at nadir
	2.07 m GSD at 20° off-nadir
Swath width	16.4 km at nadir
Repition rate	approx. 1.1 days at 1 m GSD
	approx. 3.7 days at 20° off-nadir

The spectral bands of Worldview-2 are specified with their FWHM in table 5.4. Due to close acquisition date to the HySpex VNIR campaign, same spatial resolution of both datasets and similar spectral range, Worldview-2 is an appropriate multispectral comparison for analysis of tree species discrimination.

Table 5.4: Worldview-2 band number with Wavelength [nm] and FWHM [nm] (Digital Globe)

Band	Description	Wavelength	FWHM
1	Coastal	400 - 450	51.50
2	Blue	450 - 510	60.50
3	Green	510 - 580	69.50
4	Yellow	585 - 625	38.50
5	Red	630 - 690	59.00
6	Red Edge	705 - 745	39.50
7	Near-IR1	770 - 895	117.50
8	Near-IR2	860 - 1040	92.00

Worldview-2 data are kindly provided by European Space Imaging[1].

5.2.3 LiDAR data

Additional active remote sensing data are used in form of a DEM and DSM, both derived from airborne LiDAR data. The Bavarian Mensuration Administration collected these height data in spring 2010 with last pulse point density of 5-6 points per square meter (Straub and Seitz, 2012, P. 76), a spatial resolution of 1 m and a height accuracy of approximately 20 cm LVG. The LiDAR data were delivered as smoothed DEM and DSM images.

5.3 In-situ data

Reference data were conducted for the analysis of tree species from Traunstein forest. The inventory was carried out by the forestry faculty of the Technische Universität (TU) Munich and was kindly provided for analysis by the Landesanstalt für Wald und Forstwirtschaft (LWF). On basis of these data the distribution of tree species and their location is well known. Last inventory was conducted in 2008 with 228 systematic distributed plots of 25 m diameter. Data about plot position, species composition in percentage and age was surveyed, see table 5.5 for species composition derived of these inventory data. The in-situ data are used for selecting appropriate pixel for spectra collection as described in section 6.4.

Table 5.5: Tree species composition in Traunstein forest derived from forest inventory data

Species	Percentage
Beech	23.62 %
Fir	14.14 %
Spruce	43.12 %
other Deciduous	15.97 %
other Coniferous	3.15 %

5.4 Preprocessing of remote sensing data

The collected datasets of the study area were delivered as raw data (HySpex VNIR) and as at-sensor radiance data (Worldview-2), respectively. Preprocessing is necessary to remove atmospheric and geometric distortions from the imagery, before the analysis of the forest tree classification can take place. The individual steps are stated and explained for each sensor.

[1] http://www.euspaceimaging.com/

Processing system by German Remote Sensing Data Center

The German Remote Sensing Data Centre (DFD) of the German Aerospace Center (DLR) holds a processing chain which generates standardised data products automatically that can be reproduced easily at any time (Habermeyer et al., 2005, P.67). After each step the quality control states, if the standards are achieved. The processing steps comprise system correction (Level-1) as well as geographical correction (Level-2geom) and atmospheric correction (Level-2atm). Following each step is explained and adjustments for the different sensors are stated (see Habermeyer et al. (2005) for closer explanations).

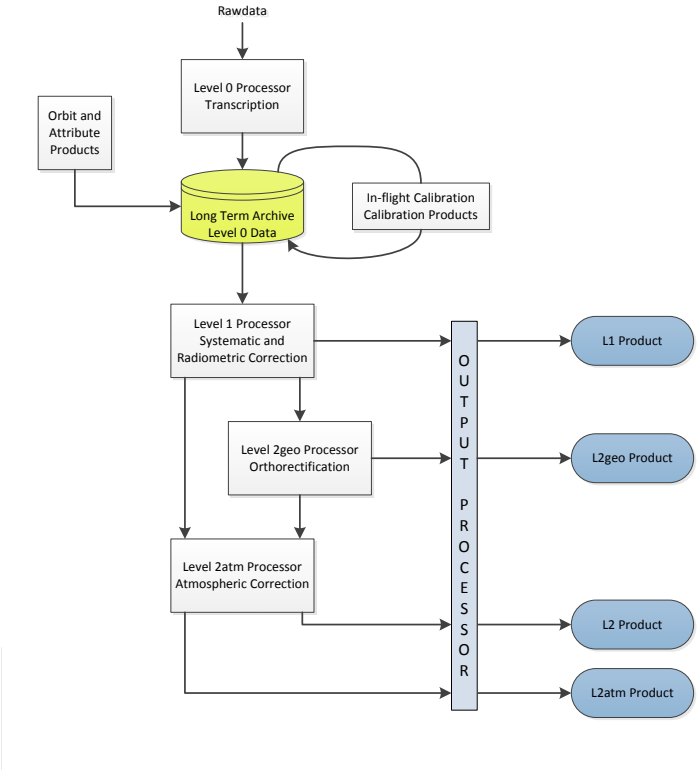

Figure 5.2: Processing chain of sensor data from data acquisition to at-sensor radiance with geographical rectification

(Bachmann et al., 2010, adapted)

1. Level-0 transcription processor collects, extracts and interprets raw data acquired from the sensor and generates image tiles and metadata
2. Level-1 systematic / radiometric correction processor transforms raw data to at-sensor radiance with calibration coefficients obtained through laboratory calibration
3. Level-2geom geometric correction processor performs geographical correction on basis of different models with or without ground control points

4. Level-2atm atmospheric correction processor generates ground reflectance values according to physical models of specific sensor
5. Output processor generates the end product with related metadata and log information including log information from prior levels

5.4.1 Ortho-rectification

During image data acquisition the geometry of the sensor towards the earth surface changes slightly. The earth surface shows altitude differences, as well within acquisition area. Both changes influence the appearance of image data. Furthermore it is necessary to address a geographical reference system to the image for subsequent analysis. Through ortho-rectification of the airborne and spaceborne sensor the geometry differences within the image are reduced. Additionally each pixel receives a geographical coordinate of a local geographical coordinate system. Especially important is this step for comparing different data sets with regard to time and sensor variability. Also the accuracy of the rectification is essential for quality of further spectral and spatial analysis of the data. Four main factors influence the geometry of sensor data, airborne in particular (Müller et al., 2002).

1. Inner orientation of the sensor, specified by laboratory calibration procedures
2. Outer orientation of the sensor, determined by Differential Global Positioning System (DGPS) for geographical position and Internal Navigation System (INS) for attitude measurements during acquisition
3. Boresight misalignment angles of navigation sensor and camera system
4. Topography of earth surface in observed area, predefined by a DEM

Since the inner orientation is known through laboratory calibration of the sensor the other three factors have to be determined during flight measurements (DGPS, INS) or prior observation (DEM). DGPS measures continuously the geographical position of the aircraft above ground and the INS records the attitude of the aircraft, which is affected by roll, pitch and yaw, see figure 5.3.

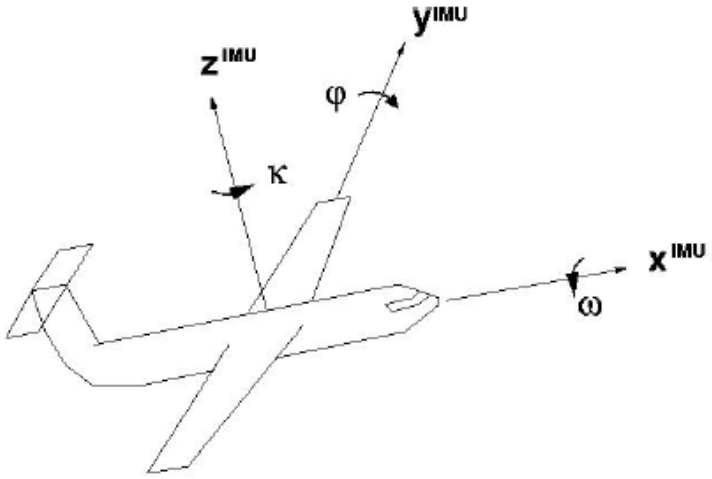

Figure 5.3: Attitude influences of airborne data acquisition; ω is equal to roll, φ is equal to pitch and κ is equal to yaw
(Müller et al., 2002)

Roll is the change of horizontal inclination of the aircraft which influences the lateral view. Pitch is the changing vertical inclination of the aircraft that affects the nadir of the sensor. Lastly yaw defines the horizontal movement change which affects the flight direction. Altitude differences of the ground influence the pixel location and size of the image to the ground. Through the application of a DEM the ground surface can be described and elevation shift within the image can be reduced.
The program used for ortho-rectification is implemented by the Remote Sensing Technology Institute (IMF) of the DLR. ORTHO uses by default a Shuttle Radar Topography Mission (SRTM) DEM with a spatial resolution of 30 m, unless a higher resolution DEM is supplied.
A fast, automatic and generic process of ortho-rectification can be applied through determining these factors (Müller et al., 2002). No ground control points and rectification by hand is necessary since a mathematical / geometrical approach is applied in ORTHO.

HySpex VNIR data

The geographical correction of the flightlines were calculated using ORTHO. Since the default DEM used in this program is SRTM data, the quality is impacted by the spatial resolution of that DEM. The spatial resolution is 30 m and the quality of surface projection is affected, as well as the image ortho-rectification.

Worldview-2 Data

The geographical correction of the Woldview-2 scene is calculated using the DEM generated of the stereoscopic panchromatic images of the same sensor and same scene. The orthorectification of the Worldview Scene was done by the IMF at DLR.

5.4.2 Atmospheric correction

The atmosphere contains several components that influence the spectral information. The aim of atmospheric correction is the conversion of at-sensor radiance with atmospheric influences to at-ground reflectance with reduced atmospheric influences. A physical overview of atmospheric effects is explained in chapter 3. The objective of atmospheric correction is to eliminate atmospheric scattering from ground surface scattering, see figure 5.4.

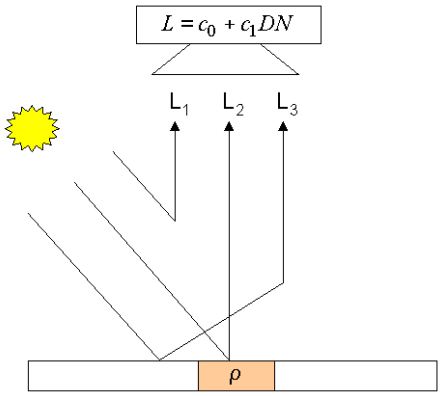

Figure 5.4: Solar radiation components and their influence on sensor radiance (Richter and Schläpfer, 2012a, P. 17)

Component L_1 is the path radiance, and it is the direct scattering of atmospheric effects without influences of ground spectra. Whereas component L_3 is the adjacency reflectance, and includes ground reflectance, as well as atmospheric scattering. L_1 and L_3 are both depending on the wavelength since shorter wavelengths are scattered more intense than longer wavelengths. In contrast to the other components L_2 is the reflected radiation from a ground pixel and is only composed of direct ground reflectance. The radiance signal L is as stated in Richter and Schläpfer (2012a) and is composed of all three components:

$$L = L_{path} + L_{reflected} + L_{adj} = L_1 + L_2 + L_3 \tag{5.2}$$

Atmospheric affected radiant components L_1 and L_3 need to be calculated and removed from L for reduction of atmospheric scattering (Richter and Schläpfer, 2012a, P. 16). With disregard of L_3 and introduction of radiometric calibration coefficients c_0 and c_1 for each

band a new equation 5.3 for L can simplify atmospheric correction. This equation describes the relation of digital number (DN) or brightness and the at-sensor radiance (Richter and Schläpfer, 2012a, P. 16).

$$L = c_0 + c_1 * DN \tag{5.3}$$

Solving the surface reflectance ρ, the global flux E_g and ground-to-sensor atmospheric transmittance τ needs to be considered with taking the sun-to-earth distance d^2 in astronomical units into account, see equation 5.4 (Richter and Schläpfer, 2012a, P. 16).

$$\rho = \frac{\pi\{d^2(c_0 + c_1 DN) - L_{path}\}}{\tau E_g} \tag{5.4}$$

HySpex VNIR data

The atmospheric correction is crucial for subsequent spectral analysis. For all three flightlines the atmospheric correction was calculated using ATCOR-4[2] with information of solar altitude and flight data, see table 5.6.

Table 5.6: Settings for atmospheric correction of HySpex VNIR mosaic

information	value flightline 1	value flightline 2	value flightline 3
altitude above ground	2590.00 m	2590.00 m	2590.00 m
altitude above sealevel	3250.00 m	3250.00 m	3250.00 m
flight direction	96.0 °	270.0 °	92.0 °
solar zenith	34.8 °	33.6 °	32.4 °
solar azimuth	123.4 °	126.3 °	129.4 °
solar elevation	55.2 °	56.4 °	57.6 °
model	flat terrain	flat terrain	flat terrain
averaged ground elevation	660.00 m	660.00 m	660.00 m
visibility	80 km	80 km	80 km

[2] algorithm is discussed in Richter and Schläpfer (2012a)

Worldview-2 data

Usually Worldview-2 data are delivered with at-sensor radiance. The atmospheric correction was calculated using ATCOR-3[3], which is specific for spaceborne sensors, see table 5.7.

Table 5.7: Settings for atmospheric correction for the Worldview-2 image

information	value
course	62.4 °
solar zenith	25.8 °
solar azimuth	156.0 °
solar elevation	64.2 °
model	flat terrain
ground elevation	600.00 m
visibility	60 m

5.4.3 Levelling of flightlines

The geometry between object, sensor and sun defines the illumination characteristics of an object. Through differing geometry during optical data acquisition overlap areas of flightlines can vary visually. Surface character of objects are diverse, and so scattering of the suns radiation is different for objects and their geometry. Also the changing topography within the image area influences the illumination of the objects. During acquisition of optical airborne data the flightlines show differences in brightness between each other, due to different ground cover per line. This implies the changed geometry of the sun towards sensor and object.

Illumination and object differences are caused by the BRDF effect. This effect describes the scattering of a light beam coming from one direction of the hemisphere into another direction of the hemisphere (Schaepman-Strub et al., 2006, P. 30). Through temporal observing differences the solar zenith angle changes and has principal effect on the reflectance of an object (Deering et al., 1995, P. 1239). Diurnal and seasonal variations in vegetation appearance influence the BRDF effect significantly.

Light scattering of an object can not be measured exactly but approximated through atmospheric correction and angular modelling (Schaepman-Strub et al., 2006, P. 33). The approximation is based on instruments that encompass the reflectance change of one object viewed from different angles. For objects with lighted and shaded areas the BRDF effect can be very strong (Richter and Schläpfer, 2012a, P. 20), such as tree canopies.

The across track illumination affects the appearance of similar objects as well. Through varying viewing angles of the sensor, objects in nadir are illuminated different than objects at the

[3] algorithm is discussed in Richter and Schläpfer (2012b)

edge of flightlines. Reducing these effects is essential for the correctness of subsequent analysis. Classification accuracies can increase with reduced across track illumination differences and BRDF effect.

Levelling of flightlines takes these effects into account and reduces the differences in illumination. This generates an enhanced mosaic with reduced spectral flightline differences. The basic requirement for levelling is the same geographical overlap area of two flightlines where only the spectral information differ. The process of levelling is as follows, see Rogge et al. (2012) and compare with figure 5.5:

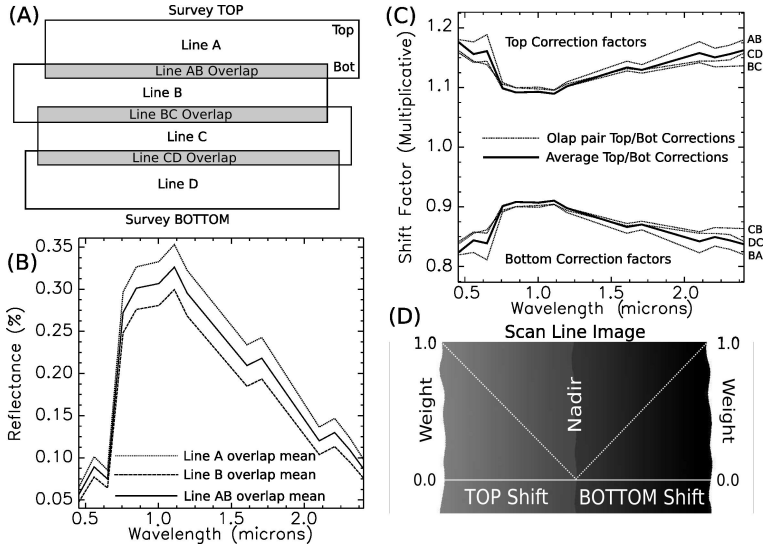

Figure 5.5: Levelling procedure showing example flight-lines with overlap regions (A), calculated overlap mean spectra for lines A, B and overlap area (B), calculated correction factors for all pair combinations of lines and the resulting average value (C), which is applied to every line and weighted relative to the scan angle from nadir (D)

(adapted Rogge et al., 2012, P. 4096)

1. Calculation of overlap areas of two flightlines, figure part (A)
2. Calculation of mean spectra for overlap area in flightline A and flightline B separately - this results A_{mean} and B_{mean} per band, figure part (B)
3. Average calculation of mean spectra from both flightlines - $Mean_{AB} = \frac{A_{mean}+B_{mean}}{2}$ (B)
4. Computation of correction factor through dividing mean spectra per flightline by average of mean, usually the correction factor is not linear within spectra, because of minimal band differences between flightlines - $corr_A = \frac{A_{mean}}{Mean_{AB}}$ equal process for B, figure part (C)

5. Determination of corrected spectra per flightline through multiplying original spectra by correction factor - $R' = corr_A * R$ and weighted relative to the scan angle from nadir, figure part (D)

Levelling is an iterative process that considers spectral differences in pairs of flightlines. Information for each pair of flightlines is combined to determine the final correction factors. In case of an erroneous geographical correction the levelling yields inadequate results.

HySpex VNIR levelling

Through levelling in the three flightlines the radiometric difference can be reduced. This decreases the spectral differences within the mosaic, see figure 5.6.

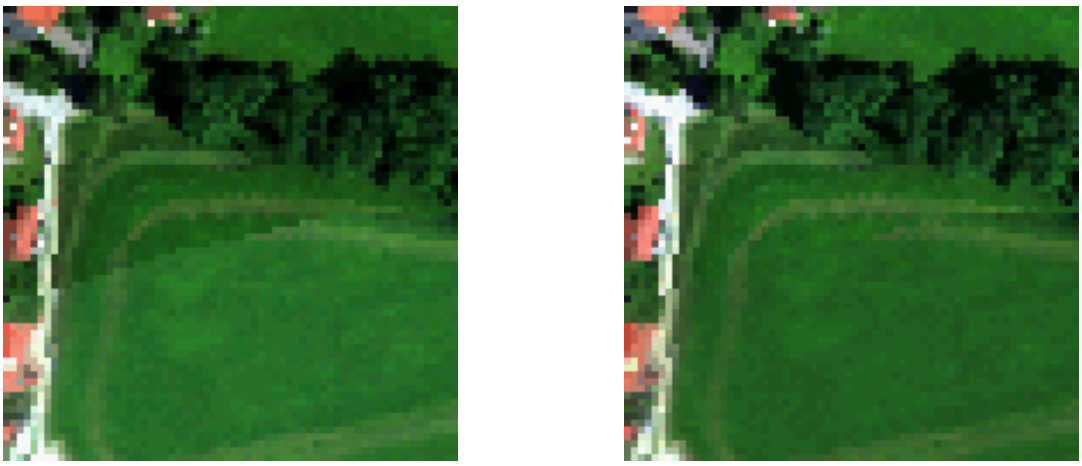

(a) HySpex VNIR zoom of two different flightlines without levelling

(b) HySpex VNIR zoom of two different flightlines after levelling applied

Figure 5.6: Comparison of HySpex VNIR mosaic with and without levelling

The levelling procedure and correction factors were calculated on the masked green vegetation. This yields better results in reason of similar spectral information.
These three flightlines were acquired approximately within 20 minutes time difference. An additional across-track illumination difference calculation is not necessary, when taking the time difference and amount of flightlines into account.

5.4.4 Spatial smoothing of flightlines

The quality of image analysis is highly dependent on the image quality itself. Several aspects can influence the quality and with this the applicability for further spectral analysis. Besides the reduction of atmospheric effects and illumination differences two more obstacles need to be diminished for spectral quality enhancement. These obstacles are random noise and intra-class variability, and they both can reduce separability among spectral classes.

Intra-class variability is the difference within one class whereas inter-class variability is the difference among classes. If intra-class exceeds inter-class variability, spectral information can overlap between objects and separability of the different classes will decline significantly. Random noise is random spectral disturbance that happened incidental during data acquisition. This also can lead to erroneous spectral analysis of image data. Usually spatial filters, such as mean or median filters, can reduce both random noise and intra-class variability effects but also blur object edges and important information, consequently.
The aim of applying the Iterative Adaptive Smoothing filter (IAS) by Rogge and Rivard (2010) is to reduce random noise and intra-class variability of similar spectral information with maintaining object edges. This filter is based on diffusion filter by Perona and Malik (1990). A kernel of an uneven number centred on a single pixel generates a weighted image of the original image, see figure 5.7.

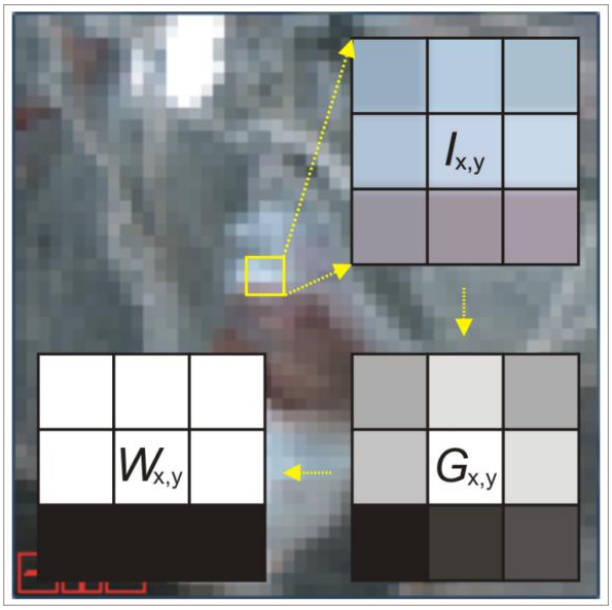

Figure 5.7: Spatial smoothing procedure showing example of a 3*3 kernel of the image ($I_{x,y}$), a derived gradient map ($G_{x,y}$) and after applying a threshold, the weighted image contains object extent ($W_{x,y}$)
(Rogge and Rivard, 2010)

The centre pixel in each kernel of the original image ($I_{x,y}$ at a time t) is weighted against every surrounding pixel. As a result the variability of each pixel in the kernel is calculated and a gradient map can be derived. The weighted image (W) contains information about the extent of objects and enables spectral smoothing only within the objects. The smoothed reflectance (R') is derived by applying the weighted image on the input reflectance (R).
The actual smoothing takes place over a defined amount of iterations. The first iteration

includes most smoothing action with a subsequent smoothing decreasing approximately exponentially.

$$
\begin{aligned}
W^t_{dx,y} &= g(\Delta D_d I^t_{dx,y}) \\
I^{t+1}_{x,y} &= (\sum_{d=1}^{9} W^t_{dx,y})^{-1} * \sum_{d=1}^{9} I^t_{dx,y} W^t_{dx,y} \\
R' &= R_{x,y} * W_{x,y}
\end{aligned}
\tag{5.5}
$$

HySpex VNIR spatial smoothing

For enhancing the spectral information and the subsequent spectral analysis, spatial filtering was applied. Three parameters need to be defined before the calculation can be done. First parameter is the amount of iterations with 5 as default. Second parameter is the size of the kernel that is $3x3$ by default. Lastly the cut-off threshold by which the weighted image is derived, is calculated by a separate algorithm, that assesses the spatial similarity of each pixel with its neighbouring pixels. This threshold serves to delimit boarders of objects. The IAS operates using two similarity metrics that may be applied after another. The Root Mean Square (RMS) is the first approach where the gradient map is derived using RMS, whereas the second approach uses the Spectral Angle (SA) for deriving the spectral similarity of the pixel within the kernel. Through this, a spectral smoothing takes place within the extent of one object such as a single tree crown, see figure 5.8.

(a) HySpex VNIR zoom of two different flightlines with applied levelling

(b) HySpex VNIR zoom of two different flightlines with applied levelling and spatial smoothing

Figure 5.8: Comparison of HySpex VNIR mosaic with (b) and without (a) spatial smoothing

6 Methodology

This chapter defines the spectral methodology that was applied on the HySpex VNIR and Worldview-2 data. Section 6.1 describes the derivation of the forest mask, and section 6.2 describes the collection of reference spectra of forest type and tree species. Subsequently section 6.3 states the spectral mean normalisation which enables the enhanced spectral analysis in section 6.4. The subsequent accuracy analysis is specified in section 6.5. Figure 6.1 shows the flowchart of forest classification. Main focus is detection of forest type and tree species.

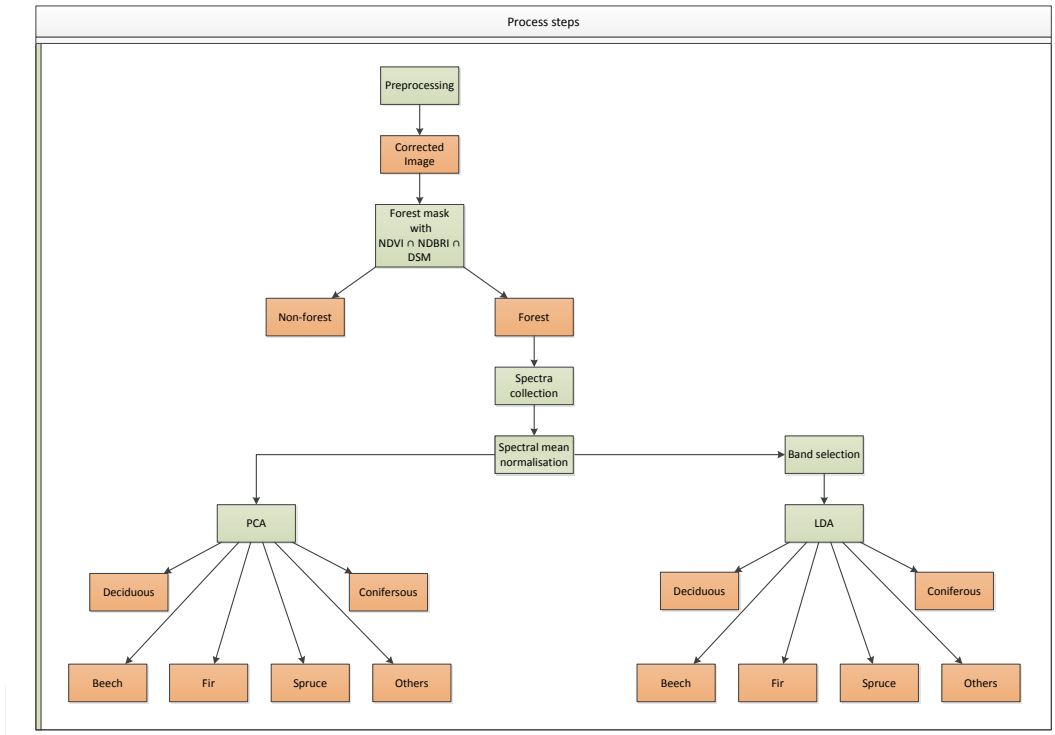

Figure 6.1: Flowchart for forest classification

Before tree species can be detected, several analysis steps are important. The separation of forest and non-forest is necessary for focussing on forest pixels only. Also partitioning the forest in deciduous and coniferous forest is of importance for making the tree species discrimination plausible. Beside spruce other, frequently distributed tree species, such as beech and fir can be analysed for discrimination based on spectral characteristics.

6.1 Creation of forest mask

Focussing on the forest as object of interest simplifies the analysis. Therefore, a forest mask was defined. This forest mask prevents misclassification of non-forested pixels in the imagery. The collection of spectra as training data and the validation of the classification will contain less error.
Three different approaches are proceeded independently and merged together for compiling the mask. The usage of LiDAR data from area Traunstein of year 2010 is used additionally to the optical remote sensing data.

1. Vegetation with different water content and greenness can be detected by applying the Normalised Difference Vegetation Index (NDVI). This index was designed to reduce the seasonal solar altitude differences and the effect of atmospheric attenuation (Rouse et al., 1974, P. 312). It shows a high sensitivity to aspect of the sensor and illumination of the object and saturates at a high Leaf Area Index (LAI) value (Roberts et al., 2004, P.560) and varies with soil influenced reflectance (Huete et al., 1985, P. 38). The range of the index is $\{-1;1\}$ and described through equation 6.1. Each vegetation type and zone demands an individual threshold for delineation of vegetation and non-vegetation.

$$NDVI = \frac{IR - R}{IR + R} \tag{6.1}$$

2. The detection of red roofs but also some spectral types of bare soil can be supported by using the normalised different brick roof index (NDBRI) which ranges from $\{-1;1\}$. The NDBRI was originally developed for Worldview-2 purposes (Zhou et al., 2012), see equation 6.2.

$$NDBRI = \frac{yellow - green}{yellow + green} \tag{6.2}$$

   Due to the lack of a reference threshold the mean range value 0 is used and proved by the histogram of the index images.

3. Calculating the absolute heights of the objects on the land surface helps to differentiate between high and low objects. The object height was derived by subtracting the DEM from the DSM. A reasonable height threshold for forest can be applied. This threshold for the forest mask was set to 5 m as part of the definition of forest by the FAO, 2000.

Since the HySpex VNIR and the Worldview-2 data have different spectral resolution, consequently the forest mask was generated for each data set independently, using different thresholds, see subsection 6.1.1 and 6.1.2. The following subsections declare the thresholds of the indices in more detail.

6.1.1 HySpex VNIR forest mask

Originally both applied indices were developed for broadband multispectral data. They had to be adapted to narrowband data, such as the HySpex VNIR spectral ranges. The adaptation was carried out by using the hyperspectral wavelength closest to the designated multispectral bands.

1. Wavelengths for NDVI were set closest to 750 nm and 705 nm, as adapted from the broadband NDVI, in order to use the red edge information (Gitelson and Merzlyak, 1994). Equation 6.3 shows the adapted index for HySpex VNIR:

$$NDVI = \frac{749\ nm - 706\ nm}{749\ nm + 706\ nm} \tag{6.3}$$

   The threshold of 0.4 is derived by slight alteration of broadband threshold by Weier and Herring (2000). Evaluating the histogram of the resulting image assisted for determining the threshold. All values below the threshold were masked out as non-vegetation.

2. Originally NDBRI was developed to fit the bands of Worldview-2. They also had to be adapted for fitting to HySpex VNIR bands and wavelengths. Equation 6.4 shows the HySpex VNIR adapted index.

$$NDBRI = \frac{600\ nm - 546\ nm}{600\ nm + 546\ nm} \tag{6.4}$$

   No threshold could be found in literature so it had to be derived by the information distribution in the histogram. The threshold was set to 0 and all values above 0 were masked out.

6.1.2 Worldview-2 forest mask

Since the indices were originally developed for broadband data, the appropriate bands had to be defined in Worldview-2 data to fit the calculations.

1. Wavelengths for NDVI were selected closest to red and near infrared range for applying the broadband NDVI index of Roberts et al. (2004). Equation 6.5 shows the index applied on Worldview-2.

$$NDVI = \frac{b7 - b5}{b7 + b5} \tag{6.5}$$

   The threshold was set to 0.6, which was stated in literature by Weier and Herring (2000). Additionally, the evaluation of the information distribution in the histogram supports the threshold.

2. For identifying red roofs the NDBRI index was applied. Following bands were selected after Zhou et al. (2012), see equation 6.6.

$$NDBRI = \frac{b4 - b3}{b4 + b3} \tag{6.6}$$

   The NDBRI index was also calculated for Worldview-2 imagery for identifying urban areas. The threshold was set to 0, such as for HySpex VNIR. The evaluation of the histogram shows a significant through of information, which is applied as threshold.

The final forest masks were derived by multiplying the three reclassified index images and masks, respectively (compare subsection 6.1). This enabled the combination of the three individual input masks with euqation 6.7

$$NDVI\ mask \cap NDBRI\ mask \cap LiDAR\ mask \tag{6.7}$$

and results a forest mask where every single input is valid regarding the definitions above. In the results the HySpex VNIR and Worldview-2 forest masks are shown in figure 7.2 and figure 7.4 and were used as input for further processing. These masks were adopted on the HySpex VNIR mosaic and the Worldview-2 image to cut out all features, that are either below 5 m or which did not exceed the threshold of the applied indices (see for this the definition of the thresholds in section 6.1).

6.2 Collection of reference spectra

Reference spectra of particular forest types and tree species are necessary for spectral analysis and discrimination. Further analysis such as band selection, classification and accuracy assessment can be examined using these important reference spectra as input data. Since the forest parameters of interest were forest type and tree species, reference spectra needed to be collected from different forest types and tree species. Forest inventory data of the LWF underlay with 228 regular spread plots within the Traunstein forest, see section 5.3. The proportion of forest type and tree species was examined for each inventory plot. Deciduous and coniferous plots were selected as forest type. Whereas European beech, European silver fir and Norway spruce were selected as tree species. Other tree species could not be included in the spectral collection as no other homogeneous plots (more than 80 %) were available in the inventory data.
The aim was to collect all spectra within homogeneous inventory plots for each forest type and tree species. The spectral sampling strategy was performed as followed:

1. Selection of inventory plots with $100\ \%$ proportion of forest type and tree species, respectively

2. Within the inventory plots, ellipsoidal regions of interest were collected with one pixel apart from the plot border, see figure 6.2
3. Each ellipsoidal region of interest counted 52 pixel. A minimum number of 100 spectra were found by selecting at least two appropriate inventory plots.

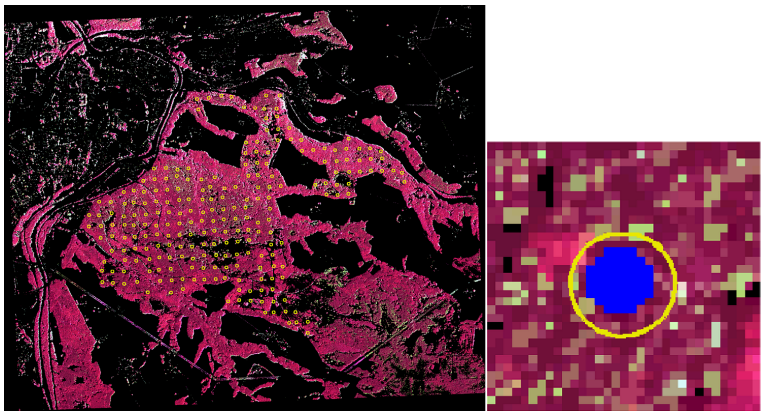

Figure 6.2: Region of interest (blue) with 52 pixel in inventory plot (yellow ring) with 100% proportion of tree specimen

6.2.1 Forest type spectra

After separation of forest from non-forest the next step is to distinguish spectral information of deciduous and coniferous forest. For this process reference spectra of deciduous and coniferous forest were necessary, using Traunstein forest inventory data from 2008, see section 5.3. All regular distributed plots with 100 % of deciduous and plots with 100 % of coniferous trees were selected, see table 7.1.
Average age and height for each specimen were also derived from inventory data and DSM. As stated in section 2.4, the study area is a stratified heterogeneous forest relating to species, age and height composition. This causes difficulties in observing small and young trees that are covered by older and higher trees. For improving the reference data, spectra of low height and young age were eliminated as they probably occur in shaded understorey. Thresholds were defined for eliminating reference spectra with tree height of less than 10 m and tree age below 30 years.

6.2.2 Tree species spectra

Another important forest parameter is tree species. In addition to forest type spectra the spectral information of different tree species were collected. Each specimen was set as class as soon as a minimum of two inventory plots were found with 100 % of that specimen.
The only two species that covered each a minimum of two inventory plots with 100 %

tree species proportion are European beech and Norway spruce. For enabling the tree species classification process at least one more specimen was needed. Since the three main species in Traunstein forest are Norway spruce, European beech and European silver fir (see section 2.4), fir was collected as third species.
Mixed plots with a minimum of $80\ \%$ fir and remaining percentage of spruce were also included due to the lack of $100\ \%$ proportion plots of fir.
Spectral collection was conducted separately for HySpex VNIR and Worldview-2, see table 7.3 for number of spectra per species and sensor.
Similar to the spectral collection of forest type, young and low trees were eliminated from tree species spectral library, see table 7.4. The collected spectra serve as reference for further spectral and statistical analysis.

6.3 Spectral mean normalisation

Brightness differences of the covered area can influence the result of a classification significantly. Varying viewing angles of the sensor, topography or illumination changes during acquisition can cause brightness differences (Zhang et al., 2005, P. 60). Also spectra of similar shape can reveal amplitude variations due to the brightness and illumination differences and can also have overlap with reflectance of other objects. The normal distribution of spectra does not exist. But the spectra need to be normal distributed for statistical analysis.
The key of this process is to remove the amplitude character of the spectra and emphasise the shape for enhanced statistical analysis. The differences in brightness shall not be confused with differences in shape for classification.
The main steps for generating the spectral mean normalisation (N) is to calculate a mean spectra value (M) per pixel (R) with n amount of bands (b). In the end the pixel spectra value is divided by the mean for normalisation, see equation 6.8 by Zhang et al. (2005).

$$\begin{aligned} N_b &= \frac{R_b}{M} \\ M &= \frac{1}{n}\sum_{b=1}^{n} R \end{aligned} \tag{6.8}$$

6.4 Spectral analysis

Several spectral evaluation methods were applied during processing. For analysing the spectral distribution, Principal Component Analysis (PCA) was calculated, afterwards a supervised classification method using LDA was applied. Following subsections explain the analysis approach. The statistical analysis was conducted using R[1], the statistical program.

[1] algorithm is discussed in The R Development Core Team (2010)

6.4.1 Principal Component Analysis

PCA is a multivariate statistical analysis for unsupervised classification. Remote sensing data shows high correlation either by overlapping spectral information of an object or by spectral band overlap due to the high number of bands. The aim of PCA is to transform correlated data into an uncorrelated coordinate system. This new coordinate system is comprised by pairwise uncorrelated Principal Components (PC). The PC are derived from a covariance matrix of a data matrix X with (x_{ij}) where i is the collected spectra and j is the band. The covariance matrix is defined by Richards and Jia (1999) as.

$$\sigma_{\mathbf{x}} = \frac{1}{n-1}\sum_{i=1}^{n}(x_i - \mu_x)(x_i - \mu_x)^T \tag{6.9}$$

In this case the PCA was calculated for identifying separation possibilities of several data groups, such as forest type and tree species. The spectra could be grouped and displayed in a two-dimensional space which reveals classification possibilities. Also intra- and inter-specific variations can be observed using the PCA. Loadings of the PCA were used for evaluating the importance of bands that comprehend most information for separating forest type and tree species, respectively. The calculation of PCs is stated below, see Bahrenberg et al. (1992) for further explanations:

1. Variables, which are the reference spectra (r) need to be standardised
2. Extraction of correlation coefficient of each variable through the covariance matrix of x_i and x_n with
   $r_{x_i x_n} = \frac{1}{2}(x_{ii}x_{in} + x_{in}x_{nn})$
3. Using these correlation coefficients for further calculations by summarising correlation coefficients per variable (r) $r_{sum} = \sum r_{x_i x_n}$ and for all variables together $r_{all} = \sum r_{sum}$
4. The square root of r_{all} results the first PC
5. The correlation of each variable with the PC, which is also known as loading, is important to calculate with
   $loadings = \frac{r_{sum}}{PC}$
6. These $(loadings)^2$ result the percentage of variance per variable on the PC
7. The sum of all $(loadings)^2$ reveal the Eigenvalue, which is a reference for the variance of all variables in the PC
8. Dividing the Eigenvalue by the amount of variables defines the variance of all variables in the PC

9. This procedure is repeated for subsequent PCs, that explain the remaining variance

The method of PC exploration can vary by program. The R package *stats*[2] uses the method of Eigenvalue extraction from a covariance matrix as explained above. It also applies the method of singular value decomposition separately. Both methods show similar results on this data basis. Results of one method can be found in section 7.4.1.

6.4.2 Band extraction

Hyperspectral data are characterised by narrow bands with a continuous spectral range. Thereby the correlation between bands is higher than compared to multispectral images with broader and fewer bands. The high amount of bands increases the computational load and distorts the modelling accuracy (Zhuo et al., 2008, P. 1), which is known as Hughes phenomenon (Shahshahani and Landgrebe, 1994, P. 1094).
Parametric classifiers, such as LDA or ML are less suited for high dimensional data than non-parametric classifiers, such as random forest or neural network. Since the LDA was set as classification method the data dimensionality needed to be reduced.
Several methods are known for feature extraction and data reduction without reduction of the information content. Trevino and Falciani (2006) have implemented a package for R that is based on medical issues. The package *galgo*[3] is based on Genetic Algorithms (GA) and is a generic software package, which was build formerly for extracting gene information from high dimensional data. Because of its origin, the feature names are related to medical issues and need to be explained in advance. The smallest element is a gene, which is equal to the hyperspectral band. Selected numbers of genes form a chromosome, which is an artificial group of bands, that pass a defined classification accuracy. This accuracy is defined in a fitness function. Figure 6.3 explains the cycle of band selection.

[2] http://stat.ethz.ch/R-manual/R-patched/library/stats/html/00Index.html
[3] http://www.bip.bham.ac.uk/vivo/galgo/AppNotesPaper.htm

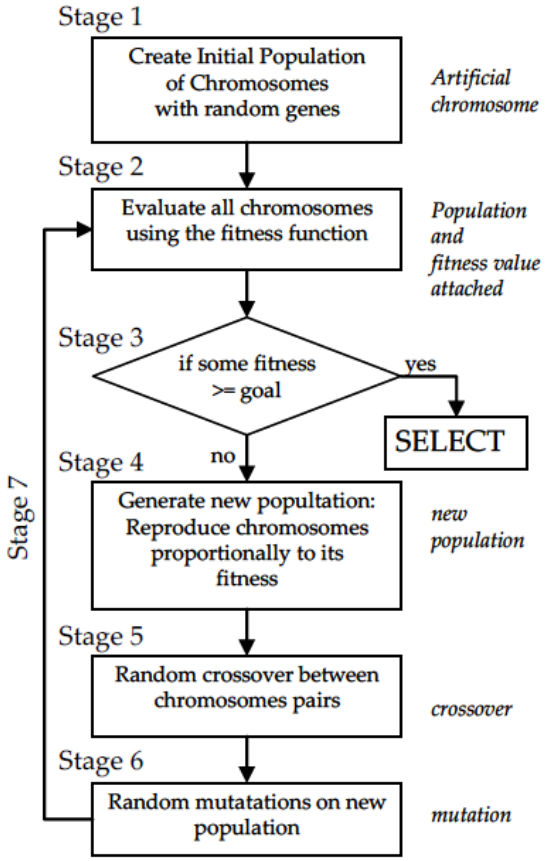

Figure 6.3: Process of band selection using a GA
Trevino and Falciani (2006, P. 5)

Stage 1 Random genes are combined to one chromosome

Stage 2 Each chromosome is evaluated regarding the fitness function; a statistical model is trained for predicting the accuracy

Stage 3 When the chromosome reaches or exceeds the accuracy, the procedure stops and a new chromosome is built and tested. If the accuracy is not reached the procedure continues with stage 4

Stage 4 Chromosomes with higher fitness scores will be replicated

Stage 5 Two randomly replicated chromosomes will be combined through genetic crossover, so that the new two chromosomes contain information of two approved chromosomes

Stage 6 Through mutation new genes are imported into replicated chromosomes

Stage 7 These two new chromosomes get into a loop back to stage 2 and will be tested for fitness

Stages 4 to 6 are called generation which will be of interest in the results.
For the set up of the GA several input data were defined. The amount of genes per chromosomes and the number of iterations are important. Also the classification method needs to be specified, since the GA uses supervised classification methods for analysing the fitness function. Whereby, the fitness function has to be defined previously.
Parameters for extracting bands with most information for separating fores type and tree species, respectively are as follows.

Forest type band extraction

- Chromosome size was constrained with 8 genes for comparison to Worldview-2 band number
- Number of iteration was 1000 for ensuring optimal results
- Classification method for band extraction and accuracy analysis was maximum likelihood, since this method is high in system performance and high in methodological value
- The fitness was set to $94\ \%$ for forest type band extraction

The selected bands were used for further analysis regarding classification and prediction of accuracy.

Tree species band extraction

- Chromosome size was constrained with 8 genes for comparison to Worldview-2 band number
- Number of iteration was 1000 for ensuring optimal results
- Classification method for band extraction and accuracy analysis was maximum likelihood, since this method is high in system performance and methodological value
- The fitness was set to $90\ \%$ for tree species band extraction, which was most possible for all three tree species

The selected bands were used for further analysis regarding classification and prediction of accuracy.

6.4.3 Linear Discriminant Analysis

LDA is a supervised classification method, that surveys predefined groups for their separability. It also allocates new members without group affiliation to an existing group (Bahrenberg et al., 1992, P. 317). Different to other classification methods, such as cluster analysis, no new groups are formed, but their distinction are tested and improved by discriminant functions. This enables the LDA for proofing a hypothesis rather than stating one (Bahrenberg et al., 1992, P. 318).
The LDA is a linear coordinate transformation that creates discriminant axes orthogonal to each other. The aim is to minimise the within group variance and maximise the between group variance (Bahrenberg et al., 1992, P. 323, 332). The discriminant function for multi-group / multi-variable approach demands discriminant coefficients v_i, derived from variables X_i. These discriminant coefficients need to be standardised using their standard deviation s_i with:

$$b_i = \frac{1}{s_i} * v_i \tag{6.10}$$

Deriving v_i, the between class σ_b and within class σ_w variation has to be calculated of matrix **X** by:

$$\begin{aligned} \sigma_w &= \sum_{g=1}^{G} \sum_{j=1}^{n_g} (y_{gj} - \overline{y}_g)^2 \\ \sigma_b &= \sum_{g=1}^{G} n_g (\overline{y}_g - \overline{y})^2 \end{aligned} \tag{6.11}$$

with G = group quantity
g = group
y_{gj} = discriminant value of element j in group g
$\overline{y}_g$ = mean discriminant value in group g
$\overline{y}$ = total amount of discriminant values of N elements

The LDA maximises the ratio of between and within class variation (Bahrenberg et al., 1992; Richards and Jia, 1999):

$$\Gamma = \frac{v * \sigma_w^x * v^T}{v * \sigma_b^x * v^T} \tag{6.12}$$

The standardised discriminant function is as follows:

$$Y = b_0 + b_1 X_1 + b_2 X_2 + b_n X_n \tag{6.13}$$

The LDA calculation was conducted using package $MASS$[4] in R. The outcome of the LDA y_i are standardised discriminant values with mean values at 0 and standard deviation at 1 (Bahrenberg et al., 1992, P. 335).

6.4.4 Image classification

The spectral analysis was conducted on the collected forest type and tree species spectra. Afterwards, the LDA classification was predicted on the HySpex VNIR and Worldview-2 images for deriving the occurrence probability of forest type and tree species within the forest area, using $raster$[5] package in R. Subsequently both forest type and the three tree species are combined choosing a minimum probability of 60 %. The combined probability distribution maps are shown in figure 7.23 and 7.27 for each sensor separately.

6.5 Accuracy assessment

The accuracy of a classification needs to be defined for estimating the quality of the classification results. Reliable reference data are highly important for comparison. The accuracy of a classification is an important issue and needs to be analysed clearly, since a high number of classes in general decreases the classification accuracy.
In this thesis the image based spectral libraries serve as input for supervised classification and also for subsequent accuracy assessment. The spectra for classification are split in two parts whereas $1/3$ is trained for the classifier and $2/3$ are test-spectra that are used for accuracy assessment. This helps to provide a confidence in separating classes that can be predicted onto the raster images. This way of accuracy assessment was chosen, because no other in-situ ground reference data were available to validate the images classification.

[4] http://cran.r-project.org/web/packages/MASS/index.html
[5] http://cran.r-project.org/web/packages/raster/

7 Results

This chapter presents the results of each method, starting with the derivation of a forest mask in section 7.1 and the collection of reference spectra in section 7.2. The results of spectral mean normalisation are stated in section 7.3, followed by the results of spectral analysis in section 7.4. The subsequent image analysis is shown in section 7.4.4. At last, the results of the accuracy assessment are presented in section 7.5.

7.1 Forest mask

7.1.1 HySpex VNIR and Worldview-2 forest mask

The forest mask, calculated on HySpex VNIR and Worldview-2 imagery, show clearly the discrimination of forest and non-forest. The images of HySpex VNIR (figure 7.1) and Worldview-2 (figure 7.3) show the distribution of forested and non-forested areas The separation of green vegetation and urban area was successfully performed using the NDVI spectral index. The additional usage of height metrics, derived from the LiDAR data, selected all objects with a minimum height of 5 m and successfully eliminated shrubs, grass land, bare soil, roads and other objects with low height. The third metric was the application of the NDBRI spectral index. This index additionally masked out urban areas, such as roads and roofs. The combination of all three metrics resulted in a mask separating low growing vegetation with a minimum of 5 m height from urban area and grass land.
In the centre of the image, the Traunstein forest is selected as white area. The masked pixels are presented in black. The area around the forest shows singular tree occurrences in urban areas (see figures 7.2 and 7.4). When applying the mask on the corresponding image, all black features are eliminated from the image and vise versa all white features remain for further analysis. The resulted forest mask was calculated separately for HySpex VNIR and Worldview-2 image. Both masks vary insignificantly by a few pixels, most likely due to the different thresholds set in the indices. The two forest masks for HySpex VNIR and for Worldview-2 are shown in figure 7.2 and 7.4.

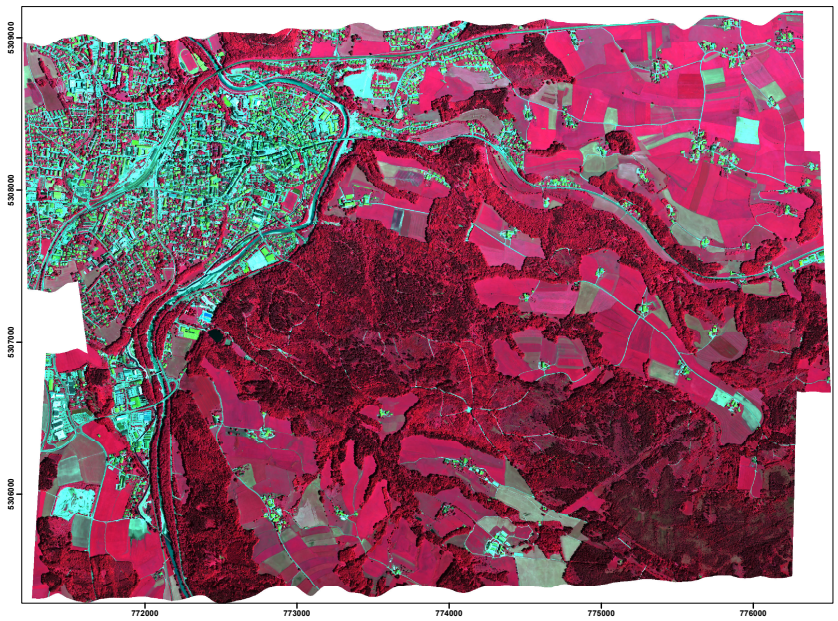

Figure 7.1: HySpex VNIR mosaic as colour infrared image

Figure 7.2: HySpex VNIR forest mask derived from LiDAR mask, NDVI mask and NDBRI mask

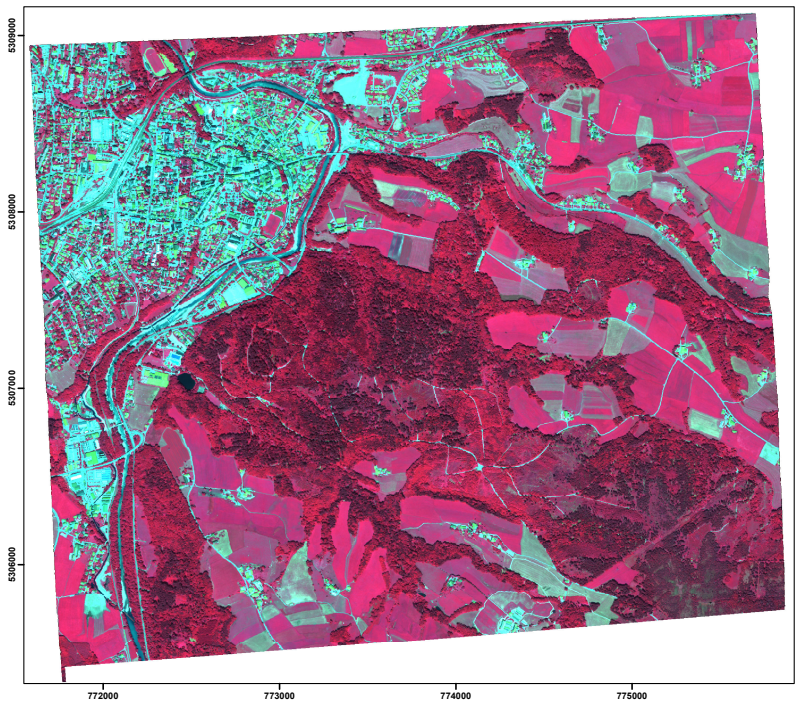

Figure 7.3: Worldview-2 as colour infrared image

Figure 7.4: Worldview forest mask derived from LiDAR mask, NDVI mask and NDBRI mask

7.2 Collection of reference spectra

Spectral analysis of forest type and tree species are dependent on the quality of reference spectra collected in the image. The image based spectral library of forest type and tree species are affected by the heterogeneous stand composition, as it was found in this study area.

Forest type spectra

Table 7.1 shows the number of reference spectra before age and height was eliminated. The amount of deciduous and coniferous reference spectra differ by over 400 spectra per sensor. Contrary the number of spectra per class among the sensors differ only by a small number. In sum 825 and 823 spectra for deciduous trees and 1270 and 1277 spectra for coniferous trees were collected from HySpex VNIR and Worldview-2 imagery, respectively (see Table 7.1). After elimination of small trees 773 and 772 spectra remained for deciduous trees, whereas the number of coniferous tree spectra reduced to 1235 and 1237 spectra for HySpex VNIR and Worldview-2 imagery, respectively (see Table 7.4).

Table 7.1: Amount of reference spectra of forest type in Traunstein forest, selected from HySpex VNIR and Worldview-2 imagery

Forest type	HySpex-VNIR	Worldview-2
Deciduous trees	825	823
Coniferous trees	1270	1277

Table 7.2 shows the number of reference spectra per sensor that remain after height and age extraction. The ratio of deciduous and coniferous spectra remain similar per sensor. Same with the ratio per forest type among the sensors.

Table 7.2: Amount of reference spectra of forest type in Traunstein forest, selected from HySpex VNIR and Worldview-2 imagery after tree height and tree age extraction

Forest type	HySpex-VNIR	Worldview-2
Deciduous trees	773	772
Coniferous trees	1235	1237

Figure 7.5 shows the number of deciduous (yellow) and coniferous (green) reflectance spectra. The standard deviation (yellow and green vertical lines) shows the maximum and minimum variation of spectra per class, which leads to a slight overlap between the two classes. This can be taken as first reference for successful forest type discrimination.

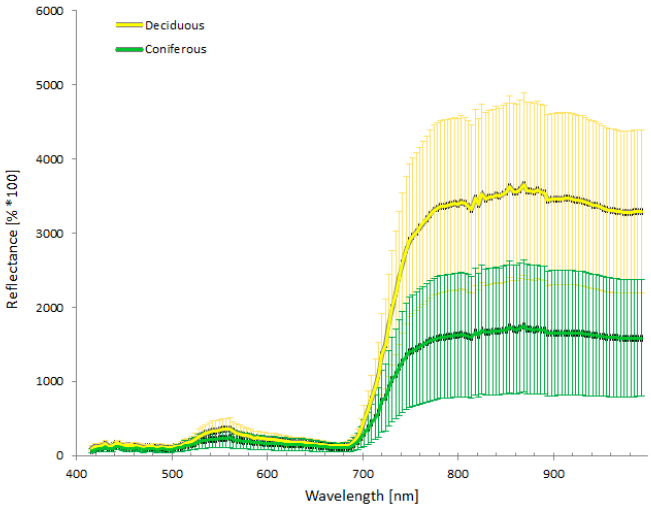

Figure 7.5: Forest type reflectance from HySpex VNIR collected reference spectra with standard deviation (coloured vertical lines)

Tree species spectra

Equal to forest type spectra the original tree species spectra were eliminated by age and height of forest, based on forest inventory data and the LiDAR derived DSM. Table 7.3 lists the number of spectra per species and sensor. The number of tree species spectra per sensor differ significantly but the number of spectra per species between the sensors is either slight (spruce) or non-existent (beech and fir). The number of spectra collected from HySpex VNIR and Worldview-2 for spruce were 596 and 595, respectively. The number of spectra for beech were 222 and number of spectra for fir were 156 for both sensors.

Table 7.3: Amount of reference spectra of three tree species in Traunstein forest, collected from HySpex VNIR and Worldview-2

Specimen	HySpex-VNIR	Worldview-2
Spruce	596	595
Beech	222	222
Fir	156	156

After extraction of spectra, that did not reach the threshold of forest age and height, remain different number of spectra, see table 7.4. The number of spectra collected from HySpex VNIR and Worldview-2 for spruce reduced to 561 and 555, whereas number of spectra for beech reduced to 203 and 201, respectively. The number of spectra for fir remained 156 for

both sensors. The ratio of spectra among species per sensor remain similar. Same with the ratio per species among the sensors.

Table 7.4: Amount of reference spectra of three tree species in Traunstein forest, selected from HySpex VNIR and Worldview-2 images, after tree height and tree age extraction

Specimen	HySpex-VNIR	Worldview-2
Spruce	561	555
Beech	203	201
Fir	156	156

Figure 7.6 shows the mean reflectance spectra of beech (yellow), fir (light green) and spruce (dark green). The standard deviation (yellow, light green and dark green vertical lines) show the maximum and minimum variation of spectra per species. The overlap of fir with beech and spruce covers almost the whole reflectance variation of fir. This could lead to difficulties in discriminating the class.

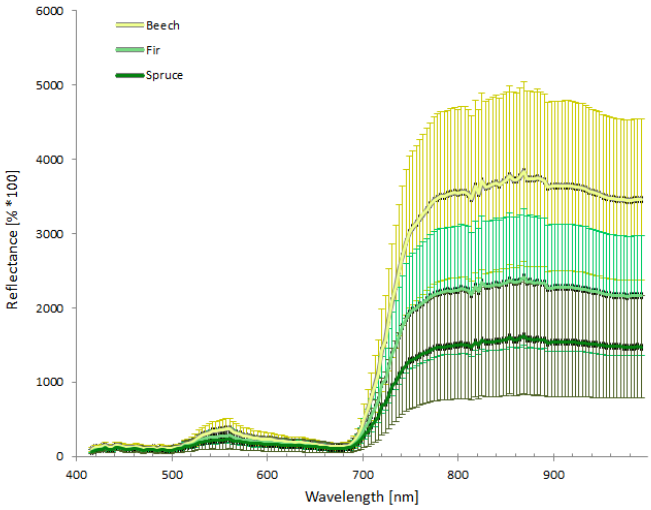

Figure 7.6: Tree species reflectance from HySpex VNIR with standard deviation (coloured vertical lines)

7.3 Spectral mean normalisation

Forest stands can contain many illumination differences. Especially tree crowns with shaded and non-shaded parts are characterised as such and can make species discrimination difficult or impossible. The spectral mean normalisation, as explained in section 6.3 reduced the illumination differences in the spectral libraries, as well as in HySpex VNIR and Worldview-2 imagery. The results are normalised spectra with focus on their spectral shape rather than illumination differences. This leads to the suppression of intra-specific variance and focuses on the inter-specific variance, which is of great importance for species discrimination and enables the comparable analysis of imagery varying in time.

7.3.1 HySpex VNIR sensor

The spectral mean normalisation enhances the statistical evaluation of the spectra.
The result of this processing step is visible in figure 7.7. The left sub-image shows the illumination differences in beech spectra. The variation of spectral information within this tree species varies intensively and results in high intra-specific variation. This leads to lower classification rates since the intra-specific variation might overcome the inter-specific variation. The right sub-image shows the normalised spectra with reduced intra-specific variation. Normalisation of spectra was conducted on every spectral library and HySpex VNIR image.

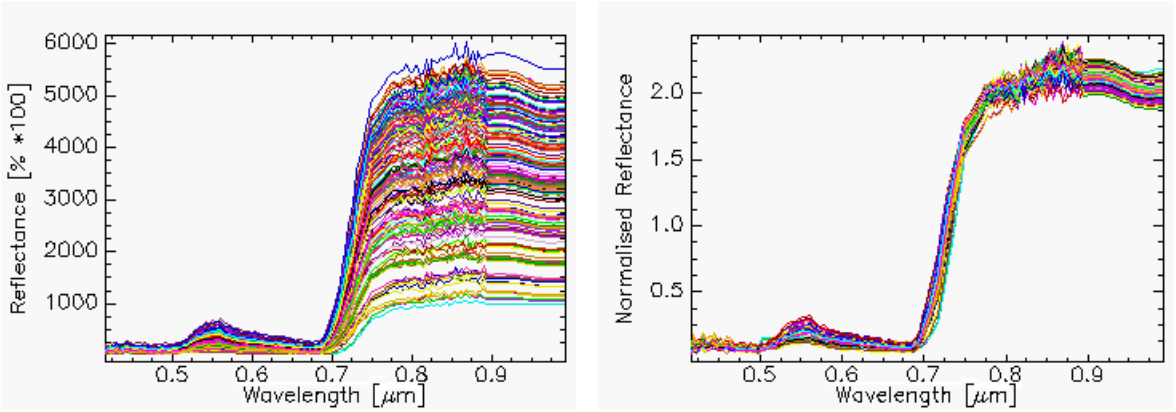

(a) HySpex VNIR spectral library of collected beech spectra

(b) HySpex VNIR normalised spectral library of collected beech spectra

Figure 7.7: Comparison of HySpex VNIR spectra with (b) and without (a) spectral mean normalisation, which highlights shape and reduces illumination differences of spectra

7.3.2 Worldview-2 sensor

Similar to the HySpex VNIR spectral libraries and image, the spectral mean normalisation was conducted on the Worldview-2 image. The reduced intra-specific variability allows the comparison of spectral analysis from both sensors. Figure 7.8 shows high variable beech spectra (left sub-image) and the normalised result (right sub-image). The reduction of these differences minimise the intra-specific variation. The right sub-image shows the normalised spectra of beech that are used for subsequent analysis.

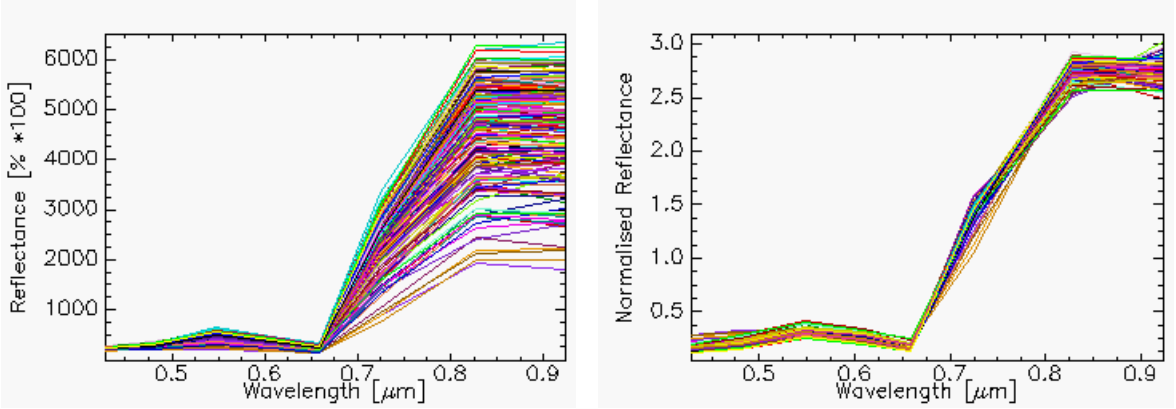

(a) Worldview-2 spectral library of collected beech spectra with high illumination differences and intra-specific variation

(b) Worldview-2 normalised spectral library of collected beech spectra with reduced illumination differences and intra-specific variation

Figure 7.8: Comparison of Worldview-2 spectra before (a) and after (b) spectral mean normalisation, which reduces illumination differences

7.4 Spectral analysis

The spectral analysis was conducted on the normalised reference spectra extracted from the images, based on forest inventory information. These reference spectra were collected separately for deciduous and coniferous as well as beech, fir and spruce within the masked images as described in section 6.2. Following subsections describe spectral analysis of species discrimination, as well as the results of classification methods in combination with the derived probability maps of each forest type and tree species distribution.

7.4.1 Principal Component Analysis

The PCA was calculated for visualising the reference data in two dimensions. It can be used as unsupervised classification method, that indicates distribution, discrimination and the overlap between classes.

Forest type PCA

The separability of forest type can quantify a statement towards possible forest type discrimination. As shown in figure 7.9 the PCA of HySpex VNIR and Worldview-2 normalised spectra show points in the plot, and each represents a single spectrum of deciduous and coniferous forest, respectively. Deciduous forest spectra (yellow points) spreads mainly within the second and third quadrant and coniferous forest spectra (green points) mainly in the first and fourth quadrant of the PCA plot. The overlap of both classes is slight and shows clear discrimination between the two classes for HySpex VNIR and Worldview-2. It confirms the information of figure 7.5 of the HySpex VNIR forest type spectra with standard deviation. It can be anticipated that forest type classes can be discriminated with both, hyperspectral and multispectral data.

The first and second principle component (PC 1 and PC 2) of normalised forest type spectra are shown in figure 7.9a for HySpex VNIR and in figure 7.9b for Worldview-2. PC 1 and PC 2 explain $85.41\ \%$ of variance for HySpex VNIR and $90.31\ \%$ for Worldview-2 spectra, respectively.

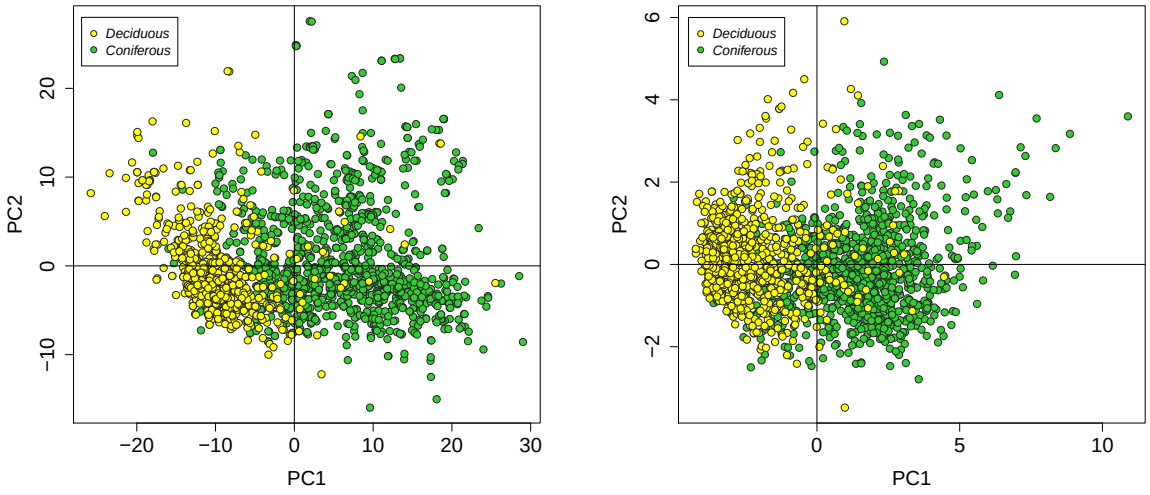

(a) PCA of forest type calculated from normalised HySpex VNIR spectra

(b) PCA calculated from normalised Worldview-2 spectra

Figure 7.9: PCA of normalised forest type spectra from HySpex VNIR and Worldview-2

The first and second PC loadings are shown in figure 7.10. They give an estimate which band might be appropriate for forest type discrimination. Peaks and troughs of the loadings graph show higher importance for forest type separation since $(loadings)^2$ is an evidence for variability of PC. Loadings of HySpex VNIR and Worldview-2 PCA show very similar results.

The main spectral ranges of variability according to the PC 1 are green to red (approximately 520 - 685 nm) and near infrared (approximately 750 - 940 nm). For PC 2 main spectral ranges are blue in visible (approximately 430 nm), red edge (approximately 735 nm) and near infrared (approximately 980 nm).

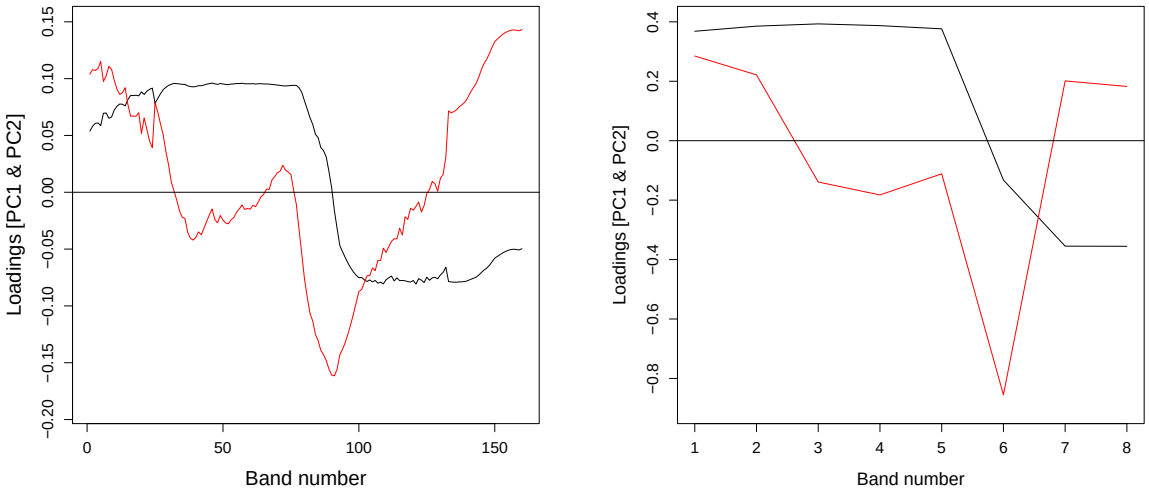

(a) PCA loadings of forest type calculated from normalised HySpex VNIR reference spectra

(b) PCA loadings calculated from normalised Worldview-2 reference spectra

Figure 7.10: PCA of normalised forest type spectra, PC 1 is coloured black and PC 2 is coloured red

Tree species PCA

The PCA of the three different tree species (beech, fir and spruce) shows a good separation of groups, see figure 7.11, which also confirms the tree species spectra with plotted standard deviation in figure 7.6. Each point in the plots represents a spectrum of the species spectral library. Beech (yellow points) and fir (light green points) spread mainly within the second and third quadrant and spruce (dark green points) spectra mainly in the first and fourth quadrant of the PC plot. The overlap of fir is significant with beech and spruce, due to the methodology of spectra collection. Beech and spruce spectra show only slight overlap. The PC 1 and 2 explain the same amount of variance (85.41% for HySpex VNIR and 90.31% for Worldview-2) as forest type.

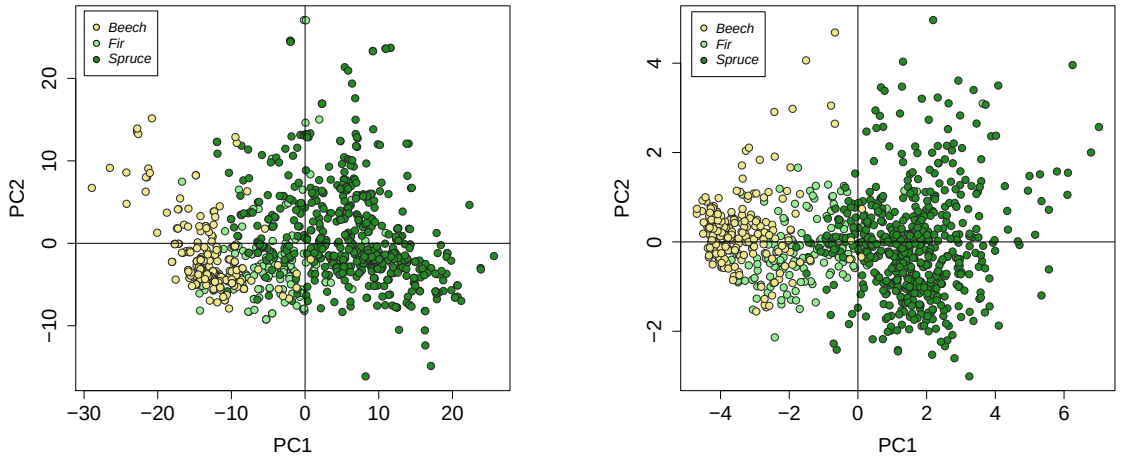

(a) PCA of tree species calculated from normalised HySpex VNIR reference spectra

(b) PCA of tree species calculated from normalised Worldview-2 reference spectra

Figure 7.11: PCA of normalised tree species reference spectra

The loadings of tree species show strong similarity to the forest type loadings. The variance is highest where loadings have maximum and minimum value, see figure 7.12. Also the main ranges are within the visible (approximately 520 - 685 nm) and near infrared (approximately 750 - 940 nm) for PC 1 and visible (approximately 430 nm), red edge (approximately 735 nm) and near infrared (approximately 980 nm) for PC 2.

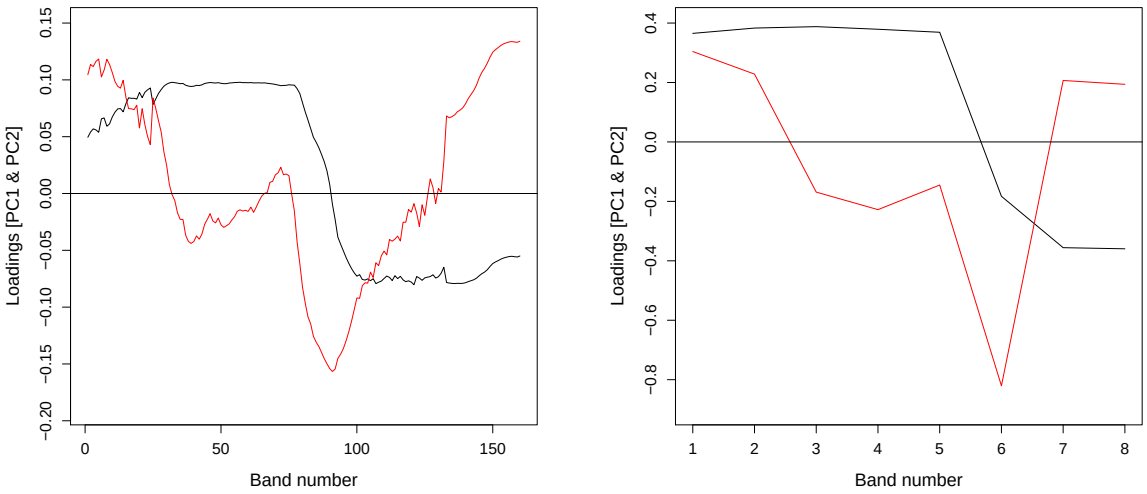

(a) PCA loadings of tree species calculated from normalised HySpex VNIR spectra

(b) PCA loadings of tree species calculated from normalised Worldview-2 spectra

Figure 7.12: Principal Component Analysis of normalised tree species spectra, PC 1 is coloured black and PC 2 is coloured red

7.4.2 Band extraction

The process of band extraction was performed on HySpex VNIR image only, due to the high number of spectral bands and their strong correlation.

Forest type band extraction

Image 7.13 shows the outcome of the GA results with the goal of selecting a maximum of eight bands, that are appropriate for forest type classification in HySpex VNIR image. The fitness function shows the fitness evolution across generations. It took 16 generations until the predefined fitness goal of $94\,\%$ accuracy was reached. The mean (all) fitness is the average fitness with considering all searches. It represents the expected fitness by generation. Mean (unfinished) is the average fitness of all searches without ending by a given generation.

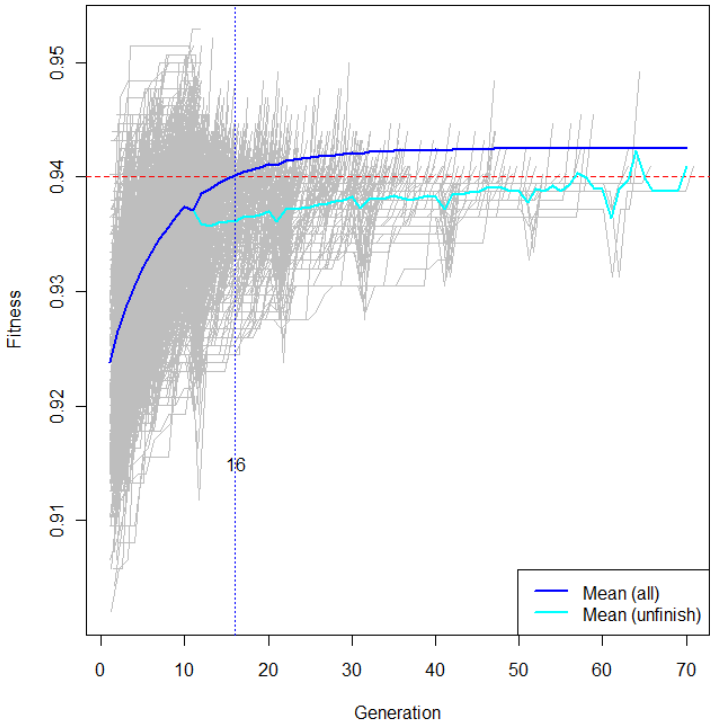

Figure 7.13: Fitness function of GA on HySpex VNIR reference spectra for forest type band extraction, with fitness function set to $94\ \%$

The GA selected bands and wavelength are listed in table 7.5. They show clear similarity to the first PC loadings of the visible range.

Table 7.5: Band numbers and wavelength of selected bands of HySpex VNIR for forest type discrimination using GA

Band number	Wavelength [nm]
20	484.49
31	524.35
40	556.96
49	589.57
59	625.80
73	676.53
80	701.89
86	723.63

These bands that were selected for optimal tree species discrimination are depicted in figure 7.14. The spectral bands that show most variation for forest type discrimination are located in the visible (6 bands) and red edge (2 band) range.

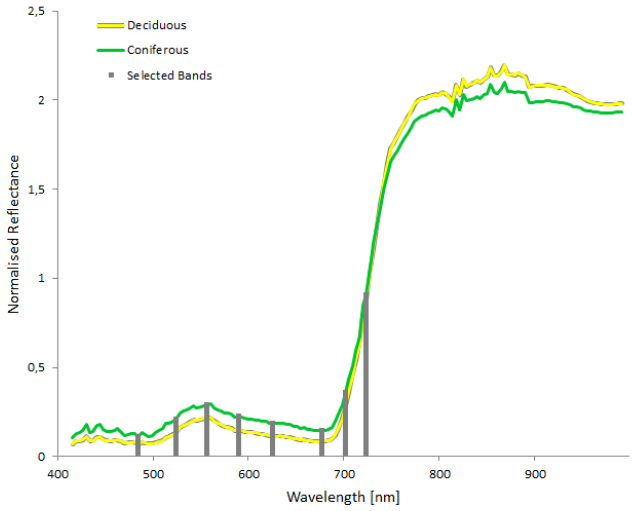

Figure 7.14: Selected bands for forest type delineation of normalised HySpex VNIR reference spectra

Tree species band extraction

Image 7.15 shows the fitness function of the GA results with the goal of selecting a maximum of eight bands appropriate for tree species classification. The fitness function shows, that it took 22 generations until the predefined fitness goal of 90 % accuracy was reached.

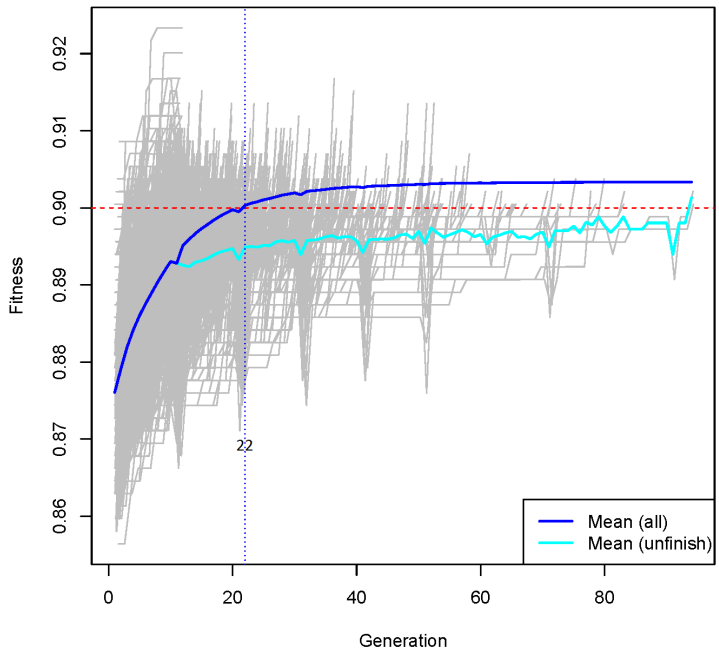

Figure 7.15: Fitness function of GA on normalised HySpex VNIR reference spectra for tree species band extraction, with fitness function set to 90 %

The selected bands are listed in table 7.6 and depicted in figure 7.16. The bands show clear similarity to the first PC loadings. Additionally the similarity to the loadings peak in the red edge range of the second PC shows high importance for tree species discrimination.

Table 7.6: Band numbers and wavelength of selected bands of HySpex VNIR for tree species discrimination using GA

Band number	Wavelength [nm]
26	506.23
55	611.31
82	709.14
93	759.00
111	814.21
114	825.08
128	875.81
140	919.29

The selected bands are more evenly spread within the spectral range of the sensor than the selected bands for forest type discrimination, see figure 7.16.

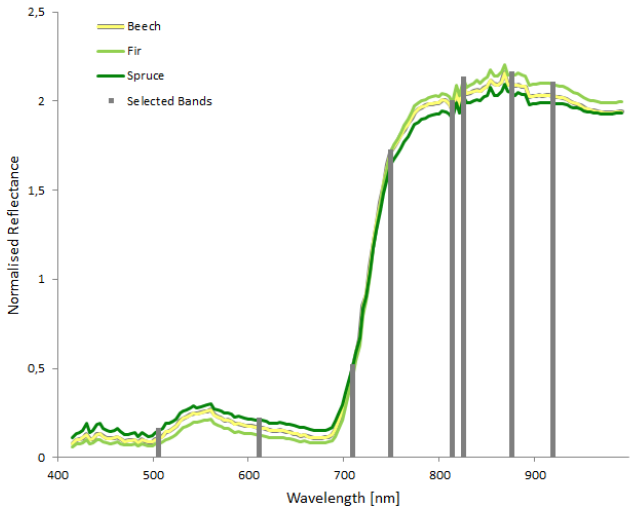

Figure 7.16: Selected bands of normalised HySpex VNIR reference spectra

7.4.3 Linear Discriminant Analysis

After applying the unsupervised classification method using PCA, the final classification of forest type and tree species was performed using the LDA, as explained in section 6.4. With LDA it was possible to delineate forest type and tree species and predict them on the image for graphical illustration of their occurrence.

Forest type classification

The plots in figure 7.17 show the separability of the forest type classes using LDA. Every density represents the test-spectra of deciduous and coniferous forest, that were predicted on the training-spectra. It shows similarity to the PCA with slight overlap between the classes, see figure 7.9. The overlap of HySpex VNIR spectra is slightly smaller than the overlap Worldview-2 spectra.

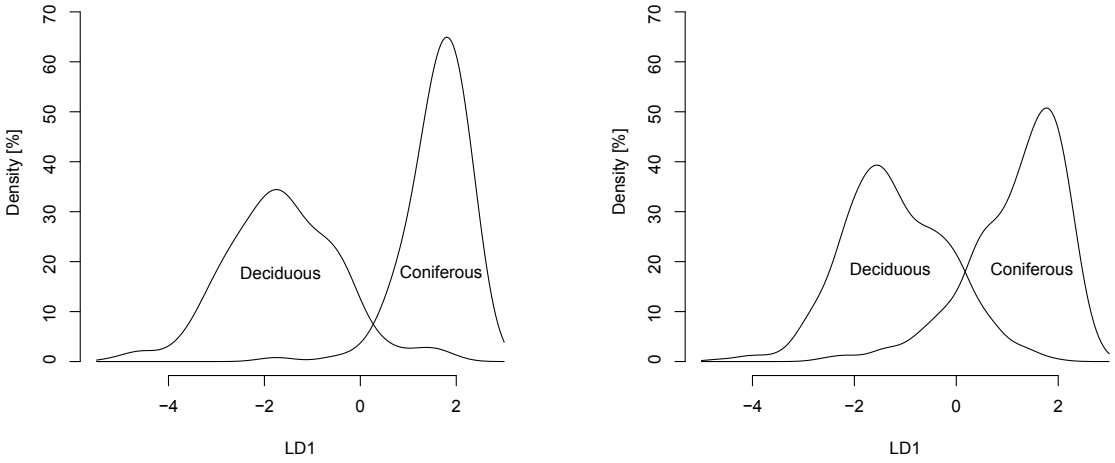

(a) LDA calculated from normalised HySpex VNIR reference spectra on basis of 8 extracted bands

(b) LDA calculated from normalised Worldview-2 reference spectra

Figure 7.17: LDA calculated with 1/3 train and 2/3 test data from normalised referenced spectra for forest type delineation

The loadings derived from LDA classification show the most variability of bands, which implies the importance for discrimination of forest type, see figure 7.18. A significantly high loading is shown in the selected band 2 of HySpex VNIR (524.35 nm) and band 3 of Worldview-2 (510-580 nm).

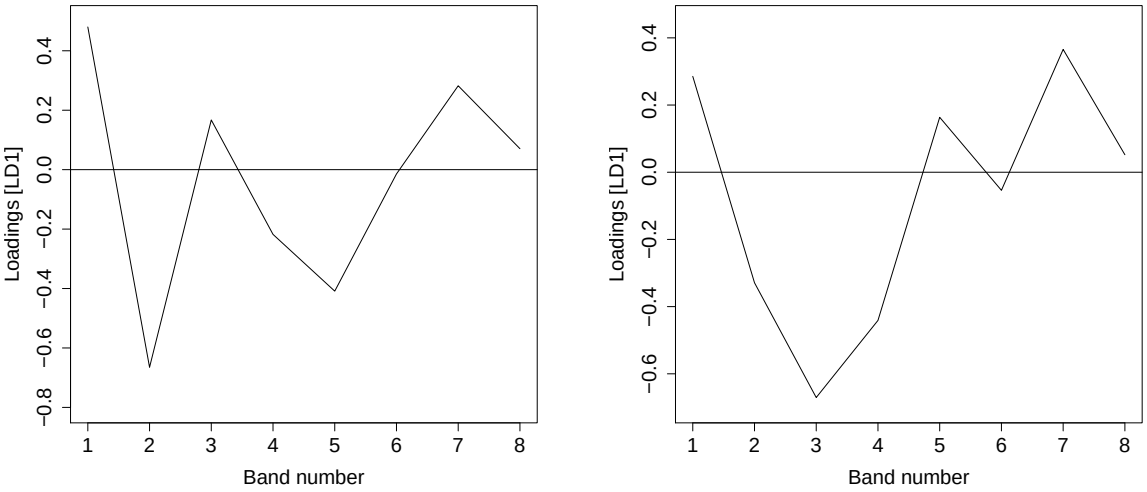

(a) LDA loadings calculated from normalised HySpex VNIR reference spectra on basis of 8 extracted bands

(b) LDA loadings calculated from normalised Worldview-2 reference spectra

Figure 7.18: LDA loadings derived from LDA classification with 1/3 train and 2/3 test spectra from normalised forest type reflectance spectra

Tree species classification

Both plots in figure 7.19 show the separability of the three tree species. The overlap of fir with beech and spruce is relatively high compared to overlap of beech and spruce. The LDA plots of HySpex VNIR and Worldview-2 show significant similarity to the PCA plot of the three tree species in figure 7.11. The HySpex VNIR LD 1 explains $97.92\,\%$ and LD 2 explains $2.08\,\%$ proportion of between-class variance. The Worldview-2 LD 1 explains $98.11\,\%$ and the LD 2 defines $1.89\ \%$ proportion of between-class variance, that is explained by successive discriminant functions.

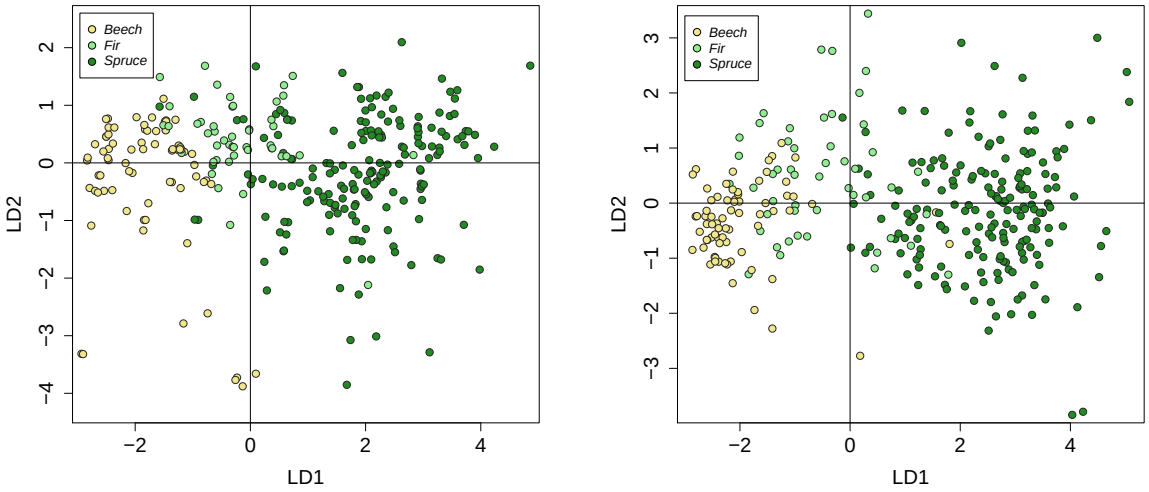

(a) LDA calculated from normalised HySpex VNIR spectra on basis of 8 extracted bands

(b) LDA calculated from normalised Worldview-2 spectra

Figure 7.19: LDA calculated with 1/3 train and 2/3 test data from normalised referenced spectra

Also the loadings derived from LDA tree species classification show the most importance of bands evenly spread for selected HySpex VNIR bands. The Worldview-2 loadings display different band importance than loadings for forest type, see figure 7.20. Significant high loadings shows the selected band 2 of HySpex VNIR for LD 1 (611.31 nm) and band 4 of LD 1 (585 - 625 nm) and band 5 in LD 2 (630 - 690) of Worldview-2.

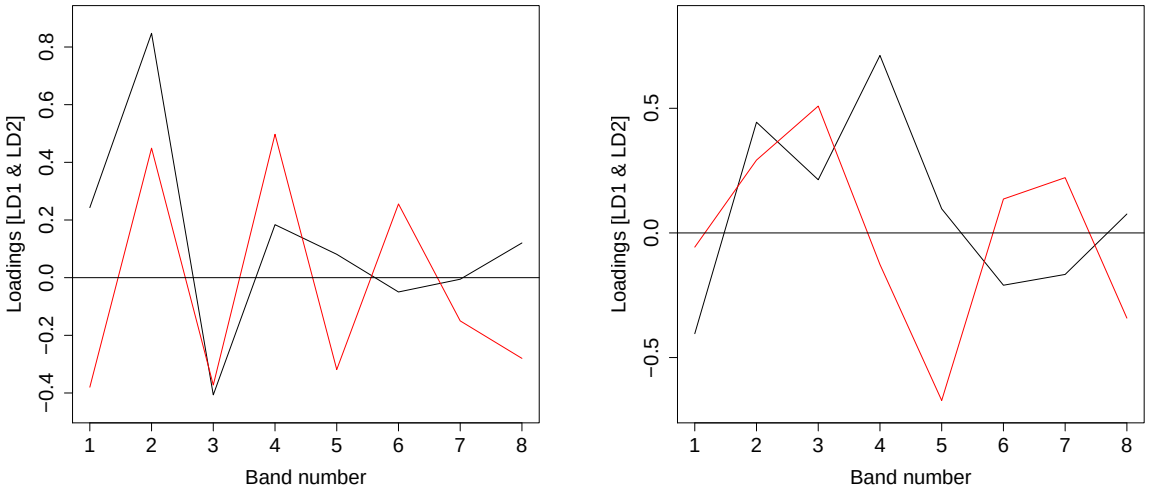

(a) LDA loadings calculated from normalised HySpex VNIR spectra on basis of 8 extracted bands

(b) LDA loadings calculated from normalised Worldview-2 spectra

Figure 7.20: LDA loadings derived from LDA classification with 1/3 train and 2/3 test data from normalised tree species reflectance spectra; LD 1 as black line and LD 2 as red line

7.4.4 Image classification

The following pages show the classification probabilities per forest type and tree species in HySpex VNIR with 8 selected bands and Worldview-2 image. Figures 7.21 and 7.22 show the classification probabilities for forest type and figures 7.24, 7.25 and 7.26 for tree species. The probability distribution for each species gives an estimate of how well the forest type and tree species were detected within each pixel. Only probabilities of 60 % and higher are displayed. Probabilities of less than 60 % are masked as unclassified and are displayed for each sensor separately in figure 7.23 and 7.27.

The distribution of spruce is similar for HySpex VNIR and Worldview-2 (figure 7.26), but beech and fir show much lower probabilities for HySpex VNIR in comparison to Worldview-2 (figure 7.24 for beech and 7.25 for fir). The discrimination of beech is similar in both sensors, but Worldview-2 shows a clearer separation of probabilities. The distribution of fir in HySpex VNIR shows only minimal probabilities, whereas Worldview-2 provides clearer separation, but also higher probabilities. Worldview-2 seems to separate the three tree species more distinct than HySpex VNIR.

Forest type classification

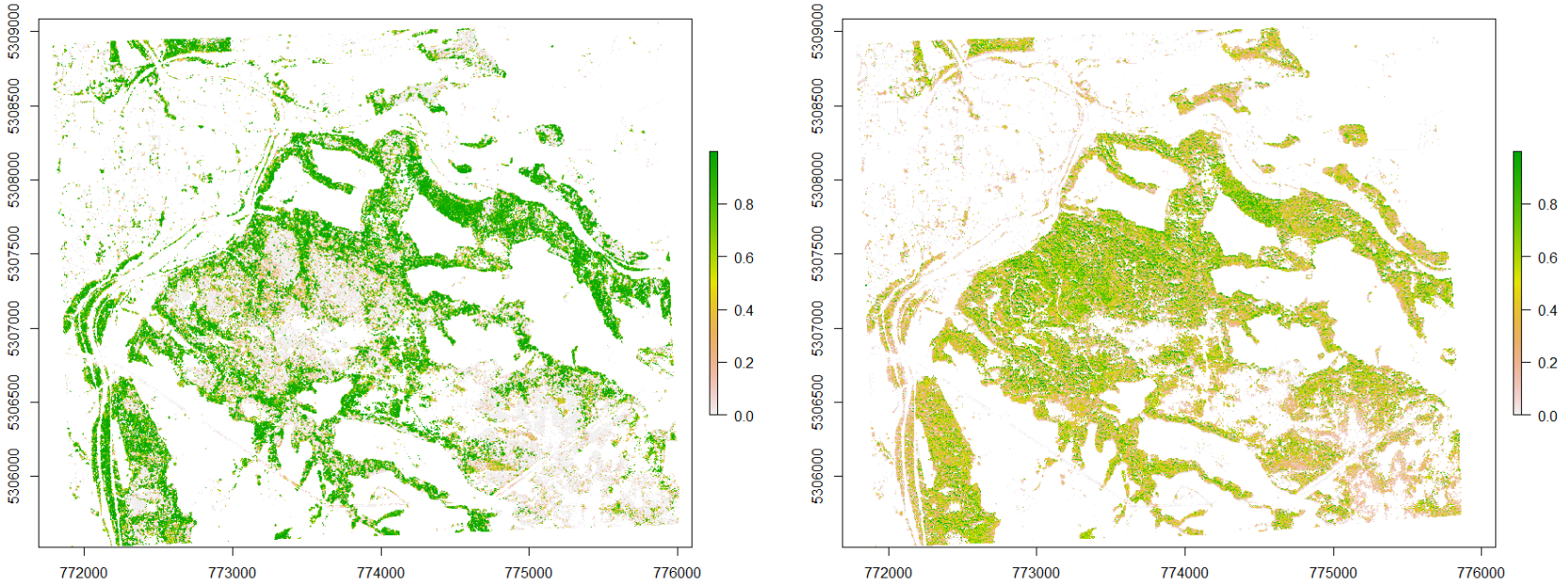

(a) Classification probabilities of deciduous trees on HySpex VNIR

(b) Classification probabilities of deciduous trees on Worldview-2

Figure 7.21: Probability distribution of deciduous forest in HySpex VNIR (a) and Worldview-2 (b) images

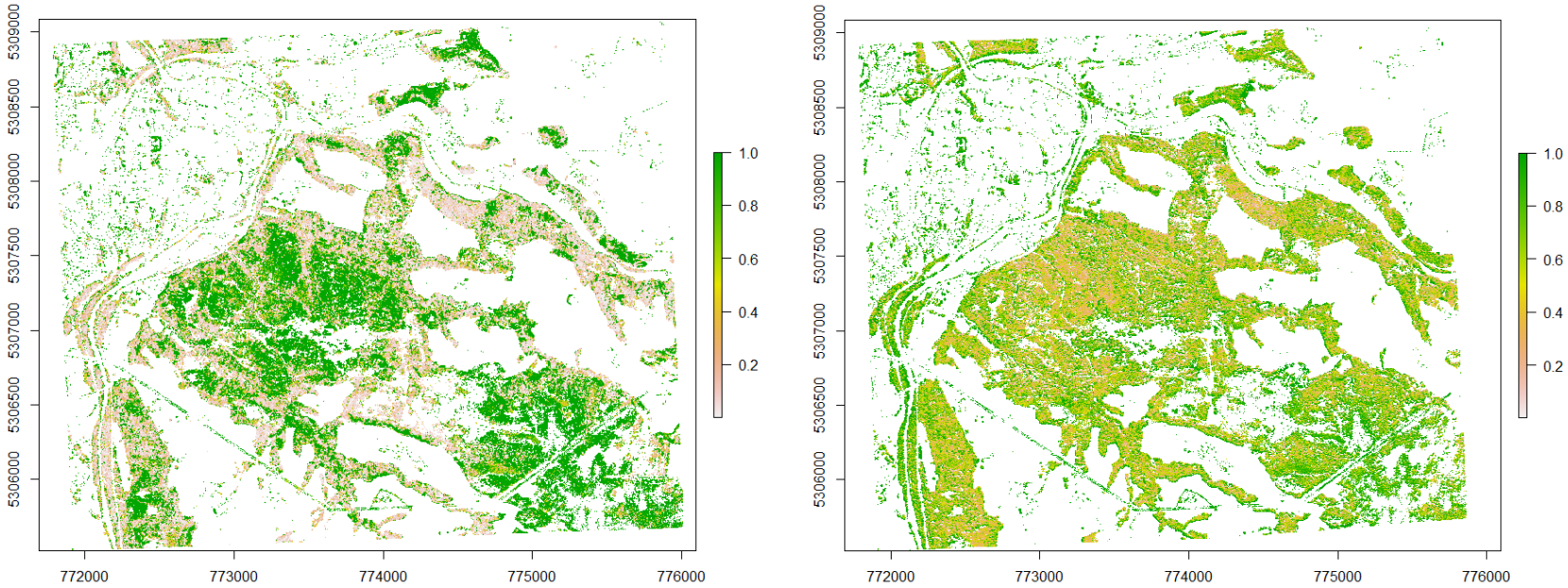

(a) Classification probabilities of coniferous trees on HySpex VNIR

(b) Classification probabilities of coniferous trees on Worldview-2

Figure 7.22: Probability distribution of coniferous forest on HySpex VNIR (a) and Worldview-2 (b) images

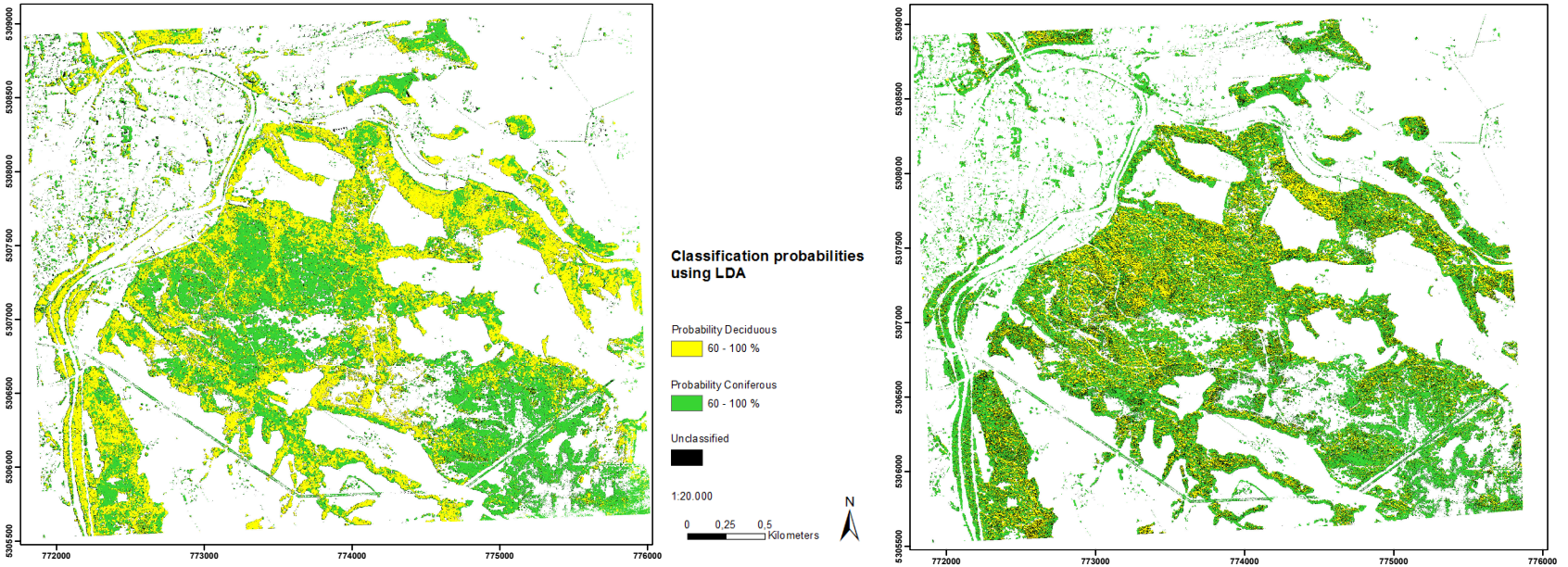

(a) Combined classification probabilities of deciduous and coniferous trees on HySpex VNIR

(b) Combined classification probabilities of deciduous and coniferous trees on Worldview-2

Figure 7.23: Combined classification probabilities with minimum of 60 % probability of occurrence of deciduous and coniferous forest on HySpex VNIR (a) and Worldview-2 (b) images

Tree species classification

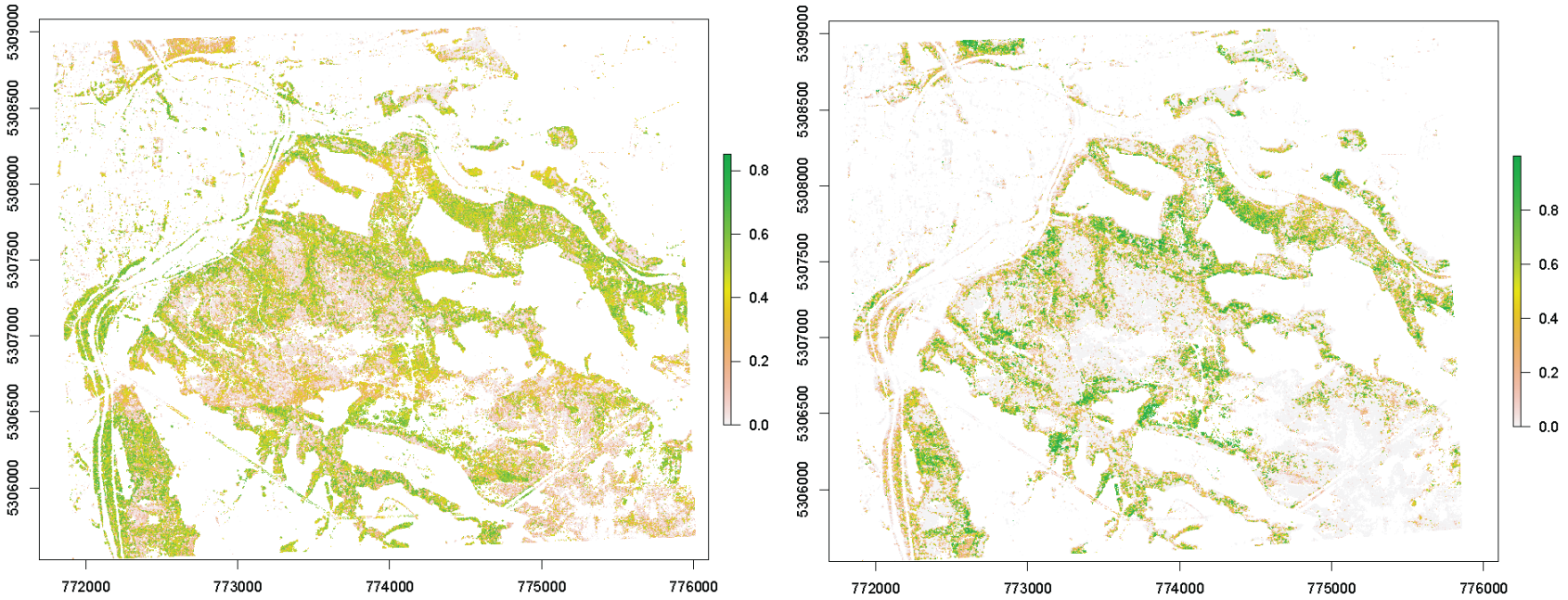

(a) Classification probabilities of beech on HySpex VNIR

(b) Classification probabilities of beech on Worldview-2

Figure 7.24: Probability distribution of European beech in HySpex VNIR (a) and Worldview-2 (b) images

(a) Classification probabilities of fir of HySpex VNIR

(b) Classification probabilities of fir of Worldview-2

Figure 7.25: Probability distribution of European silver fir in HySpex VNIR (a) and Worldview-2 (b) images

(a) Classification probabilities of spruce of HySpex VNIR

(b) Classification probabilities of spruce of Worldview-2

Figure 7.26: Probability distribution of Norway spruce in HySpex VNIR (a) and Worldview-2 (b) images

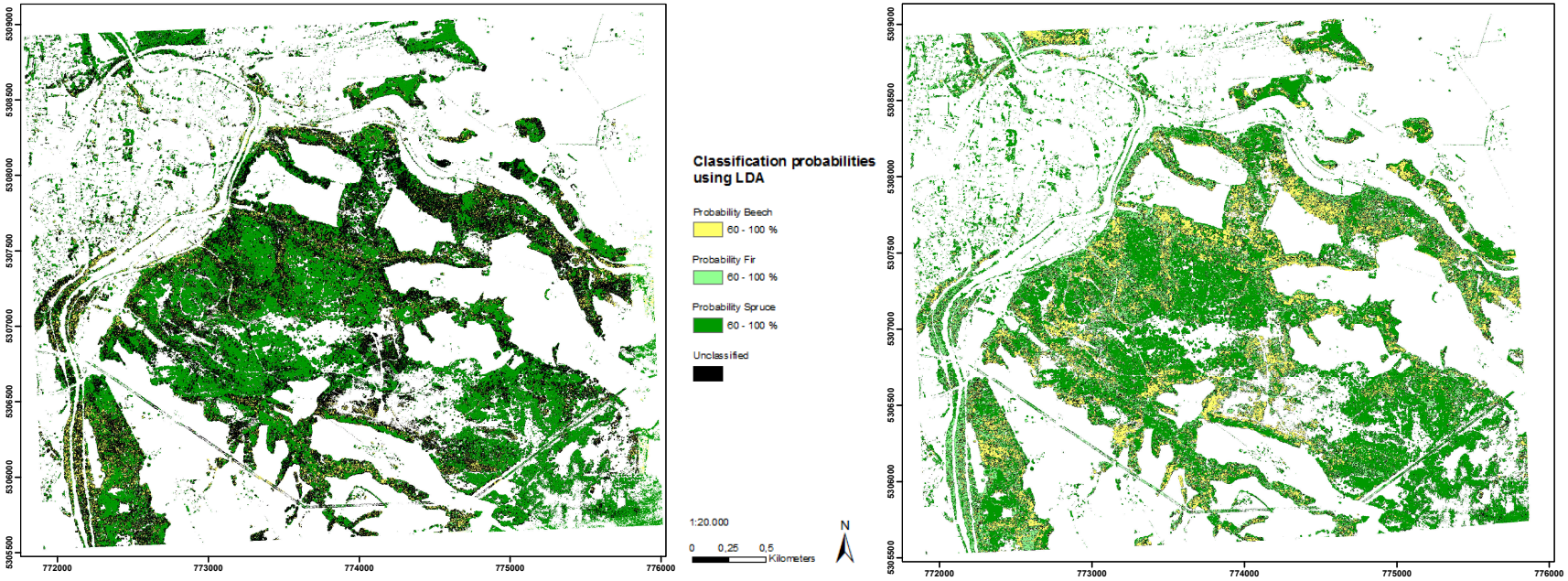

(a) Combined classification probabilities of beech, fir and spruce on HySpex VNIR

(b) Combined probabilities classification of beech, fir and spruce on Worldview-2

Figure 7.27: Combined probability classification with minimum of 60 % probability for European beech, European silver fir and Norway spruce on HySpex VNIR (a) and Worldview-2 (b) images

7.5 Accuracy assessment

The accuracy assessment is important for quantifying the classification method and the results. Tables 7.7 and 7.8 reveal the accuracy of the hyperspectral and multispectral forest type discrimination approach with an overall accuracy of $94.40\ \%$ and $87.76\ \%$, using selected reference spectra. Additionally, tables 7.9 and 7.10 show the accuracy assessment of the hyperspectral and multispectral tree species classification with an overall accuracy of $88.27\ \%$ and $86.68\ \%$. The accuracy assessment was conducted each on $2/3$ test spectra.

Forest type accuracy assessment

Table 7.7: User, Producer and Overall accuracy of LDA forest type classification of normalised HySpex VNIR test spectra

Forest type	Deciduous	Coniferous	Total	User accuracy
Deciduous	**487**	15	502	97.01 %
Coniferous	60	**777**	837	92.83 %
Total	547	792	**1264**	
Producer accuracy	89.03 %	98.12 %		**Overall accuracy: 94.40 %**

Table 7.8: User, Producer and Overall accuracy of LDA forest type classification of normalised Worldview-2 test spectra

Forest type	Deciduous	Coniferous	Total	User accuracy
Deciduous	**428**	60	488	87.70 %
Coniferous	104	**748**	852	87.79 %
Total	532	808	**1340**	
Producer accuracy	80.45 %	92.57 %		**Overall accuracy: 87.76 %**

The discrimination of tree species group using HySpex VNIR and Worldview-2 spectra show significant difference in accuracy. HySpex VNIR discriminated forest type by $94.40\ \%$ overall accuracy and producer and user accuracy show high values as well. Whereas the overall accuracy of forest type using Worldview-2 spectra shows an accuracy of 87.76%. The values for producer and user accuracy is similar to the overall accuracy.

Tree species accuracy assessment

Table 7.9: User, Producer and Overall accuracy of LDA classification of normalised HySpex VNIR test spectra

Specimen	Beech	Fir	Spruce	Total	User accuracy
Beech	**126**	1	0	127	99.21 %
Fir	21	**58**	30	109	53.21 %
Spruce	10	10	**358**	378	94.71 %
Total	157	69	388	**614**	
Producer accuracy	80.25 %	84.06 %	92.27 %		**Overall accuracy: 88.27 %**

Table 7.10: User, Producer and Overall accuracy of LDA classification of normalised Worldview-2 test spectra

Specimen	Beech	Fir	Spruce	Total	User accuracy
Beech	**112**	15	3	130	86.15 %
Fir	20	**55**	31	106	51.89 %
Spruce	2	10	**360**	372	96.77 %
Total	134	80	394	**608**	
Producer accuracy	83.58 %	68.75 %	91.37 %		**Overall accuracy: 86.68 %**

The discrimination of tree species, using HySpex VNIR and Worldview-2 spectra show slight difference in accuracy. HySpex VNIR discriminated tree species with $88.27\,\%$ overall accuracy, but producer and user accuracy show distinct values. Fir has lowest producer and user accuracy. Whereas the overall accuracy of tree species using Worldview-2 spectra shows a similar accuracy of $86.68\,\%$. The values for producer and user accuracy shows also distinct values, especially for fir.

8 Discussion and Outlook

This chapter discusses the applied methods and results, with possible improvements for them given in section 8.1. Section 8.2 evaluates the results of this analysis and gives an indication for applicability.

8.1 Evaluation of reference spectra collection

Following subsections evaluate the applied methodology and the influence of intra-specific variability for subsequent spectral analysis.

8.1.1 Spectral discrimination of forest tree species

The main goal of this thesis was to separate forest parameters, in particular forest type and tree species, based on their spectral characteristics. Figure 7.5 shows clear separation of forest type and figure 7.6 of tree species using mean reflectance with standard deviation. This suggests that discrimination of tree species based on spectral information is possible, taking into account, that three tree species were observed and more species might result in more overlap. Their difference in physiology especially the foliage, crown structure and of course the aspect of leaves and needles lead to different spectral characteristics. Certainly the main difference of deciduous and coniferous spectra result from phenology characteristics. Main phenology difference is the regrowth of completely shed leaves (deciduous) and regrowth of needles additional to remaining needles from past years (coniferous), that generates uneven amount of shading within the crown.

Spectral data

The reference spectra were derived from each image separately on basis of forest inventory data. Every spectra was defined by affiliation to species, type and age. Additional height metrics were extracted on basis of an existing DSM from 2010, see section 5.2. Through calculation of a forest mask and application on the images only tree spectra were collected. The aim of collecting was to gather reference spectra in pure stands (100 % proportion) per type and species. This was problematic, because Traunstein forest is comprised of heterogeneous forest stands with species and age variation as well as vertical and horizontal structure. This complicated the collection of several pure stands of more than two tree species (beech and spruce) out of the inventory plots. The purity had to be set down to 80 % for fir. This enabled the collection of three different tree species, beech, fir and spruce. The result was the collection of reference spectra from two species with pure stands and one specimen with a mixture of 20 % other tree species, in this case 80 % fir was mixed with 20 % spruce.

This explains the low classification rate for fir compared to beech or spruce, which are delineated with high percentages in user and producer accuracies, see below. So there is need for improvement regarding the reference spectra collection with aim of collecting more tree species with pure spectra.
After observing the collected spectra, height and age were grouped and trees under 10 m of height and under 30 years of age were culled in forest type to eliminate shaded trees. Traunstein as heterogeneous forest is characterised by multi-storeys and multi-ages and trees of lower age and height compared to surrounding trees might affect the classification rate negatively.
Reuter (2010) have used a similar method of sorting out shaded in-situ data by eliminating low reflectance values. That approach was considered as not appropriate, because it distorts the intra-specific variability, which is characteristic for each specimen.

8.1.2 Intra-specific variation of in-situ data reflectance spectra

Every spectral library collected from in-situ data showed high variability of spectra. This is highly influenced by the physiology of trees and their crowns, but also by the forest structure. Tree spectra can vary significantly by season and crown part. The crown is comprised of shaded and non-shaded leaves and they different optically. Also seasonal aspects influence the reflectance of tree species. Flowering trees and trees with fruits, such as beechmast and cones can vary in their reflectance. The acquisition date of HySpex VNIR and Worldview-2 data, which varied by one week in June 2012, influence the reflectance probably slightly, due to permanent phenological changes within the vegetation period. Usually beech begins to sprout in April to May and the leave surface appears different than later on in the year, see section 2.4. Also coniferous trees show these differences even if needles remain at the tree for several years, additional needles regrow every spring time. Additionally, the aspect of leaves and needles on the tree have an impact on the appearance since upper and lower surface differ slightly by colour (Clark et al., 2005, P. 377). Volume scattering is a typical phenomenon in tree crowns, where the reflectance is scattered several times within the crown before it reaches the sensor. This influences the intra-specific variance. However, every tree specimen has a typical crown structure through genetic characteristic and also varying by crown space (Vieilledent et al., 2010, P. 759), which influences the inter-specific variation. Figure 7.7 shows how much the intra-specific variance spreads and that this was successfully reduced by preprocessing for enhancing the ratio of inter- and intra-specific variation.

8.1.3 Error of collecting in-situ data reflectance spectra

The problems of spectra collection, discussed in subsection 8.1.1, shows that there are several points for improvement in that methodology. Reflectance spectra were derived from

the remote sensing imagery, using forest type and tree species percentage of inventory plots. This enables on one hand the comparability of spectral data from different imagery, but also inhabits possible inventory and position inaccuracies. The classification is only as good as the forest inventory data. The forest inventory was conducted in year 2008, which varies by four years to acquisition date of HySpex VNIR and Worldview-2 data, and can contain severe stand alteration. Also the LiDAR data were acquired in a different year (2010) and can vary in height distribution of June 2012.
Additional to temporal shift of data, spatial shift is an important factor. The inventory data were centred by ground reference of global positioning system (GPS). Due to less satellite reception within dense forest the positioning was probably of lower accuracy, which lead to a spatial shift of inventory plots and pixel collection of different tree species, consequently.
Also the influence of neighbouring trees from outside the plot might affect the reference spectra with crown overlap from different tree species. Furthermore, spectral mixture of leaves and substrate influenced probably the reference spectra, compare to section 4.1.
An improvement of spectral library would be to obtain inventory data simultaneously to remote sensing data acquisition and ground spectra collection of tree species obtaining ground truth data . With this method the problem of mixed spectra within a plot and exact allocation to tree species would be improved.

8.2 Assessment of methodology - Evaluation of spectral analyses

The statistical analysis of the reflectance spectra is the main part of this thesis and important for evaluating the information content of tree species classification. Since the classification is based on reference spectra, evaluated in section before, the classification results enclose the irregularities of reference spectra collection. This is clearly noticeable through accuracy assessment in table 7.9 and 7.10. The producer accuracy, which represents how well reference spectra are classified, are acceptable for the impure spectral library of fir. The user accuracy, which represents the probability that a reference spectra was classified into a given species, is definitely not of acceptance compared to the high accuracies of beech and spruce. This again results from the methodology of collecting reference spectra for the tree species.
The result of the classification accuracy gives an estimation how well the forest type and species were separated and with which confidence their prediction in the image was possible, discussed in subsection 8.2.3 and 8.2.4.

8.2.1 Results of the PCA and their value of information

The results of the PCA show overlap of forest type and tree species spectra, respectively. This shows the contained inconsistency of spectra collection, due to impure fir spectra. The overlap of fir with beech and spruce reveals the difficult discrimination of fir from the other

two species.
The PCA loadings were helpful to explore important and unimportant wavelengths for forest type and tree species discrimination. Variance of band information is derived of $(loadings)^2$, the higher the distance of band loading from $y = 0$, the more information contain these bands for forest type and tree species delineation. The loadings of forest type PCA show clearly that most important wavelength are located in the blue and near infrared and especially the red edge range. Chubey et al. (2006) and Holmgren and Persson (2004) stated, that differentiating between coniferous and deciduous forest is not difficult when near infrared wavelengths were obtainable, compare figure 7.9.
Also Clark and Roberts (2012) and Ozdemir and Karnieli (2011) stated the importance of red-edge for tree species classification. Blue range importance can be explained by varying chlorophyll a and chlorophyll b content of foliar, which is causal related to red-edge reflectance (Curran et al., 1990, P. 35) and the phenological state of vegetation (Blackburn, 2007, P. 856). The information derived from the PCA serve as first evidence for possibility of forest type and tree species discrimination for both sensors. In comparison to PCA results the band extraction for HySpex VNIR shows clearly similarities.

8.2.2 Band extraction of hyperspectral HySpex VNIR data and their relation to PCA results

In this thesis a GA, $galgo$ in R was used for feature extraction and is based on a supervised classification method (the maximum likelihood classifier). The GA extracts bands, that reach combined the best classification accuracy. The iterative process of selecting band combinations, that contain important information for forest type and tree species discrimination is explained in section 6.4.
The selected bands are described with their wavelength information in table 7.5 for forest type, and table 7.6 describes the selected bands for tree species discrimination. The number of bands extracted, was set to the Worldview-2 band amount for comparison.
The band selection for forest type shows slight correlation to the important bands from PCA loadings, compare selected bands in figure 7.14 to figure 7.10. However, this contradicts Chubey et al. (2006) and Holmgren and Persson (2004), that near infrared is important for forest type discrimination, since no important band was found in that spectral range. It needs to be mentioned, that the spectral mean normalisation reduced amplitude variations of deciduous and coniferous forest. These variations are significantly in the near infrared region and influenced the band selection, probably. Contrary to forest type, the trend shows, that red-edge and near infrared ranges contain obviously most information for tree species classification, since six of eight bands were selected in these regions, see figure 7.16. This shows the statement of Clark and Roberts (2012) and Ozdemir and Karnieli (2011), that

these spectral ranges are important for tree species discrimination. Apart from that, the spectral noise, obvious in the near infrared region, may has contributed to the high number of 4 extracted bands in near infrared, see figure 7.16. Contrary the band extraction for forest type showed same noise, but no bands were extracted in the noise influenced spectral range. Therefore, spectral smoothing of the HySpex VNIR spectra was not considered, due to the resulting reduction of spectral characteristics, that is important for forest type and tree species discrimination. Also the impure spectra for fir may have contributed to the band selection. It is possible, that different bands might be extracted when the reference spectra are evenly spread in number and purity.
Pinnel (2007); Latifi et al. (2012) and Zhuo et al. (2008) have also applied a GA successfully for hyperspectral feature extraction. Since the results for forest type and tree species yielded satisfying classification outcomes, the GA would be used in next analyses based on hyperspectral data. It needs to be mentioned, that more than one chromosome and band combination is appropriate for further classification. Also the outcome of separate GA calculations with same input parameters show different results. Additional to this, distinct amount of classes to be separated, changes the fitness goal and the band combination as logical reasoning.
Further spectral analysis was based on these selected bands for improving the classification results and the time of processing.

8.2.3 Classification of forest type and tree species applying LDA

The aim of this thesis was to compare HySpex VNIR and Worldview-2 data for forest type and tree species classification, and therefore were eight bands selected from HySpex VNIR, see section 6.4. Utilisation of these bands reached an overall accuracy regrading forest type of $94.40\ \%$ for HySpex VNIR and $87.76\ \%$ for Worldview-2. In comparison, the sensors attained an overall accuracy of $88.27\ \%$ and $86.68\ \%$ regarding tree species discrimination with same amount of bands.
The PCA analysis of reflectance data and their information content for tree species discrimination showed, that the classification can be successfully applied. The classification accuracy in section 7.5, showed higher differences in forest type discrimination, than tree species discrimination for HySpex VNIR ($94.40\ \%$) and Worldview-2 ($87.76\ \%$). Both times revealed HySpex VNIR with different bands per classification the highest accuracy but Worldview-2 accuracy dropped only by approximately 1% percent from forest type to tree species classification. Whereas HySpex VNIR classification of tree species did drop by 6% from forest type accuracy. This results in similar accuracies of tree species for HySpex VNIR with $88.27\ \%$ and Worldview-2 with $86.68\ \%$. This reveals that Worldview-2 is comparable in tree species detection to HySpex VNIR sensor.

Possible errors of classification again arise from reference spectra collection and their unequal numbers and mixture percentages. Also of course the LDA classification with R in package $MASS$ has several parameters that can be set and they might affect the classification rate. Using a reference image for accuracy prediction on image basis also might improve the classification, due to statements of pure tree species pixel locations. Certainly all errors from prior analysis steps that prepared the classification were carried through to the final result.

8.2.4 Image classification of forest type and tree species predicting LDA classification

The classification of reference spectra was predicted on the related forest mask of HySpex VNIR and Worldview-2. The probability distribution within the forested areas are shown for forest type in figures 7.21 and 7.22, and for tree species in figures 7.24, 7.25 and 7.26. This gives an estimate of forest type and tree species distribution in Traunstein forest. Additional to that, a combined map of forest type and separately all three species per sensor with a minimal occurrence probability of 60 % was generated, see figures 7.23 and 7.27.
HySpex VNIR shows for forest type discrimination the highest accuracies. This can also be seen in the probability maps per class and combined, which shows clearer separation than the Worldview-2 image. In contrary to that, the probability images and the combined images for tree species are obviously variant in probability prediction. Even if HySpex VNIR reveals a higher accuracy than Worldview-2, the prediction on the image shows, that Worldview-2 separated the tree species with higher probability. Only spruce was predicted with high occurrence in the probability maps of both sensors. As a consequence, spruce is the tree species that can be discriminated of both sensors with high probability within the image.
The variant probability of HySpex VNIR and Worldview-2 might result from the much narrower bands from HySpex VNIR compared to Wolrdview-2 FWHM, see table 5.2 and 5.4. The FWHM of HySpex VNIR is evenly distributed with 3.5 nm per band, whereas Worldview-2 shows broader FWHM for all bands. Also the spectral range covered in a HySpex VNIR band is much narrower but more selective than the broad and averaged range covered in a Worldview-2 band. This leads to a higher rate of spectral features detected in HySpex VNIR bands than the bands of Worldview-2. This also could be an indicator for more sensitivity of HySpex VNIR than Worldview-2 towards the discrimination of a higher amount of classes. It is important to state, that the probability estimation of these tree species in the Worldview-2 image is not of higher quality only because the delineation is more intense. A higher amount of classes may set clearer distinction between HySpex VNIR and Worldview-2 and states probably better which sensor is more appropriate for tree species classification.

8.3 Outlook for prospective forest parameter detection

The presented approach of forest parameter detection and classification was based on spectral analysis and the information content, that can be derived using same spatial resolution, but diverse spectral information of imagery. Further research based only on spectral information can be enhanced by using equal amount of reference spectra with equal validity per class, since the subsequent analysis is based on the collected spectra and an unequal amount of spectra, and their purity affect the result and validity. Also a higher amount of tree species might show more distinctive results and could stabilise the applicability of sensor type. The selection of at least two tree species for deciduous and two for coniferous forst will help to increase the significance of discrimination. When using a higher spatial resolution more parameters could be analysed and through crown segmentation single trees with their characteristic physiology might be detectable. However, the drawbacks of higher spatial resolution, such as high computational load and higher spectral complexity of different objects, should not be neglected.

Crown segmentation could be applied in general, if higher spatial resolution of 1 m and more existed, since single trees in a dense multi-storey forest might be difficult to detect. The advantage of crown delineation could be observed, if it improves the classification significantly.

Forest parameters need to be observed in regular time intervals for forest inventory and remote sensing becomes more important for inventory. The analysis of fast response after short-termed impacts, using remote sensing data could also be applicable and combined with inventory. An automated operational and objective approach for tree species and ongoing parameters, such as vitality, might be useful.

By avoiding the high costs of airborne hyperspectral data acquisition, several new sensors are planned and might be practicable for large-scale hyperspectral forest parameter detection. The Environmental Mapping and Analysis Program (EnMAP) is a spaceborne sensor system with high spectral but low spatial resolution. Since the sensor covers more area, it would be a cost-effective alternative to airborne HySpex VNIR or Worldview-2 data.

9 Conclusion

Forest type and three tree species as reference classes were used with different amount of spectra. These classes were deciduous and coniferous forest as forest type and tree species were European beech, European silver fir and Norway spruce. The final analysis of reference spectra showed that PCA and following LDA was successful delineating forest type with approximately 94 and 88 % for HySpex VNIR and Worldview-2. Tree species were classified also with high accuracies of approximately 88 and 86 % for both sensors which enables to conclude that HySpex VNIR and Worldview-2 are both suitable for forest parameter detection.

Higher amount of tree species and purer reference spectra might find more intense differences that could enable to a more distinctive conclusion of sensor suitability for the study objective. Recommended bands that are important for tree species discrimination are spread in chlorophyll absorption regions in blue and red range. Also important is the red edge region where at least one band should be present and the near infrared region with important information about tree species discrimination. Since the classification results were appropriate using 8 bands the ideal sensor for tree species discrimination should have approximately 8 bands as well.

A final probability distribution map per forest type and tree species as combined image was prepared for descriptive display of spatial tree species occurrence.

An outlook for possible analysis enhancement of the deployed methods and of different methods was given which might lead to further studies having similar objectives.

10 Summary

Cost-effective forest parameter detection is an important issue in modern forestry management since inventory is time consuming and expensive. Detection of forest and tree species becomes more important in climate change with high impact on Norway spruce which is main tree species in Bavaria. Due to its anthropogenic influenced high distribution on unsuited sites towards soil type, water supply and climate influences, spruce is highly predisposed for biotic and abiotic impacts. Detecting forest parameters, such as tree species helps to observe their distribution and possible damage.
Remote sensing enables such forest parameter detection, using different sources of information available. The latest state of the art uses hyperspectral, multispectral and LiDAR data separate or combined.

In this thesis hyperspectral airborne sensor data from HySpex VNIR were analysed, classified and compared to multispectral spaceborne data from Worldview-2. The aim was to evaluate the information content of HySpex VNIR data in respect to delineating spectral forest parameter and transferring these results to Worldview-2 sensor. Imaging spectroscopy is not yet well established as regular repeatable and cost-effective data acquisition with high areal coverage compared to satellite data but offers more spectral information and mostly higher spatial resolution than spaceborne sensors. For widespread forest cover classification alternatives of multispectral satellites might be important.
Therefore similar spatial resolution of both sensors was chosen for equal condition in this analysis. Also the acquisition date was within one week in June 2012 which reduced the possible errors by phenology differences of the observed forest.
The preprocessing of the sensor data was deducted using Atcor-3 and Atcor-4 for atmospheric correction and ORTHO for ortho-rectification. Several more procedure were performed that enhanced the data and normalised them for better comparison and reduction of illumination effects arising from different acquisition dates and BRDF effects within the images.
Further processes for forest masking were performed using ENVI IDL 4.8 and ArcGIS 10.1 and the final analysis of the reference spectra and the preprocessed images were realised using R 12.2 and 15.2 combined with different packages.

Bibliography

Albertz, J., 2009. Einführung in die Fernerkundung, 4th Edition. Wissenschaftliche Buchgesellschaft, Darmstadt.

Bachmann, M., Habermeyer, M., Müller, A., Müller, R., Schneider, M., Storch, T., 2010. Operational quality control for hyperspectral data. In: ESA Hyperspectral Workshop.

Bahrenberg, G., Giese, E., Nipper, J., 1992. Statistische Methoden in der Geographie, 2nd Edition. Vol. 2 Multivariate Statistik. Teubner Verlag.

Baumann, P. R., 2009. History of Remote Sensing, Satellite Imagery, Part II. http://www.oneonta.edu/faculty/baumanpr/geosat2/RS20History20II/RS-History-Part-2.html, [accessed online 13-March-2013].

Blackburn, G. A., 1998. Quantifying Chlorophylls and Caroteniods at Leaf and Canopy Scales: An Evaluation of Some Hyperspectral Approaches. Remote Sensing of Environment 66 (3), 273–285.

Blackburn, G. A., 2007. Hyperspectral remote sensing of plant pigments. Journal of experimental botany 58 (4), 855–867.

BMELV (Bundesministerium für Ernährung, Landwirtschaft und Verbraucherschutz), 2002. Bundeswaldinventur^2. http://www.bundeswaldinventur.de/enid/31.html, [accessed online 06-February-2013].

Breiman, L., 2001. Random forests. Machine Learning 45 (1), 5–32.

Bucher, H., 2004. Abies alba. In: Schütt, Weisgerber, Schuck, Lang, Roloff, Stimm (Eds.), Lexikon der Nadelbäume. Nicol Verlagsgesellschaft mbH & Co. KG, pp. 2–5, 9, 12–14.

Buddenbaum, H., Schlerf, M., Hill, J., 2005. Classification of coniferous tree species and age classes using hyperspectral data and geostatistical methods. International Journal of Remote Sensing 26 (24), 5453–5465.

Bunting, P., Lucas, R., 2006. The delineation of tree crowns in Australian mixed species forests using hyperspectral Compact Airborne Spectrographic Imager (CASI) data. Remote Sensing of Environment 101 (2), 230–248.

Campbell, J. B., 2006. Introduction to Remote Sensing. Taylor & Francis.

Carter, G., Knapp, A., 2001. Leaf optical properties in higher plants: Linking spectral characteristics to stress and chlorophyll concentration. American Journal of Botany 88 (4), 677–684.

Cho, M. A., Mathieu, R., Asner, G. P., Naidoo, L., van Aardt, J., Ramoelo, A., Debba, P., Wessels, K., Main, R., Smit, I. P. J., Erasmus, B., 2012. Mapping tree species composition in South African savannas using an integrated airborne spectral and LiDAR system. Remote Sensing of Environment 125, 214–226.

Chubey, M. S., Franklin, S. E., Wulder, M. A., 2006. Object-based Analysis if Ikonos-2 Imagery for Extraction of Forest Inventory Parameters. Photogrammetric Engineering & Remote Sensing 72 (4), 383–394.

Clark, M., Roberts, D., Clark, D., 2005. Hyperspectral discrimination of tropical rain forest tree species at leaf to crown scales. Remote Sensing of Environment 96 (3-4), 375–398.

Clark, M. L., Roberts, D. A., 2012. Species-Level Differences in Hyperspectral Metrics among Tropical Rainforest Trees as Determined by a Tree-Based Classifier. Remote Sensing 4 (6), 1820–1855.

Curran, P., Dungan, J., Gholz, H., 1990. Exploring the Relationship between Reflectance Red Edge and Chlorophyll Content in Slash Pine. Tree physiology 7 (1-4), 33–48.

Cutler, D. R., Edwards, Jr., T. C., Beard, K. H., Cutler, A., Hess, K. T., 2007. Random forests for classification in ecology. Ecology 88 (11), 2783–2792.

Dalponte, M., Bruzzone, L., Gianelle, D., 2008. Fusion of hyperspectral and LIDAR remote sensing data for classification of complex forest areas. IEEE Transactions on Geoscience and Remote Sensing 46 (5), 1416–1427.

Darga, R., 2009. Auf den Spuren des Inn-Chiemsee-Gletschers -Übersicht-. Wanderungen in die Erdgeschichte. Verlag Dr. Friedrich Pfeil.

de Boer, T. A., 1993. Botanical Characteristics of Vegetation and their Influence on Remote Sensing. In: Buiten, H. J., Clevers, J. G. (Eds.), Land Observation by Remote Sensing, 1st Edition. Current Topics in Remote Sensing. Gordon and Breach Science Publishers, pp. 89 – 103.

Deering, D., Ahmad, S., Eck, T., Banerjee, B., 1995. Temporal attributes of the bidirectional reflectance for three boreal forest canopies. IEEE.

Digital Globe, unknown. WorldView-2 Data sheet. http://www.digitalglobe.com/downloads/WorldView2-DS-WV2-Web.pdf, accessed online 17-February-2013.

Elatawneh, A., Tian, J., Schneider, T., Reinartz, P., 2012. Erkennen von Strukturveränderungen in heterogener Waldgebiete: Welche Auflösung wird für Aussagen auf Betriebsebene benötigt? AFZ-Der Wald 18, 17–19.

FAO (Food and Agriculture Organization of the United Nations - Forestry Department), 2000. On Definitions of Forest and Forest Change. Working Paper 33, 7.

Felbermeier, B., Mosandl, R., 2006. Fagus sylvatica. In: Schütt, Weisgerber, Schuck, Lang, Roloff, Stimm (Eds.), Enzyklopädie der Laubbäume. Nicol Verlagsgesellschaft mbH & Co. KG, pp. 242–247, 253–255.

Feret, J.-B., Asner, G. P., 2012. Semi-Supervised Methods to Identify Individual Crowns of Lowland Tropical Canopy Species Using Imaging Spectroscopy and LiDAR. Remote Sensing 4 (8), 2457–2476.

Gitelson, A., Gritz, Y., Merzlyak, M., 2003. Relationships between leaf chlorophyll content and spectral reflectance and algorithms for non-destructive chlorophyll assessment in higher plant leaves. Journal of Plant Physiology 160 (3), 271–282.

Gitelson, A., Merzlyak, M. N., 1994. Spectral Reflectance Changes Associated with Autumn Senescence of Aesculus hippocastanum L. and Acer platanoides L. Leaves. Spectral Features and Relation to Chlorophyll Estimation. Journal of Plant Physiology 143 (3), 286–292.

Goel, N. S., 1988. Models of vegetation canopy reflectance and their use in estimation of biophysical parameters from reflectance data. Remote Sensing Reviews 4 (1), 1–212.

Goetz, A. F. H., 1992. Principles of Narrow Band Spectrometry in the Visible and IR: Instruments and Data Analysis. In: Toselli, F., Bodechtel, J. (Eds.), Imaging Spectroscopy: Fundamentals and Prospective Applications. Kluwer Academic Publishers, pp. 21 – 32.

Goetz, A. F. H., Gregg, V., 1985. Imaging Spectroscopy for Earth Remote Sensing. Science 228 (4704), 1147–1153.

Habermeyer, M., Müller, A., Holzwarth, S., Richter, R., Müller, R., Bachmann, M., Seitz, K.-H., Seifert, P., Strobl, P., 2005. Implementation of the Automatic Processing Chain for ARES. In: EARSeL Workshop on Imaging Spectroscopy. pp. 67–75, proceedings of 4th EARSeL Workshop on Imaging Spectroscopy. New quality in environmental studies.

Hapfelmeier, A., Ulm, K., 2013. A new variable selection approach using Random Forests. Computational Statistics & Data Analysis 60, 50–69.

Heinzel, J., Koch, B., 2012. Investigating multiple data sources for tree species classification in temperate forest and use for single tree delineation. International Journal of Applied Earth Observation and Geoinformation 18, 101–110.

Holmgren, J., Persson, A., 2004. Identifying species of individual trees using airborne laser scanner. Remote Sensing of Environment 90 (4), 415–423.

Howard, J. A., 1991. Remote Sensing of Forest Resources, 1st Edition. Remote Sensing Applications. Chapman & Hall.

Huete, A., Jackson, R., Post, D., 1985. Spectral Response of a Plant Canopy with Different Soil Backgrounds. Remote Sensing of Environment 17 (1), 37–53.

Jacquemoud, S., Baret, F., 1990. Prospect - a Model of Leaf Optical-Properties Spectra. Remote Sensing of Environment 34 (2), 75–91.

Jäger, E. J., Neumann, S., Ohmann, E., 2003. Botanik, 5th Edition. Spektrum Akademischer Verlag.

Jones, H. G., Vaughan, R. A., 2010. Remote sensing of vegetation, 1st Edition. Oxford University Press.

Jones, T. G., Coops, N. C., Sharma, T., 2010. Assessing the utility of airborne hyperspectral and LiDAR data for species distribution mapping in the coastal Pacific Northwest, Canada. Remote Sensing of Environment 114 (12), 2841–2852.

Kölling, C., Ammer, C., 2006. Waldumbau unter den Vorzeichen des Klimawandels. AFZ/Der Wald 20, 1086–1089.

Landesamt für Vermessung und Geoinformation, unknown. Digitales Geländemodell 1 (DGM 1) aus Laserscanning. http://vermessung.bayern.de/geobasis_lvg/gelaendemodell/DGM1.html, [accessed online 11-March-2013].

Latifi, H., Fassnacht, F., Koch, B., 2012. Forest structure modeling with combined airborne hyperspectral and LiDAR data. Remote Sensing of Environment 121, 10–25.

Leckie, D. G., Gougeon, F. A., Walsworth, N., Paradine, D., 2003. Stand delineation and composition estimation using semi-automated individual tree crown analysis. Remote Sensing of Environment 85 (3), 355–369.

Lee, K., Cohen, W., Kennedy, R., Maiersperger, T., Gower, S., 2004. Hyperspectral versus multispectral data for estimating leaf area index in four different biomes. Remote Sensing of Environment 91 (3-4), 508–520.

LfU (Bayerisches Landesamt für Umwelt), 2010. Altmoräne, Jungmoräne mit Wallform.

LfU (Bayerisches Landesamt für Umwelt), 2012. Der Klimawandel in Bayern Auswertung regionaler Klimaprojektionen Klimabericht Bayern.

Lillesand, T. M., Kiefer, R. W., 1994. Remote Sensing and Image Interpretation, 3rd Edition. John Wiley & Sons, Inc.

Measures, R. M., 1992. Laser Remote Sensing, 2nd Edition. Krieger Publishing Company.

Müller, R., Lehner, M., Müller, R., Reinartz, P., Schroeder, M., Vollmer, B., 2002. A program for direct georeferencing of airborne and spaceborne line scanner images. In: ISPRS, Commission I, WG I/5. Vol. 103. pp. 148–153.

Müller-Kroehling, S., Walentowski, H., Bußler, H., Kölling, C., 2009. Natürliche Fichtenwälder im Klimawandel - Hochgradig gefährdete Ökosysteme. In: Fichtenwälder im Klimawandel. Bayerische Landesanstalt für Wald und Forstwirtschaft, LWF Wissen 63, pp. 677–684.

Norsk Electro Optikk AS, 2012. General brochure HySpex.

Ozdemir, I., Karnieli, A., 2011. Predicting forest structural parameters using the image texture derived from WorldView-2 multispectral imagery in a dryland forest, Israel. International Journal of Applied Earth Observation and Geoinformation 13 (5), 701–710.

Perona, P., Malik, J., 1990. Scale-Space and Edge Detection Using Anisotropic Diffusion. IEEE Transactions On Pattern Analysis And Machine Intelligence 12, 629–639.

Pinnel, N., 2007. A method for mapping submerged macrophytes in lakes using hyperspectral remote sensing. Ph.D. thesis, Technische Universität München.

Reuter, R. (Ed.), 2010. Tree Species Classification Based on the Analysis of Hyperspectral Remote Sensing Data. EARSel.

Richards, J. A., Jia, X., 1999. Remote Sensing Digital Image Analysis: An Introduction, 3rd Edition. Springer-Verlag New York, Inc.

Richter, R., Schläpfer, D., 2012a. Atmospheric / Topographic Correction for Airborne Imagery (ATCOR-4 User Guide). Tech. rep., German Aerospace Center.

Richter, R., Schläpfer, D., 2012b. Atmospheric/Topographic Correction for Satellite Imagery (ATCOR-2/3 User Guide). Tech. rep., German Aerospace Center.

Roberts, D., Ustin, S., Ogunjemiyo, S., Greenberg, J., Dobrowski, S., Chen, J., Hinckley, T., 2004. Spectral and structural measures of northwest forest vegetation at leaf to landscape scales. Ecosystems 7 (5), 545–562.

Rodriguez-Galiano, V. F., Abarca-Hernandez, F., Ghimire, B., Chica-Olmo, M., Atkinson, P. M., Jeganathan, C., 2011. Incorporating Spatial Variability Measures in Land-cover Classification using Random Forest. In: Stein, A and Pebesma, E and Heuvelink, G (Ed.), 1st Conference on Spatial Statistics 2011 - Mapping Global Change. Vol. 3 of Procedia Environmental Sciences. pp. 44–49.

Rogge, D., Bachmann, M., Rivard, B., Feng, J., 2012. Hyperspectral Flight-Line Leveling and Scattering Correction for Image Mosaics. 2012 IEEE International Geoscience and Remote Sensing Symposium (Igarss), 4094–4097.

Rogge, D. M., Rivard, B., 2010. Iterative spatial filtering for reducing intra-class spectral variability and noise. In: Hyperspectral Image and Signal Processing: Evolution in Remote Sensing (WHISPERS), 2010 2nd Workshop on. pp. 1–4.

Rouse, J. W., J., Haas, R. H., Schell, J. A., Deering, D. W., 1974. Monitoring Vegetation Systems in the Great Plains with ERTS.

Schaepman-Strub, G., Schaepman, M. E., Painter, T. H., Dangel, S., Martonchik, J. V., 2006. Reflectance quantities in optical remote sensing-definitions and case studies. Remote Sensing of Environment 103 (1), 27–42.

Schelhaas, M., Nabuurs, G., Schuck, A., 2003. Natural disturbances in the European forests in the 19th and 20th centuries. Global Change Biology 9 (11), 1620–1633.

Schlerf, M., Atzberger, C., Hill, J., 2003. Tree species and age class mapping in a Central European woodland using optical remote sensing imagery and orthophoto derived stem density - Performance of multispectral and hyperspectral sensors. Millpress Science Publishers.

Schmidt, P., 2004. Picea. In: Schütt, Weisgerber, Schuck, Lang, Roloff, Stimm (Eds.), Lexikon der Nadelbäume. Nicol Verlagsgesellschaft mbH & Co. KG, pp. 269–273.

Shahshahani, B. M., Landgrebe, D. A., 1994. The Effect of Unlabeled Samples in Reducing the Small Sample Size Problem and Mitigating the Hughes Phenomenon. IEEE Transactions on Geoscience and Remote Sensing 32 (5), 1087–1095.

Stadtverwaltung Traunstein, unknown. Stadtforst. http://www.traunstein.de/Rathaus-Politik/StaedtEinrichtungen.aspx?view= /kxp/orgdata/default&orgid=f06f7208-c694-4fab-9082-3dc21ffc2721, [accessed online 12-November-2012].

Stiftung Unternehmen Wald, unknowna. Die Buche (Fagus Sylvatica). http://www.wald.de/die-rotbuche-fagus-sylvatica/#more-42, [accessed online 31-January-2013].

Stiftung Unternehmen Wald, unknownb. Die Fichte (Picea abies). http://www.wald.de/die-fichte-picea-abies-l, [accessed online 04-February-2013].

Stiftung Unternehmen Wald, unknownc. Weißtanne (Abies alba)). http://www.wald.de/weisstanne-abies-alba/#more-40, [accessed online 31-January-2013].

StMELF (Bayerisches Staatsministerium für Ernährung, Landwirtschaft und Forsten), 2009. 10.000 Jahre Wald in Bayern Wald und Mensch in Bayern. http://www.stmelf.bayern.de/wald/forstpolitik/wald-in-zahlen/005185/index.php, [accessed online 22-November-2012].

Straub, C., Seitz, R., 2012. Schätzung von forstlichen Kenngrößen auf der Grundlage von Punktwolken aus digitaler Photogrammetrie und flugzeuggetragener Laserscannermessung. DGPF Tagungsband 21, 75–82.

The R Development Core Team, 2010. R: A Language and Environment for Statistical Computing.

Thenkabail, P., Lyon, J., Huete, A., 2011. Advances in Hyperspectral Remote Sensing of Vegetation and Agricultural Croplands. In: Thenkabail, P. S., Lyon, J. G., Huete, A. (Eds.), Hyperspectral Remote Sensing Of Vegetation. CRC Press, pp. 3–36.

Trevino, V., Falciani, F., 2006. Galgo.

Ustin, S., Xiao, Q., 2001. Mapping successional boreal forests in interior central Alaska. International Journal of Remote Sensing 22 (9), 1779–1797.

Vieilledent, G., Courbaud, B., Kunstler, G., Dhote, J.-F., Clark, J. S., 2010. Individual variability in tree allometry determines light resource allocation in forest ecosystems: a hierarchical Bayesian approach. Oecologia 163 (3), 759–773.

Wang, Z., Boesch, R., Ginzler, C., 2008. Integration of High Resolution Aerial Images and Airborne LiDAR Data for Forest Delineation. The International Archives of the Photogrammetry, Remote Sensing and Spatial Information Sciences Vol. XXXVII. 2008 (Part B7), 1203–1208.

Weier, J., Herring, D., 2000. Measuring Vegetation (NDVI & EVI). http://earthobservatory.nasa.gov/Features/MeasuringVegetation, [accessed online 18-December-2012].

Zhang, J., Rivard, B., Sanchez-Azofeifa, A., 2005. Spectral unmixing of normalized reflectance data for the deconvolution of lichen and rock mixtures. Remote Sensing of Environment 95 (1), 57–66.

Zhang, J., Rivard, B., Sanchez-Azofeifa, A., Castro-Esau, K., 2006. Intra and inter-class spectral variability of tropical tree species at La Selva, Costa Rica: Implications for species identification using HYDICE imagery. Remote Sensing of Environment 105 (2), 129–141.

Zhou, X., Jancsó, T., Chen, C., Vero”né, M. W., 2012. Urban Land Cover Mapping Based on Object Oriented Classification Using WorldView 2 Satellite Remote Sensing Images. International Scientific Conference on Sustainable Development & Ecological Footprint, 1–10.

Zhuo, L., Zheng, J., Li, X., Wang, F., Ai, B., Qian, J., 2008. A genetic algorithm based wrapper feature selection method for classification of hyperspectral images using support vector machine. In: Geoinformatics 2008 and Joint Conference on GIS and Built Environment: Classification of Remote Sensing Images. International Society for Optics and Photonics, pp. 1–9.

Appendix

Programs	Process
Atcor-3[6]	Atmospheric correction WV2 image
Atcor-4[7]	Atmospheric correction HySpex VNIR flightlines
ArcGIS 10.1	Forest mask creation for WV2
	Evaluation of forest inventory data
ENVI IDL 4.8	ORTHO geocorrection
	Levelling
	Spatial smoothing
	Normalisation
	Index calculation for WV2 scene and HySpex VNIR mosaic
	Forest mask creation for HySpex VNIR mosaic
	Collection of spectra in WV2 mask and HySpex VNIR mask
R 2.12.2 /	Calculation Principal Component Analysis using R Package *stats*[9]
R 2.15.2[8]	Band extraction with genetic algorithm using R Package *galgo*[10]
	Calculating Linear Discriminant Analysis using R Package *MASS*[11]
	Probability classification of WV2 mask and HySpex VNIR mask using Package *raster*[12]

Table 10.1: Applied programs for processes and analyses on data basis

[6] algorithm is discussed in Richter and Schläpfer (2012b)
[7] algorithm is discussed in Richter and Schläpfer (2012a)
[8] algorithm is discussed in The R Development Core Team (2010)
[9] http://stat.ethz.ch/R-manual/R-patched/library/stats/html/00Index.html
[10] http://www.bip.bham.ac.uk/vivo/galgo/AppNotesPaper.htm
[11] http://cran.r-project.org/web/packages/MASS/index.html
[12] http://cran.r-project.org/web/packages/raster/

Acknowledgement

I would like to thank Prof. Dr. Martin Oczipka (HTW Dresden) who supported me in the cooperation with the German Remote Sensing Data Centre. For helping me through my thesis I also want to give great thanks to Dr. Nicole Pinnel (DLR Oberpfaffenhofen) who was a great and tireless supervisor and mentor with guidance to and in R, the statistical language. Many thanks goes to Dr. Derek Rogge (DLR Oberpfaffenhofen), who explained me in great patience spectra and its characteristics, as well as many methodological issues. I also want to thank Dr. Xingjuan Wang (DLR Oberpfaffenhofen) for improving my atmospheric explanations and Mr. Christoph Ehrler (DLR Oberpfaffenhofen) for his IT-support.

Additional the whole team applied spectroscopy deserves my thanks for giving me the warmest and most sociable time I could have for writing my thesis.
Also all the opportunities, that were given to me, I would never want to miss. Of course my thanks also goes to Mr. Andreas Müller (DLR Oberpfaffenhofen), who allowed me to accomplish my thesis at the department land surface of the German Remote Sensing Data Centre.

Helping me through R I often reached my limits, but Mr. Carsten Neumann (GFZ in Potsdam) helped me through this successfully.
Without appropriate data to work on, this thesis would not have been possible. Many thanks to the German Remote Sensing Data Centre for supporting me with great HySpex VNIR data. Also thanks to European Space Imaging who provided me with great Worldview-2 data. The Landesanstalt für Wald und Forstwirtschaft (LWF) as well as Technische Universität (TU) in Munich supported me with in-situ inventory data from Traunstein forest, which enabled my spectral approach of tree species discrimination. Special thanks goes to Dr. Christoph Straub (LWF Freising) and Ralf Moshammer (TU Munich) for supporting me with answers to my questions about the inventory data. For giving me valuable comments on my thesis I thank Dr. Thomas Schneider (TU Munich).

And of course without the financial and mental support of my family I would not have been able to accomplish my studies this way.

Thank you all.

Erklärung über die eigenständige Erstellung der Arbeit

Hiermit erkläre ich, dass ich die vorgelegte Arbeit mit dem Titel
Detection of forest parameters using imaging spectroscopy
selbständig verfasst, keine anderen als die angegebenen Quellen und Hilfsmittel benutzt sowie alle wörtlich oder sinngemäß übernommenen Stellen in der Arbeit als solche und durch Angabe der Quelle gekennzeichnet habe. Dies gilt auch für Zeichnungen, Skizzen, bildliche Darstellungen sowie für Quellen aus dem Internet. Mir ist bewusst, dass die Hochschule für Technik und Wirtschaft Dresden Prüfungsarbeiten stichprobenartig mittels der Verwendung von Software zur Erkennung von Plagiaten überprüft.

Ort, Datum	Unterschrift Studentin